

**DEVELOPING CONTROL STRATEGIES TO MITIGATE INJURY AFTER
FALLING BACKWARD WITH A LOWER LIMB EXOSKELETON**

by

Mahsa Khalili

B.Sc., Sharif University of Technology, 2010

MASc., Sharif University of Technology, 2012

A THESIS SUBMITTED IN PARTIAL FULFILLMENT OF
THE REQUIREMENTS FOR THE DEGREE OF

MASTER OF APPLIED SCIENCE

in

THE FACULTY OF GRADUATE AND POSTDOCTORAL STUDIES
(Mechanical Engineering)

THE UNIVERSITY OF BRITISH COLUMBIA
(Vancouver)

December 2016

© Mahsa Khalili, 2016

Abstract

Powered lower limb exoskeletons (LLEs) are wearable robotic aids that provide mobility assistance for people with mobility impairments. Despite their advanced design, LLEs are still far from being effective assistive devices that can be used to perform activities of daily living. The main challenge in the operation of a LLE is to ensure that balance is maintained. However, maintaining an upright stance is not always achievable and regardless of the quality of user skill and training, inevitably falls will occur. Currently, there is no control strategy developed or implemented in LLEs that help reduce the user's risk of injury in the case of an unexpected fall.

In this thesis, an optimization methodology was developed and used to create a safer strategy for exoskeletons falling backwards in a simulation environment. Due to the data available regarding the biomechanics of human falls, the optimization methodology was first developed to study falls with simulation parameters characteristic of healthy people. The resulting optimal fall strategy in this study had similar kinematic and dynamic characteristics to the findings of previous studies on human falls. Rapid knee flexion at the onset of the fall, and knee extension prior to ground contact are examples of these characteristics. Following this, the optimization methodology was extended to include the characteristics of an exoskeleton. The results revealed that the hip impact velocity was reduced by 58% when the optimal fall strategy was employed compared to the case where the exoskeleton fell with locked joints. It was also shown that in both cases of optimal human and human-exoskeleton falls, the models contacted the ground with an upright trunk with a near-zero trunk angular velocity to avoid head impact. These results achieved the thesis goal of developing an effective safe fall control strategy. This strategy was then implemented in a prototype exoskeleton test device. The experimental results validated the simulation outcomes and support the feasibility of implementing this control

strategy. Future studies are needed to further examine the effectiveness of applying this strategy in an actual LLE.

Preface

This thesis is submitted in partial fulfillment of the requirements for a Masters of Applied Science in Mechanical Engineering at the University of British Columbia. It contains work done from May 2014 to December 2016, in the Collaborative Advanced Robotics and Intelligent Systems Laboratory. The test setup presented in Section 5.2 of Chapter 5 is based on work completed by a team of undergraduate students (Todd Darcie, Bryan Pawlina, Oliver Gadsby, and Saman Shariat Jaffari) as a capstone project with the author in the role of the client.

Table of Contents

Abstract.....	ii
Preface.....	iv
Table of Contents	v
List of Tables	x
List of Figures.....	xi
Acknowledgements	xiii
Chapter 1: Introduction	1
1.1 Mobility Impairments and Lower Limb Assistive Technologies	1
1.2 Motivation and Objectives	3
1.3 Thesis Outline	5
Chapter 2: Previous Studies and Related Work	6
2.1 Studies on Human Falls	6
2.1.1 Governing Dynamics of Human Falls	6
2.1.2 Characteristics of Human Falls	9
2.1.2.1 Prevalence of Human Falls.....	9
2.1.2.2 Average Fall Duration	9
2.1.2.3 Impact Velocities	10
2.2 Studies on Humanoid Robot Falls.....	11
2.3 Studies on Loss of Balance and Falls with Exoskeletons	13
Chapter 3: Development of an Optimization Methodology to Study an Optimal Fall	
Strategy	14
3.1 Introduction	14

3.2	Methods.....	15
3.2.1	Dynamic Modelling of a Human Backward Fall	15
3.2.2	Optimizing a Human Backward Fall	17
3.2.2.1	Design Variables	18
3.2.2.2	Constraints	20
3.2.2.3	Objective Function	21
3.2.2.4	Optimization Technique	22
3.2.2.5	Initial Guess	24
3.2.3	Development and Analysis of Optimized Human Falls.....	25
3.3	Results	26
3.3.1	Optimizing the Fall of a One-link Model.....	26
3.3.1.1	Effects of Available Torque Constraints at the Joint on the Optimal Solution of a One-link Model	26
3.3.1.2	Effects of the Initial Guess on the Optimal Solution of a One-link Model	28
3.3.2	Optimizing the Fall of a Two-link Model.....	28
3.3.2.1	Effects of the Available Torque Constraints at the Joints on the Optimal Solution of a Two-link Model.....	29
3.3.2.2	Effects of the Initial Guess on the Optimal Solution of a Two-link Model	30
3.3.3	Optimizing the Fall of a Three-link Model.....	31
3.3.3.1	Effects of the Fall Duration on the Value of the Objective Function.....	32
3.3.3.2	Effects of the Initial Guess on the Optimal Solution of a Three-link Model ...	35
3.3.3.3	Effects of the Initial Condition on the Optimal Solution	41
3.3.4	Joint Characteristics of an Optimal Solution	42

3.4	Discussion	51
3.4.1	Optimization Validation.....	51
3.4.2	Examining the Characteristics of an Optimized Fall Strategy	52
3.4.3	Limitations	54
3.5	Summary	54
Chapter 4: Human-Exoskeleton Falls Modelling and Optimization		56
4.1	Introduction	56
4.1.1	Methods.....	56
4.1.2	Dynamic Modelling of a Backward Fall with an Exoskeleton	56
4.1.3	Optimizing a Human-Exoskeleton Backward Fall	57
4.1.3.1	Design Variables	57
4.1.3.2	Constraints	58
4.1.3.3	Objective Function	59
4.1.3.4	Optimization Technique	59
4.1.3.5	Initial Guess	59
4.1.4	Development and Analysis of Optimized Human-Exoskeleton Falls	59
4.2	Results	60
4.2.1	Effects of Fall Duration and Initial Guess on the Value of the Objective Function ..	60
4.2.2	Effects of Coefficient of Friction Constraint on the Value of the Objective Function ..	62
4.2.3	Effects of Acceleration/Deceleration Time Constraint on the Value of the Objective Function	64
4.2.4	Joint Characteristics of an Optimal Human-Exoskeleton Fall	66

4.3 Discussion	74
4.3.1 Limitations	77
4.4 Summary	78
Chapter 5: Numerical and Experimental Validations.....	79
5.1 Numerical Validation Methods	79
5.2 Experimental Validation	83
5.2.1 Introduction	83
5.2.2 Test Bed Design	83
5.2.3 Experimental Procedure	85
5.2.3.1 Data Collection	85
5.2.3.2 Data Analysis.....	85
5.2.4 Results	86
5.3 Discussion	89
Chapter 6: Conclusions	91
6.1 Summary of Contributions	91
6.2 Recommendations and Future Work.....	93
Bibliography	95
Appendices.....	102
Appendix A : Governing Equations of Motion of a One-link, Two-link, and Three-link Model	
.....	102
A.1 One-Link Model.....	102
A.2 Two-Link Model	103
A.3 Three-Link Model	105

Appendix B : Design Variables	110
Appendix C : Constraints Governing the Motion of a Falling Human Model	112
Appendix D : Optimization Problems.....	114
Appendix E : Model of a Human-Exoskeleton Fall.....	116
Appendix F : Acceleration/Deceleration Time Calculations	121

List of Tables

Table 3-1	Design variables representing the dynamics of the one-link, two-link, and three-link models	19
Table 3-2	Parameters defining the structure of the optimization problem	24
Table 3-3	Examining the effect of the available torque at the joint on the optimal solution of the one-link model	27
Table 3-4	Examining the effect of the initial guess on the optimal solution of the one-link model	28
Table 3-5	Examining the Effect of Available Torque on the Optimal Solution of a Two-link Model	29
Table 3-6	Examining the effect of the initial guess on the optimal solution of the two-link model	30
Table 3-7	Examining the effect of the fall duration on the optimal solution of the three-link model	34

List of Figures

Figure 3.1 One-link, two-link, and three-link models of a human body The human is facing toward the right.	15
Figure 3.2 Value of the objective function for different fall durations	34
Figure 3.3 Hip linear velocity and trunk angular velocity at impact for different fall durations.	35
Figure 3.4 Value of the objective function for optimization trials (fall duration = 0.58 seconds)..	36
Figure 3.5 Hip linear velocity and trunk angular velocity at impact.....	36
Figure 3.6 Value of the objective function for optimization trials (fall duration = 0.55 seconds)..	38
Figure 3.7 Body configurations at specific instants during the fall.....	40
Figure 3.8 Joint trajectories of optimal solutions	41
Figure 3.9 Effects of the initial ankle angle on the optimal solution	42
Figure 3.10 Optimized kinematics and dynamics characteristics of ankle joint	43
Figure 3.11 Optimized dynamic and kinematic characteristics of the knee joint.....	45
Figure 3.12 Optimized dynamics and kinematics characteristics of the hip joint.....	47
Figure 3.13 Optimized angular velocity of the joints plotted in the global reference frame.....	49
Figure 3.14 Optimized hip linear velocity	50
Figure 4.1 Value of the objective function for different fall durations and two initial guesses ...	61
Figure 4.2 Value of the objective function for different ground surface conditions	63
Figure 4.3 Body configuration at specific instants of optimal falls with different coefficients of friction (CoF)	63

Figure 4.4 Value of the objective function for different fall durations with different actuator constraints	65
Figure 4.5 Optimized kinematics and dynamics characteristics of ankle joint (human-exoskeleton fall)	67
Figure 4.6 Optimized dynamic and kinematic characteristics of the knee joint (human-exoskeleton fall)	68
Figure 4.7 Optimized dynamic and kinematic characteristics of the hip joint (human-exoskeleton fall)	70
Figure 4.8 Optimized angular velocity of the joints plotted in the global reference frame (human-exoskeleton fall)	72
Figure 4.9 Optimized hip linear velocity (human-exoskeleton fall)	73
Figure 5.1 Comparing joint trajectories obtained from forward difference analysis and optimization	81
Figure 5.2 Comparing joint trajectories obtained using ode45 solver and optimization.....	82
Figure 5.3 Mechanical test setup	84
Figure 5.4 Comparison of joint angles between the simulation and experimental results	87
Figure 5.5 Comparison of joint angular velocity between the simulation and experimental results	88
Figure 5.6 Comparison of hip linear velocity between the simulation and experimental results	89

Acknowledgements

I would like to thank my supervisors, Dr. Machiel Van der Loos, Dr. Jaimie Borisoff for their guidance, motivation, encouragement, and support. I would also like to thank Dr. Ian Mitchell and Dr. Elizabeth Croft for their valuable knowledge and feedback throughout my work. I would like to thank my lab mates, especially Navid and Shalaleh whose support and help were always encouraging. Finally, I would like to specially thank my family, my parents and sisters for their support throughout my education and for teaching me to always strive for excellence.

This thesis is dedicated to my beloved family for their constant support and inspiration
throughout my life.

Chapter 1: Introduction

1.1 Mobility Impairments and Lower Limb Assistive Technologies

The ability to stand and walk plays an important role in performing activities of daily living and maintaining an independent life. However, mobility impairments impact many people's lives all over the world, and have significant effects on their quality of life. Mobility disability was identified as the most prevalent type of disability in the United States and the third most common disability in Canada [1],[2]. Several diseases lead to mobility disability, and among those are injuries to the spinal cord, with a high prevalence of occurrence [3]. According to a survey conducted in 2010, over 85,000 Canadians were living with an SCI [4]. It is also estimated that about 282,000 Americans are living with spinal cord injury in 2016, and approximately 17,000 new cases are added every year [5].

SCI has various consequences such as motor and/or sensory deficits, often including partial or complete impairment with walking. As a result, assistive technologies have been developed and used to help affected people maintain their independence and/or improve their functional mobility to perform activities of daily living [6]. For example, wheelchairs, orthoses, crutches, canes, and walking frames are used to improve mobility of people with disabilities [7]. Among these, wheelchairs are the most common assistive devices. Although wheelchairs do provide some form of mobility for their users, there are certain limitations and drawbacks regarding their long term use. Those include health concerns such as skin problems, cardiovascular disease, and psychological issues, as well as accessibility and usability limitations [8]. Beside these limitations, wheelchairs also do not provide therapeutic benefits, and would not improve mobility or other health conditions of their users.

On the other hand, standing is an effective way to overcome the drawbacks of constant sitting. It improves blood circulation, reduces muscle spasticity, reduces the occurrence of pressure sores, and enhances psychological well-being [9]. Hip-Knee-Ankle-Foot-Orthoses (HKAFO) and other passive orthoses are types of assistive devices that provide the benefit of standing and limited walking ability to their users. However, these types of mobility aids haven't been commonly accepted in the community due to the inherent limitations in their design, usability, and safety [10].

To meet the growing need for effective assistive technologies and rehabilitation goals, the concept of enhancing passive orthoses with powered actuators has gained more attention during the past few years [11]. Such wearable robotic aids that are developed for people with lower limb impairments are usually referred to as powered orthotic devices or lower limb exoskeletons (LLEs). According to the US Food and Drug Administration (FDA): "A powered exoskeleton is a prescription device that is composed of an external, powered, motorized orthosis used for medical purposes that is placed over a person's paralyzed or weakened limbs for the purpose of providing ambulation" [12].

LLEs normally consist of a brace that is attached to the legs and part of the trunk through straps and supports those body segments. Usually, the hip and knee joints of these devices are actuated, and control signals are applied at these joints to replicate a gait cycle. A variety of sensors, including inertial measurement units (IMUs) and pressure sensors, are used to determine the postural configuration of the user and provide the required feedback to the controller. A backpack, which is usually placed around the waist, houses the controller and the power supply system. Apart from all of these components, other assistive aids like a walker, cane, or crutches are usually used as an adjunct to LLEs to help maintain balance [13].

Results of previous studies show that exoskeletons, when used as therapeutic devices, improve their users' health conditions [14],[15],[16]. The benefits that exoskeletons provide for their users include improving functional mobility (not by only being used as an assistive device but when used over time and for incomplete SCI users who can improve their mobility) and blood circulation, reduction in pressure sores and muscle spasticity. LLEs have been designed to be used for both clinical and personal purposes [17]. There are currently two LLEs available on the market that have received FDA approval for personal use. These devices include: ReWalk™, Indego®. However, safety concerns are still among the most challenging barriers to the acceptance and use of LLEs in the community. The FDA has identified “instability, falls, and associated injuries” as the primary risk associated specifically with these devices [13]. Thus, LLEs should be used under constant supervision and assistance from a trained companion according to FDA regulations [18].

1.2 Motivation and Objectives

In the case where an internal or external perturbation is applied to an exoskeleton or the user, the exoskeleton's function might be perturbed, eventually leading to the destabilization and fall of the device and user. To enhance the safety of the user, the state of balance of the system should be monitored constantly. This could be done by the use of available data from different sensors mounted on the exoskeleton and balance-detection algorithms. Different decisions could be made to handle the case when loss of balance is detected. First, a fall could be prevented by the application of balance recovery techniques. If this is successful, the exoskeleton would continue its function. However, if the application of a fall prevention strategy is not successful, the control system would switch to a safe-fall control strategy.

Regardless of the substantial development in gait control strategies for exoskeletons, no control strategy has yet been developed for LLEs to ensure balance recovery in the case of loss of balance. In the case of a fall with an exoskeleton, the impact velocity when hitting the ground is large enough to cause traumatic brain injury, bone fracture or bruises. Normally persons living with an SCI have fragile bones, with low bone mineral density due to lack of physical movement. Therefore, the consequences of a fall could be even worse for these individuals [19]. In one study where a LLE was used by a group of persons with SCI, the exoskeleton lost its balance 16 times, each time resulting in the engagement of a tether, which was used for safety considerations. The findings of this study confirm the risks associated with the use of LLEs [20]. A survey of potential end users of exoskeletons and individuals who have experience working with mobility impairments reported safety to be the primary concern when using a LLE [21].

Addressing the safety issues associated with the use of LLEs is a top priority as these devices are expected to assist individuals in performing activities of daily living independently. Therefore, the goal of the author of this thesis is to enhance LLE user safety by reducing the risk and the severity of injury in the case of an unrecoverable loss of balance. In case of a fall, the most important part of the body that should be protected against any possible impact is the head. Thus, one approach to enhance the user's safety is to avoid any head impacts.

A study showed that the severity of an injury is related to the velocity of the body segments at impact [22]. Therefore, one should minimize impact velocity to minimize the severity of the resulting injury. Depending on the type of fall, different parts of the body may come into contact with the ground. This thesis focuses exclusively on cases of backward falls with exoskeletons. One reason is due to the potential for catastrophic head injury in the case of a backward fall. Another reason to study this type of fall is the high prevalence of backward falls observed among

healthy individuals [23]. In the case of a backward fall for healthy individuals, the hip or hands would be the first contact point with the ground. However, when exoskeletons are in use, hands are usually occupied with a walking aid such as a walker or a crutch. As a result, the first contact point with the ground when falling backward is assumed to be the hip. Based on this assumption, the following statement summarizes the objectives of this thesis:

To reduce the risk and severity of injuries in the case of a human-exoskeleton backward fall, by avoiding head impact and minimizing the hip linear velocity at the moment of ground contact.

1.3 Thesis Outline

The current chapter of this thesis discusses the motivation of this work and presents the objectives. Chapter 2 provides the background literature related to this work, including a review of the biomechanics of human falls, an overview of safe-fall strategies for bipedal robots, and proposed safe-fall strategies for a falling exoskeleton. Optimization methods are also reviewed in that chapter to provide the basis for the methodology developed in this thesis. Then, Chapter 3 explains the optimization methodology developed for a human fall model. First, a human fall is modelled in a simulation environment. Then, the dynamics of the fall are optimized and the corresponding results are presented and discussed. Chapter 4 details the development of a safe-fall strategy for the model of a human-exoskeleton fall, and the characteristics of an optimal fall are presented. Chapter 5 examines the validity of the safe-fall strategy developed to achieve the objectives of this thesis. A mechanical test setup was built, and experiments were conducted to examine the simulation results. Finally, Chapter 6 concludes this thesis with a focus on summarizing the findings of the work, contributions, and recommendations for future research.

Chapter 2: Previous Studies and Related Work

As discussed in the previous chapter, safety issues regarding the use of exoskeletons become a serious concern when these devices are used as assistive technologies in performing daily activities. However, the current state-of-the-art technology is not capable of safe and functional operation without external assistance, as there are no control strategies developed to safeguard the user and device against falling. Moreover, no safety considerations have been implemented on the exoskeletons currently being used that could lessen the severity of impact to the user in the case of a fall. This thesis focuses on eliminating this gap by developing a safe fall control strategy to enhance user safety in the event of a human-exoskeleton fall.

As mentioned above, fall mitigation and recovery strategies and falls with exoskeletons have not been studied previously, and there are no data available regarding the characteristics of a human-exoskeleton fall. However, fall-related studies in the healthy population have been the focus of previous research. The related literature was reviewed to gain a better understanding of the underlying kinematics and dynamics of human falling (Section 2.1). In addition, there are studies on developing safe fall strategies for humanoid robots, reviewed in Section 2.2. A few safe-landing concepts were previously proposed to improve the safety of exoskeletons in the case of a loss of balance. These proposed ideas are examined and summarized in Section 2.3.

2.1 Studies on Human Falls

2.1.1 Governing Dynamics of Human Falls

The centre of mass of a standing human is located at a relatively high distance from the base of support, the ground. In some studies, the human body is regarded as an unstable inverted pendulum in which an active control system is constantly maintaining its upright balance [24]. Therefore, in the case of an external or internal perturbation, humans may lose their upright

balance. Depending on the severity of the perturbation, different balance recovery strategies could be employed [25]. Most of the time, these balance recovery strategies are successful and can recover upright balance. However, in more severe cases where falls are not preventable, people do fall and hit the ground or other surrounding objects.

Different factors that cause human falls are generally categorized into intrinsic and extrinsic. Intrinsic factors are related to physiological deficiencies whereas extrinsic factors have environmental origins [26]. Fall-related injuries often reduce mobility, independence, and the quality of life of the injured person. Among the older population in the United States, falls are reported to be a leading cause of death from injury [27]. According to the report “Leading Causes of Nonfatal Injury”, between the years of 2001 to 2014, unintentional falls were the most common cause of nonfatal unintentional injury for all ages in the United States [28]. In Canada, between the years of 2005 and 2013, broken or fractured bones (37%) were the most common types of fall-related injury [29]. The two most common injuries were reported to be hip and upper extremity fractures [30]. In one study, fall-related injuries were studied among groups of young and old adults. The results of this study reveal that the percentage of people who suffered a pelvic injury was 27% in the older and 15% in the younger group [31].

A theoretical analysis of falls from a standing height suggest that forces at impact are an order of magnitude greater than the force required to break any bone of an elderly woman [32]. In another study, it was shown that if the potential energy at standing height is directly converted to kinetic energy at the moment of ground contact, it is 40 times greater than the kinetic energy required to fracture the femoral neck [33].

Nevertheless, experimental work that studied the biomechanics of the human body during a fall reveal that most of the impulsive force in a fall is absorbed by muscle contraction and soft

tissue. It also found that no more than 10% of falls in older people result in bone fractures [32]. The results of other research confirmed that the actual rate of any kind of fracture in the cases of human falls is a lot less than the theoretical prediction [34],[35],[36]. All these results indicate that people constantly use injury-mitigation strategies to reduce the occurrence of fall-related injuries [37].

The abovementioned protective responses have been examined in previous research. One injury mitigation technique is to share the contact energy between different body segments. The application of this strategy was observed in several cases of falls where subjects hit the ground with outstretched hands, simultaneously, slightly before, or slightly after the hip, knee, or head hit [23],[38]. Lower hip impact velocities were observed in cases where subjects' hands came into contact with the ground before the hip [39].

Activation of the lower limb muscles throughout the fall was found to be another safe fall technique that is employed by healthy individuals [22]. Synergistic patterns of muscle contractions in the lower extremity lead to the application of braking torques at the lower limb joints. These torques are applied to the joints to resist joint motion in the direction of the fall and lead to mitigation of the impact velocity or the impact kinetic energy. In the case of a backward fall, these synergistic patterns of muscle contractions are found to result in a series of body movements throughout the fall. These movements start with a quick knee flexion at an early stage of the fall, followed by knee extension starting in mid-fall, and end at ground impact while maintaining an upright trunk [39],[40],[41].

The effectiveness of these protective responses was found to be influenced by several factors. The first and the most important factor is the falling technique [41]. The available strength in the lower limb muscles is another factor that influences the severity of the fall. It has

been shown that the severity of the injury increases with age [42]. Another factor is how fast the loss of balance is detected and how fast the injury mitigation strategy is initiated. In other words, the sooner the safe fall strategy is activated, the lower the severity of the injury [40],[43],[44].

2.1.2 Characteristics of Human Falls

In the remaining parts of this section, the biomechanical characteristics of human falls are examined in more details. It is worth noting that most of the research conducted in the field of human falls is limited to cases of simulated, mechanically induced, or self-initiated falls. There are very few studies conducted to study the characteristics of real-life human falls [45].

2.1.2.1 Prevalence of Human Falls

The prevalence of different types of falls has been studied in previous literature. In one study, randomly varied perturbations were applied to a platform and subjects were asked to maintain their balance as much as possible. The results of this study revealed that the rate of balance recovery is lower for cases of backward falls compared to forward or sideways falls [23]. In another study, in which falls were monitored in long term facilities among older adults, backward falls were found to have a higher rate of occurrence (84%) compared to other types of falls [46]. In the same study, major contact points were found to be the hip (in 100% of the falls), hand (in 84% of the falls), and head (48% of the falls) [23],[38].

2.1.2.2 Average Fall Duration

The fall duration is commonly defined as the interval between the initiation of imbalance and the time at which one of the body parts hits the ground. In a group of young adults where sudden perturbations were applied to the base of support, the average fall duration was measured to be 715 ± 160 ms [23]. In another study, in which healthy young adults were released from an unbalanced standing position and were asked to maintain their balance as much as possible, the

average fall duration was recorded to be 749 ms [39]. The average fall duration (the time interval between imbalance initiation and impact), in real-life falls among older adults, was found to be 1271 ± 648 ms. Also, the average descent time, which is defined as the time interval between fall initiation and impact, was reported to be 593 ± 255 ms among the same group of individuals [38].

2.1.2.3 Impact Velocities

The two main indicators of fall severity are the position at which the body comes into contact with the ground and the impact velocity of the contact point [40]. Impact velocity is influenced by the conditions under which the fall is performed. Studies on human falls could be categorized into different types including: self-initiated falls, tether-released falls, mechanically-induced falls, and real-life falls. The results from previous research on sideways falls reveal that the average impact velocity is lower in self-initiated falls (2.75 ± 0.42 m/s) compared to mechanically-induced falls (3.01 ± 0.83 m/s) [47], [48]. The same relationship is observed in studies where impact velocity in backward falls was examined. The vertical component of the impact velocity was found to be lower in self-initiated falls (1.45 ± 0.5 m/s in one study and 1.86 ± 0.47 m/s in another study), compared to mechanically-induced falls (2.55 ± 0.85 m/s) [23],[22],[49]. These results suggest that protective responses are more effective in self-initiated falls where users are ready to employ those strategies as quickly as possible. In one study, where real-life falls were examined among older adults, the average impact velocity was found to be 2.14 ± 0.63 m/s [38].

It was also shown that the initial conditions of the fall had an influence on the severity of the impact velocity. In cases where safe fall strategies were employed later after the onset of imbalance, the effectiveness of the strategy was lower. In other words, when less time is available to implement the safe fall strategy, the fall impact velocity is higher [49].

2.2 Studies on Humanoid Robot Falls

The development of safe fall strategies has been the focus of research in the field of humanoid robots for some time. Similar to humans, humanoid robots are inherently unstable structures. The control systems of most humanoid robots are designed to maintain balance in the case where weak perturbations are applied to the robot. However, in cases of large disturbances, balance recovery techniques might not be effective and falls are inevitable [50]. Due to the importance of preventing physical damage to the robot as well as considering human and environmental safety, safe fall control strategies have been studied, developed and implemented in bipedal robots [51].

The first step in the implementation of a safe fall strategy in a humanoid robot is to detect the state of imbalance. This is a complex procedure and could be done by the use of sensors mounted on the robot. The next step is then to switch from the task-directing control strategy (e.g., walking, turning, etc.), or possibly a fall-prevention control strategy, to a “safe-landing” control strategy [52],[53]. In the remainder of this section, different safe fall strategies that have been developed for humanoid robots are described.

In one study, a stepping technique was proposed to orient the robot towards an optimal fall direction that results in minimum damage to the robot [54]. Another safe-landing strategy was developed based on the techniques of martial arts. Considering the conservation of energy, it is known that decreasing the potential energy at the very early stage of a fall could lead to the reduction of kinetic energy at impact and consequently decrease of the velocity at impact. The proposed strategy was executed by lowering the mass center of the robot by quickly bending the knees at the very beginning of the fall. Resisting torque was generated at the lower limb joints of the robot to further damp the existing potential energy. This safe-landing strategy was utilized in

conjunction with the use of protective structures. The protective structures were installed on segments that were identified to be at high risk of impacting the ground [32],[51].

In a follow-up study, a model of a one-link, variable length, passive-joint inverted pendulum was developed to study the dynamics of a humanoid robot fall in a simulation environment. The safe fall strategy was executed in two steps. The first step was to quickly shrink the legs after the initiation of the fall. Then, the legs were extended when the centre of mass of the robot reached a certain height. This height was chosen to minimize the impact velocity. The results of this study revealed that the angular velocity of the pendulum, and consequently the vertical linear velocity at impact, was reduced when the safe-landing strategy was employed. Also, it was shown that using a high-jump mat reduced the impact by 7-fold compared to the case of directly hitting the floor [55].

In a later study from the same research group, an optimization technique was used to improve the effectiveness of the safe-fall control strategy. In this study, the objective was to minimize the landing speed of the centre of gravity of the robot and to optimize the time that takes to complete the fall. The results of this work revealed that by performing a squatting motion at an early stage of the fall, the landing impact velocity of the system was suppressed [52],[56]. In a more recent study, a model of a quadruple inverted pendulum was used to simulate the humanoid forward fall. In this study, a minimization technique was used to optimize the falling motion of the robot. The objective function included the joint dynamics during the fall and the impact dynamics at landing. The optimization was then performed for different fall durations and results compared. The fall duration with which the value of the objective function was minimized was selected as the optimal fall duration. The joint kinematics and dynamics corresponding to this fall duration were chosen as the optimal solution [57]. Taken together,

these studies on humanoid robot falls confirmed that less damage is transferred to the robot when safe-landing control strategies were used [32],[50],[53],[54].

2.3 Studies on Loss of Balance and Falls with Exoskeletons

The focus of the exoskeleton-related studies has been mostly on the development of human-like movements such as standing, walking, turning, sitting, and more recently climbing up or down stairs. Fall-related studies in the field of exoskeletons are a relatively a new area of research. After the expansion of the use of exoskeletons outside of rehabilitation centres, safety concerns regarding the use of these devices became more critical. To the best knowledge of the author, there has been no study on the development of safe-fall strategies for the case of a human-exoskeleton fall. However, just recently, a few safe-fall techniques were proposed to enhance the safety of exoskeletons. One proposed strategy is to augment the device with an advanced fall detection technology. This technology could be then combined with the use of an airbag system, which is activated in the case of detection of loss of balance [58].

In a recently published patent, three protective strategies were proposed to be implemented in a lower limb exoskeleton. The first strategy is to provide a cushioning mechanism that is used to absorb energy or spread the force at impact. The second strategy is to detect the state of imbalance and reduce the kinetic energy by generating braking torques at the joints of the exoskeleton. The third strategy is a hybrid technique to use joint work to actively position the system during the fall to maximize the effectiveness of the cushioning mechanism [59]. It is worth recalling that none of these proposed strategies have been implemented or used in any of the existing exoskeletons, nor have they studied the potential injury- or impact velocity-reduction that might result from the use of such techniques.

Chapter 3: Development of an Optimization Methodology to Study an Optimal Fall Strategy

3.1 Introduction

The prior chapters introduced the motivation for the development of a safe fall strategy in powered lower limb exoskeletons. This thesis considers the specific case of a backward fall because of the risks and severity of injuries associated with this type of fall, specifically as a result of head and hip impact. The basis of this research objective relies on fall-related studies that were performed with healthy participants. Results of these studies reveal that there are some protective responses that prevent the occurrence of severe damage to the human body in the case of a fall. The kinematics and dynamics of lower limb joints during falls in these studies provided the foundation for my first study, which was to develop the methodology to optimize a safe fall strategy for the case of a human backward fall and to compare the results with available data regarding real-life human falls. If the validity of the developed optimization methodology was verified, then the methodology could be extended to the development of a safe fall strategy in the case of a human-exoskeleton backward fall. The next chapter provides further details regarding the development of the safe fall strategy for the model of a human-exoskeleton.

This chapter describes the details regarding the establishment of an optimal, safe fall strategy to reduce the risk and severity of injury in the case of a human backward fall. The governing dynamics of a simplified human model were derived and used to simulate human falls. An optimization method was then developed in the simulation environment to obtain the dynamics of the lower limb joints when performing a safe fall. Finally, to examine the validity of the developed optimization technique, results of this work were compared with the results of previous fall-related studies.

3.2 Methods

3.2.1 Dynamic Modelling of a Human Backward Fall

In the field of biomechanics, it is common to represent the dynamics of the human body with a model of an inverted pendulum. Depending on the complexity of the task that is being studied or the required accuracy, various models based on an inverted pendulum, including one-link, two-link, and three-link models have been used [24],[60],[61]. More specifically, models of a single or multi-link inverted pendulum have been developed to study falls in the field of humanoid robots [55],[57].

In this work, one-, two-, and three-link models were created to determine the dynamics of different representations of human backward falls [62],[63]. These models are shown in Figure 3.1. The governing equations of motion for each model are described in Appendix A. For all the models, the human body was assumed to have a total height of 1.6 m and body mass of 53.7 kg¹. For each model, anthropometric characteristics of corresponding body segments were calculated separately [64].

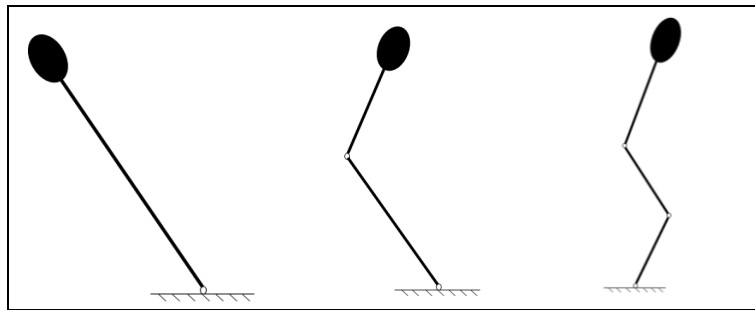


Figure 3.1 One-link, two-link, and three-link models of a human body

The human is facing toward the right.

¹ These values were selected from a similar study in which human falls were modeled in a simulation environment [41].

The model of a one-link inverted pendulum represents the case where the whole body is considered as one, rigid, straight, fixed-length link, in which the hip and knee joints are considered to be locked, and the whole body pivots about the ankles. Although this model is not a realistic model of a human fall, it does replicate the condition under which most of the currently used exoskeletons fall when losing balance. Also, the governing dynamics of a one-link system are simple to derive and the model can be easily created and validated in a simulation environment.

The model of a two-link inverted pendulum represents the case where the upper and lower body are modelled as two separate, rigid links that are connected together through the hip joint. In this model, the first joint replicates the dynamics of the ankle joint; the shin and thigh are aligned, and the knee joint is considered to be locked. This model could be an example of falling with a passive orthotic device (e.g., a Knee-Ankle-Foot Orthosis), in which the knee joints are locked but the user has some control over positioning the trunk.

In the model of a three-link inverted pendulum, the foot and shin are represented as the first link that is connected to the ground through the ankle joint. The thigh is the second link, which is connected on one side to the shin through the knee joint, and connected to the upper body through the hip joint, on the other end.

Other assumptions that were made throughout the development of these models in the simulation environment are listed below:

- Falls are assumed to be symmetric and studied in the sagittal plane.
- Throughout the fall, both feet remain in contact with the ground.
- The effects of friction and damping at each joint are neglected.

- The net torque applied at the lower limb joints represents the sum of the corresponding muscle contractions.
- It is assumed that the available torque at the joints could be applied instantaneously and with no time delay.
- Except for the one-link model, the hip (i.e., representing the pelvis/buttocks) is considered to be the only contact point to the ground at impact.
- Each joint's angular velocity is assumed to be zero at the onset of the fall

3.2.2 Optimizing a Human Backward Fall

As discussed before, prior to the development of the safe fall strategy, the two main goals of the strategy were defined as avoiding head impact and reducing hip impact velocity. These objectives were achieved through the application of an optimal torque profile at the joints. According to the governing dynamics of the motion, there is a one-to-one relation between the joint trajectories and the applied torque to the joints. Thus, joint trajectories were also optimized while optimal torque profiles were generated.

The first step in the development of the safe fall strategy was to formulate the characteristics of the problem, that is, to define the *design variables*. Following this, the *constraints* that had to be satisfied and the *objective function* were defined. Next, based on the form of the constraints and the objective function, an appropriate *optimization technique* was selected to solve the optimization problem. Lastly, based on the type of the optimization algorithm and model studied, an *initial guess* for the design variables had to be provided to the optimization.

3.2.2.1 Design Variables

As described in Appendix A, the Euler-Lagrange equations of motion for a one-link, two-link, and three-link models were derived in the state-variable space format. The general form of these equations is shown in (3.1):

$$I(\Theta)\ddot{\Theta} + \dot{I}(\Theta, \dot{\Theta})\dot{\Theta} - \frac{1}{2} \left[\frac{\partial(I\dot{\Theta})}{\partial \Theta} \right]^T \dot{\Theta} + \frac{\partial V}{\partial \Theta} = \Phi_n \quad (3.1)$$

In this equation, Θ is a one-, two-, or three-dimensional vector including ankle², and/or knee, and/or hip joint angles, for one-, two-, or three-link models, respectively. $\dot{\Theta}, \ddot{\Theta}$ are the first and second derivative of Θ with respect to time, respectively. I is the generalized inertia matrix, and \dot{I} is its first derivative with respect to time. V represents the system's potential energy and in the case of this problem, where friction at the joints was neglected, Φ_n is the total torque delivered to the lower limb joints. The vector of the design variables is defined to include the joint angles, angular velocities, and the torque applied at each joint from the initiation of the fall until the moment of ground impact. The design variables take different forms for each model, as defined in Table 3-1.

² In all the three models, it was assumed that the shank and foot are represented as a single segment (locked ankle joint). However, in order to keep the consistency of the biomechanical representation of the joints and with no effect on the obtained results, the angle between the heel and the ground was labeled as the ankle angle.

Table 3-1 Design variables representing the dynamics of the one-link, two-link, and three-link models

Model	Joint Angle Θ	Joint Angular Velocity $\dot{\Theta}$	Joint Torque T
One-link	θ_{Ankle}	$\dot{\theta}_{Ankle}$	τ_{Ankle}
Two-link	$[\theta_{Ankle}, \theta_{Hip}]$	$[\dot{\theta}_{Ankle}, \dot{\theta}_{Hip}]$	$[\tau_{Ankle}, \tau_{Hip}]$
Three-link	$[\theta_{Ankle}, \theta_{Knee}, \theta_{Hip}]$	$[\dot{\theta}_{Ankle}, \dot{\theta}_{Knee}, \dot{\theta}_{Hip}]$	$[\tau_{Ankle}, \tau_{Knee}, \tau_{Hip}]$

In the case of a one-link model, there is only one link that represents the characteristics of the human body and the only unmovable pin joint in this model represents the dynamics of the ankle angle throughout the fall. The vector of the design variables has the form described in (3.2), in which Θ_{Ankle} , $\dot{\Theta}_{Ankle}$, and T_{Ankle} are vectors of joint angle, joint angular velocity, and joint torque that contain the value of each design variable at specific instants of fall. More details regarding the definition of the vector of the design variables are provided in Appendix B.

$$[\Theta_{Ankle}, \dot{\Theta}_{Ankle}, T_{Ankle}] \quad (3.2)$$

In the case of a two-link model, where the knee joint is assumed to be locked, the two joints in the model represent the characteristics of the ankle and the hip joints. The design variables are defined in a vector format as described in (3.3), in which each parameter is a vector itself.

$$[\Theta_{Ankle}, \Theta_{Hip}, \dot{\Theta}_{Ankle}, \dot{\Theta}_{Hip}, T_{Ankle}, T_{Hip}] \quad (3.3)$$

In the case of a three-link model, the design variables are defined in a vector as described in (3.4). As will be discussed later, in the three-link model, the ankle is assumed to be passive and no torque is applied to the joint throughout the fall.

$$\left[\Theta_{Ankle}, \Theta_{Knee}, \Theta_{Hip}, \dot{\Theta}_{Ankle}, \dot{\Theta}_{Knee}, \dot{\Theta}_{Hip}, T_{Knee}, T_{Hip} \right] \quad (3.4)$$

3.2.2.2 Constraints

The biomechanical characteristics of a human body impose several constraints on the motion of the lower limb joints. These constraints include the range of motion, range of angular velocity, and the range of available torque at each joint. More specifically, these constraints are defined as the upper and lower bounds of the design variables, and the corresponding values for each of these variables for healthy individuals were obtained from previous studies [41],[65].

The initial condition from which the fall is initiated is another constraint that had to be satisfied when developing the safe fall strategy. The initial condition is defined by the joint angles and angular velocities at the onset of a fall. Initial joint angles and angular velocities were set equal to constant values and were defined in the form of linear constraints.

When developing the optimal safe fall strategy, the dynamics of the fall strategy must still be in compliance with the previously derived equations of motion throughout the fall. This assumption imposes a set of nonlinear constraints that have to be satisfied when optimizing the fall. Details regarding the definition of these constraints are provided in Appendix C.

By examining the dynamics of the human fall, it can be observed that the time required to complete a fall is directly influenced by the torque that is applied to the joints throughout the fall. So the fall duration or impact time is an unknown parameter when initializing the optimization since the optimal torque profiles and the joint trajectories are undetermined at that point. Due to the complexity of the three-link model and the constraints that were imposed on this model, this was a challenge specifically when the optimal fall strategy was developed for the three-link model. Ultimately, the fall duration was defined as a constraint that had to be satisfied. The time

of impact was defined as the moment where the hip height changes sign from a positive value to a negative value. In each optimization trial, the fall duration was predetermined and the value of the hip height was constrained to be negative and positive at the last and the one-before-the-last step of the fall, respectively. More details on how this issue was approached and resolved are described in Appendix B.

3.2.2.3 Objective Function

In the case of a one-link model, the objective function was defined as the angular velocity of the ankle joint at the moment of impact. In this case, both the angular velocity of the ankle joint and the linear velocity of the hip or head at the moment of impact have equivalent representations.

In the case of a two-link model, the objective function was defined as the linear impact velocity of the hip, and head impact avoidance was achieved through the specified joint constraints. In this case, the available extension torque was limited to avoid the backward inclination of the trunk to reduce the risk of head impact.

In the case of a three-link model, due to the complexity of the fall dynamics, a more specific objective function had to be defined. As described previously, the goal in the development of the safe fall strategy was to avoid head impact and to minimize the linear hip impact velocity. In cases of real-life falls, head impact could be prevented by positioning the trunk throughout the fall and/or by the use of the upper extremities, specifically the hands. In my work, the upper extremities were not included in the control strategy, and head impact avoidance was achieved by a trunk positioning strategy. Thus, when defining the objective function of the three-link model, the possibility of head impact was assumed to be correlated with the value of the angular velocity of the trunk at the moment of hip impact. The reason behind this assumption

was that if the angular velocity of trunk would be high, the residual angular momentum in the system might be high and may lead to the rotation of the whole body about the contact point. Considering that the other goal was to minimize the impact velocity of the hip when hitting the ground, the general form of the objective function was defined as presented in (3.5). In this equation, $\dot{\theta}(t)_{Trunk}^2$ is the square of the trunk angular velocity at the moment of impact (to avoid both forward or backward rotation of the trunk in order to avoid the risk of head injury and prevent other potential collisions), and $(\dot{x}(t)^2 + \dot{y}(t)^2)_{Hip}$ is the square of the total linear velocity of the hip at the moment of ground contact. Since the units of the impact trunk angular velocity and the hip linear velocity are not the same, weighting factors α and β were added. The optimization was performed for a few trials and the order of magnitude of each objective was examined individually. These factors were then chosen to equalize the weight of each objective.

$$F = \alpha \dot{\theta}(t)_{Hip}^2 + \beta (\dot{x}(t)^2 + \dot{y}(t)^2)_{Hip} \quad @ \quad t = t_{impact} \quad (3.5)$$

3.2.2.4 Optimization Technique

Considering the dynamics of the fall and the form of the objective function, the problem was identified as a multivariable, smooth, nonlinear, and non-convex optimization problem with a set of smooth linear and nonlinear equality and inequality constraints that needed to be satisfied (Refer to Appendix D for more details on optimization problems). As discussed in the previous chapter, there is no analytical solution for a non-convex, nonlinear optimization problem. In this case, a numerical technique is considered the best option to solve the optimization problem. In previous studies, to solve a similar minimization problem, numerical optimization techniques based on the variational principle, steepest descent method, and Pontryagin's minimum principle

were used to find the optimal safe fall strategy for humanoid robots [57],[56]. More recently, various powerful software toolboxes that employ highly efficient optimization techniques have been developed and are available to be used for finding a solution to a general form of an optimization problem. Among the available resources, the Optimization Toolbox in MATLAB (2013b; MathWorks, Natick, MA) was identified to be an appropriate option to be used in the case of the current optimization problem.

This toolbox provides a large set of different optimization algorithms to solve various types of optimization problems. An optimization decision table provided by MATLAB was used to identify the appropriate optimization method for the discussed optimization problem. Since the objective function and the constraints had a nonlinear general smooth form, FMINCON was chosen [66]. This function finds the local minimum of a constrained nonlinear multivariable function, as specified in (3.6). The general form of the syntax used to define the optimization problem is described in (3.7) and details regarding the definition of each parameter are described in Table 3-2.

In MATLAB R2013b, FMINCON provides four optimization algorithms, including: ‘trust-region-reflective (default)’, ‘interior-point’, ‘sequential quadratic programming (sqp)’, and ‘active-set’. ‘Trust-region-reflective’ and ‘interior-point’ algorithms were not used because of their clear deficiencies in defining the constraints in the case of the current problem. It has been found that the set of linear algebra routines to solve the ‘sqp’ are more efficient in both memory usage and speed than the ‘active-set’ routines [67]. The results of both optimizations were similar, however, in the case of the current optimization problem, the execution time of the optimization was 35% lower when the ‘active-set’ algorithm was used compared to the case

where the ‘sqp’ algorithm was used. Ultimately, the ‘active-set’ algorithm was determined to be the best option in the case of the present optimization problem.

$$\min_x f(x) \text{ such that } \begin{cases} c(x) \leq 0 \\ ceq(x) = 0 \\ A.x \leq b \\ Aeq.x = beq \\ lb \leq x \leq ub \end{cases} \quad (3.6)$$

$$x = \text{fmincon}(f, x_0, A, b, Aeq, beq, lb, ub, \text{nonlcon}) \quad (3.7)$$

Table 3-2 Parameters defining the structure of the optimization problem

Field Name	Description	Field Name	Description
x	Vector or matrix of design variables	A	Matrix for linear inequality constraints
x_0	Initial guess for x	b	Vector for linear inequality constraints
$f(x)$	Objective function	Aeq	Matrix for linear equality constraints
$c(x)$	Function to define nonlinear inequality	beq	Vector for linear equality constraints
$ceq(x)$	Function to define nonlinear equality	lb	Vector of lower bounds
nonlcon	Nonlinear constraint function that includes $c(x)$, $ceq(x)$	ub	Vector of upper bounds

3.2.2.5 Initial Guess

An initial guess for the design variables needs to be provided to an optimization strategy when numerical routines are used. In this case, the optimization iteratively alters the initial guess in an attempt to converge to an optimal solution. The initial guess has exactly the same vector structure as the design variables. Thus, the initial guess consisted of a feasible set of joint angle trajectories, joint angular velocities, and corresponding torque profiles that were applied to the joints throughout the fall. The strategy that was used in this work was to apply a constant torque to the joints and use the resultant joint angles and angular velocities, which were determined by a forward kinematics calculation, as an initial guess for the design variables.

When using local optimization methods, one should consider that the optimal solution might be affected by the choice of the initial guess that is provided to the optimization. To examine this fact, various optimization trials were performed with different initial guesses. The value of the objective function was obtained for each optimization trial and the dependency of the optimal solution on the initial guess was examined.

3.2.3 Development and Analysis of Optimized Human Falls

The development of the optimization methodology initially used the one-link model of a human fall. When the validity of the optimization was confirmed for this model, the optimization method was extended for the two-link model of a human fall. The dynamics of the fall were more complicated in the case of the two-link model and the optimization routine had to evolve correspondingly. Next, the effectiveness of the developed optimization technique was verified for the two-link model, ultimately leading to the development of the optimization methodology for the three-link model of a human fall. This model was the most representative model of a human fall compared to the previously discussed models and was ultimately used in the development of the safe fall strategy. Due to the complexity of the three-link model, more detailed investigations were conducted to verify the efficacy of the developed optimization methodology. Corresponding results and validation of the optimization of the one-, two-, and three-link models are presented in Sections 3.3.1, 3.3.2, and 3.3.3, respectively. Finally, the joint characteristics for the optimal solution of a backwards-falling human are presented in Section 3.3.4.

3.3 Results

3.3.1 Optimizing the Fall of a One-link Model

An optimal safe fall strategy was determined for the one-link model of a human fall. The validity of the optimization technique was then assessed for two conditions. The first condition was to examine the congruency of the optimal solution to the governing dynamics of the human fall. It was hypothesized that if enough torque is made available at the joint, the optimal safe fall strategy would stop the link from falling and stabilize it³. Also, in cases where lower non-stabilizing torques are available, it was hypothesized that higher torques would result in lower impact velocities. To test these hypotheses, the constraints of available torque at the ankle joint were adjusted and the optimal solutions were compared against each other. The second condition ascertained the robustness of the results by investigating the dependency of the optimal solution on the choice of the initial guess. Optimizations performed with different initial guesses were compared.

3.3.1.1 Effects of Available Torque Constraints at the Joint on the Optimal Solution of a One-link Model

In all optimization trials to examine the effect of available ankle torque on the optimal solution, the upper bound of available torque was equal to zero (to prevent the forward inclination of the body), and the lower bound varied from 0 to -25 Nm. The initial ankle angle at which the fall was initiated was 92° (For more details regarding the sign conventions refer to Appendix A, Section A.1). It should be emphasized that the case where no torque is made available at the ankle joint corresponds to a simple free fall; this is also the situation for current

³ Available torque at the joint indicates the resultant effects of muscle activity at that joint

exoskeletons which fall with no mitigation strategy, and thus serves as the worst case fall scenario. For all the trials, the initial guess was assumed to be the joint characteristics of a free fall. The corresponding results for this study are summarized in Table 3-3.

Table 3-3 Examining the effect of the available torque at the joint on the optimal solution of the one-link model

Trial No.	Optimization Constraints	Optimal Solution	
	[Lower, Upper] Range of the Available Torque at the Ankle Joint (Nm)	Head Impact Velocity (m/s)	Fall Duration (s)
1	0	-6.88	1.51
2	[-5,0]	-6.67	1.62
3	[-10,0]	-6.54	1.81
4	[-15,0]	-6.48	2.35
5	[-20,0]	0	-

A simple statics analysis of the one-link model revealed that the model could be held at the initial position from which it is released, if a torque of -16.22 Nm is applied at the ankle joint and in a direction to resist the fall. The results of this study confirmed that when the available torque at the joint was constrained higher than that value, the model remained balanced at the initial angle and did not fall. This justified the observed zero velocity of the head when a negative torque greater in magnitude than 16.22 Nm was made available at the joint. It was also found that in trials constrained with lower available torques, the model was not stabilized and it fell. However, in these trials, the impact velocity was lower and the duration of fall was higher when higher torque was available at the joint. As a result of this optimization study, the hypothesis of higher available torque lowering the impact velocity was verified.

3.3.1.2 Effects of the Initial Guess on the Optimal Solution of a One-link Model

The dependency of the optimal solution on the choice of the initial guess was examined with four different initial guesses. In each trial, a constant torque was applied to the joint and the resultant dynamic characteristics of the joint, including the joint angle and angular velocity, were used as the starting point of the optimization. Since analyzing the dynamics of the fall was the focus of this study and not the cases in which the model was stabilized, the range of the available torque at the joint was set equal to $[-15, 0]$ Nm. The initial ankle angle from which the fall was initiated was 92° (in other words, 2° leaning forward from vertical). The result of each trial is summarized in Table 3-4.

Optimization converged to the same optimal solution in all the four trials. Therefore, it was concluded that the optimization method developed for the one-link model provides an optimal solution unique and independent of the initial guess.

Table 3-4 Examining the effect of the initial guess on the optimal solution of the one-link model

Trial No.	Optimization Condition	Initial Guess		Optimal Solution	
	Applied Torque to the Joint (Nm)	Head Impact Velocity (m/s)	Fall Duration (s)	Head Impact Velocity (m/s)	Fall Duration (s)
1	0	-6.88	1.51	-6.48	2.35
2	-5	-6.81	1.63	-6.48	2.35
3	-10	-6.69	1.82	-6.48	2.35
4	-15	-6.48	2.35	-6.48	2.35

3.3.2 Optimizing the Fall of a Two-link Model

The model was then extended to two links and the validity of the optimization technique examined under the same conditions as for the one-link model. In this model, both the effects of available torque constraints at the ankle joint and the effect of different initial guesses on the

optimal solution were examined. Corresponding results for these optimized models of falls are described in Sections 3.3.2.1 and 3.3.2.2.

3.3.2.1 Effects of the Available Torque Constraints at the Joints on the Optimal Solution of a Two-link Model

In this study, the optimization was performed for different ranges of available torque at the ankle joint to examine the effect of the available torque on the optimal solution. In all the trials, the upper bound of the available torque at the joint was set equal to zero, and the lower bound was varied from 0 to -90 Nm. The lower and upper limits of the available torque at the hip joint were constant for all the trials and were equal to -130 Nm and 5 Nm, respectively. The initial ankle and hip angle from which the fall was initiated was 120° and -20° , respectively (for more details regarding the sign conventions, refer to Appendix A, Section A.2). The initial guess for the optimization, for all the trials, was considered to be the joint characteristics of a free fall, where no torque is applied to the joints. The results of this study are summarized in Table 3-5.

Table 3-5 Examining the Effect of Available Torque on the Optimal Solution of a Two-link Model

Trial No.	Optimization Condition	Optimal Solution	
	[Lower, Upper] Bounds of the Available Torque at the Ankle Joint (Nm)	Hip Impact Velocity (m/s)	Fall Duration (s)
1	0	-4.01	0.48
2	[-10,0]	-3.88	0.50
3	[-30,0]	-3.77	0.53
4	[-50,0]	-3.56	0.56
5	[-70,0]	-3.46	0.61
6	[-90,0]	-3.20	0.67

By performing a simple static analysis, while considering the biomechanical limits of the joints, it was noticed that the fall was initiated from an initial condition from which stable

balance could not have been recovered. Therefore, the model could not have been stabilized in any of the trials. However, as expected, the impact velocity of the hip was lower and the fall duration was higher when higher torque was available at the ankle joint.

3.3.2.2 Effects of the Initial Guess on the Optimal Solution of a Two-link Model

Ten pairs of different constant torques were applied at the hip and ankle joint of a two-link model to generate ten sets of initial guesses for the optimization trials. The joint characteristics of the case of a free fall, where no torque is applied to the joints, were provided as in initial guess to the optimization. The limits of the available torque at the ankle and hip joints were $[-90, 0]$ Nm and $[-130, 0]$ Nm, respectively. The initial ankle and hip angle from which the fall was initiated were 120° and -20° , respectively. Results of this study are summarized in Table 3-6.

Table 3-6 Examining the effect of the initial guess on the optimal solution of the two-link model

Trial No.	Optimization Condition		Initial Guess		Optimal Solution	
	Applied Torque to the Joints (Nm)		Hip Impact Velocity (m/s)	Fall Duration (s)	Hip Impact Velocity (m/s)	Fall Duration (s)
	Ankle	Hip				
1	0	0	-4.01	0.48	-3.20	0.67
2	-90	0	-3.33	0.63	-3.20	0.67
3	-90	-5	-3.31	0.61	-3.20	0.67
4	-50	0	-3.70	0.55	-3.20	0.67
5	-50	-5	-3.57	0.53	-3.20	0.67
6	-50	-10	-3.46	0.52	-3.20	0.67
7	-10	0	-3.92	0.49	-3.20	0.67
8	-10	-5	-3.89	0.48	-3.20	0.67
9	-10	-10	-3.79	0.47	-3.20	0.67
10	-10	10	-3.77	0.51	-3.20	0.67
11	-10	20	-3.51	0.56	-3.20	0.67

By examining the results, it was confirmed that all the optimized solutions had lower hip impact velocity compared to the case of the free fall or the initial guess. It was also observed that despite the variability of the dynamics of the initial guesses that were provided to the optimization, the optimal solution converged to a constant value for all the trials. Therefore, it was concluded that the optimization method for the two-link model provides an optimal solution that is unique and independent of the starting point of the optimization.

3.3.3 Optimizing the Fall of a Three-link Model

Due to its joint and limb congruency with a human, a three-link model represents the biomechanics of human falls more realistically than the simpler models. This model was ultimately used to develop the safe human fall strategy. The results of my model analysis to optimize a backward fall strategy in a human are presented in Section 3.3.4. Before moving forward with confidence and using this model to analyze a human-exoskeleton fall strategy (the subject of Chapter 4), the previous model validations were extended to this three-link model. First, it was observed that in the three-link model, and in part due to the optimization algorithm chosen and complexity of the model studied, using predefined fall duration has a direct impact on the optimal solution. As a result, the effect of the fall duration on the optimal solution was studied for the three-link model and corresponding outcomes are detailed in Section 3.3.3.1. Next, the effects of the choice of the initial guess on the optimal solution were examined. Results of this investigation are presented in Section 3.3.3.2. As discussed earlier, previous studies show that the effectiveness of the protective safe fall strategy is determined by how fast it is employed in the case of an imbalance. To verify this phenomenon in the developed optimization technique, the effectiveness of the optimal strategy was compared for different cases of falls with different initial conditions. In these studies, the initial ankle angle from which the fall was initiated

represented the stage of the fall at which the optimal control strategy is activated. The results of this investigation are presented in Section 3.3.3.3.

Additional assumptions that were made in the development of the safe fall strategy for the three-link model of a human fall are listed below:

- In the case of a three-link model of a human fall, the ankle joint was considered as a passive joint. This was due to the fact that previous studies revealed that the effect of the generated torque at this joint is negligible [22].
- A half-plane model of a human body was used to simulate the fall in the sagittal plane.
- In all trials, the limits of the available torque at the knee and hip joints were equal to $[-175, 75]$ Nm and $[-65, 125]$ Nm, respectively.
- In all the trials, the initial knee and hip angles from which the fall was initiated were 40° and -40° , respectively. These values were chosen similar to a previous study done on human falls modelling [41].

3.3.3.1 Effects of the Fall Duration on the Value of the Objective Function

As described before, the fall duration is predefined when the optimization settings are initialized. However, theoretically the fall duration is affected by the torque that is applied to the joints throughout the fall and the ultimate resulting trajectory, both of which are unknown when the optimization is initialized. It was shown previously that for the one- and two-link models of a human fall, the optimal solution is not influenced by the predefined fall duration, and the results of the optimization converged to the same value in all trials (Table 3-4 and Table 3-6).

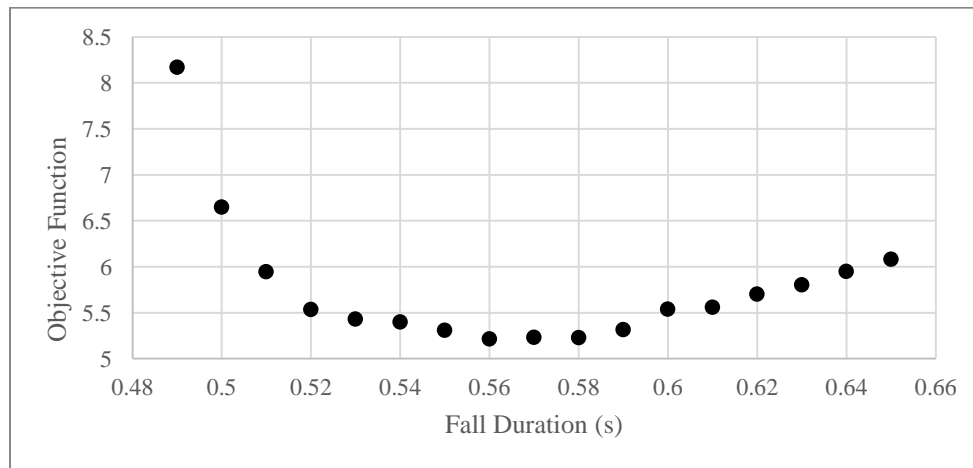
Throughout the development of the optimization technique, it was found that unlike the one- and two-link models, optimizing a three-link model of a human fall is directly influenced by the choice of the fall duration. To investigate the effect of the fall duration on the optimal solution,

optimizations were performed for a range of different fall durations, and the results of each trial were compared. To generate the initial guess for each optimization trial, -16 Nm and 9 Nm torque were applied to the knee and hip joints, respectively. The initial ankle angle from which the fall was initiated was 95° (For more details regarding the sign conventions, refer to Appendix A, Section A.3). Under these conditions, the optimal fall duration was 0.56 sec.

Results corresponding to this study are summarized in Table 3-7, and the value of the objective function for each fall duration is shown in Figure 3.2. The results of these optimization trials confirmed that the predetermined value of the fall duration would directly affect the results of the optimization. It was observed that no feasible solution existed in the case where fall duration was set lower than 0.49 sec or higher than 0.65 sec. This meant that the optimization constraints could not have been satisfied under the required conditions, in the case where a fall took shorter than 0.49 or longer than 0.65 sec. According to Figure 3.2, the objective function obtained its lowest value when the fall duration was equal to 0.56 sec. According to Table 3-7, both objectives, that are the hip linear velocity and angular velocity of the trunk at impact, obtained their lowest value in the case where the fall duration was equal to 0.56 sec (Figure 3.3). This analysis confirmed the need to analyze varying fall durations for each optimization analysis.

Table 3-7 Examining the effect of the fall duration on the optimal solution of the three-link model

Trial No.	Fall Duration (s)	Hip Impact Velocity (m/s)	Trunk Angular Velocity at Impact (rad/s)	Value of the Objective Function
1	0.49	2.86	0.016	8.17
2	0.50	2.58	0.013	6.65
3	0.51	2.44	0.012	5.95
4	0.52	2.35	0.010	5.54
5	0.53	2.33	0.010	5.43
6	0.54	2.32	0.008	5.40
7	0.55	2.30	0.005	5.31
8	0.56	2.28	0.005	5.22
9	0.57	2.29	0.005	5.23
10	0.58	2.29	0.007	5.23
11	0.59	2.30	0.008	5.32
12	0.60	2.35	0.008	5.54
13	0.61	2.36	0.008	5.56
14	0.62	2.39	0.008	5.70
15	0.63	2.41	0.009	5.80
16	0.64	2.44	0.010	5.95
17	0.65	2.46	0.010	6.08

**Figure 3.2 Value of the objective function for different fall durations**

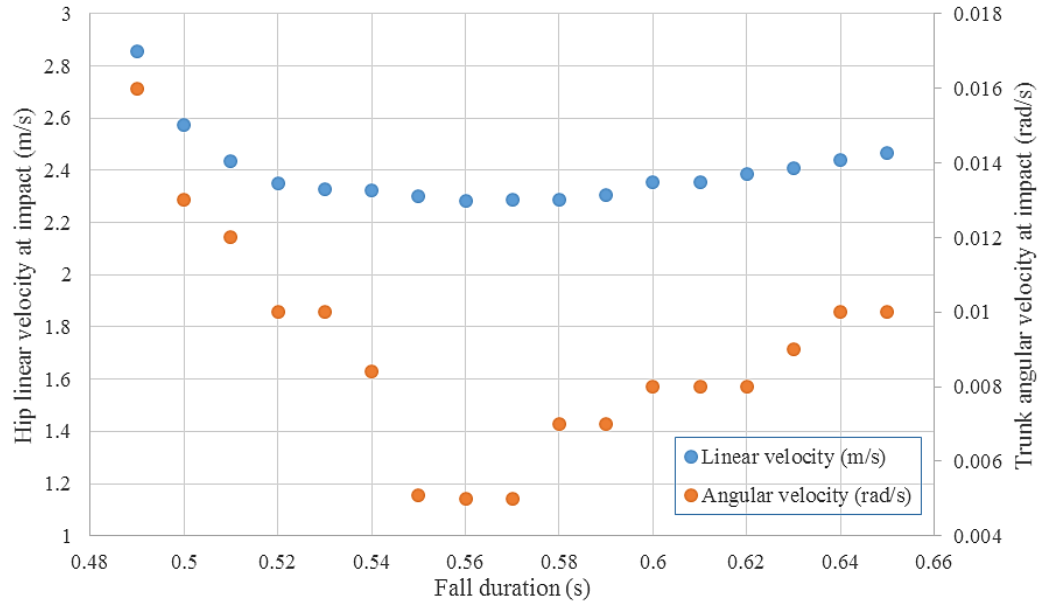


Figure 3.3 Hip linear velocity and trunk angular velocity at impact for different fall durations

3.3.3.2 Effects of the Initial Guess on the Optimal Solution of a Three-link Model

To examine the effects of the initial guess on the optimization results, multiple pairs of different constant torques were applied to the hip and knee joints of the three-link model to provide dissimilar initial guesses for the optimization trials. The value of the objective function for each initial guess and the corresponding optimal solution were examined for each optimization trial. To further examine the details of the obtained optimal solutions, the value of the hip impact velocity as well as the value of the trunk angular velocity at impact were evaluated separately. The results of this study are shown in Figure 3.4 and Figure 3.5. The ankle angle from which the fall initiated was 95° and the duration of the fall for all the optimization trials was equal to 0.58 sec.

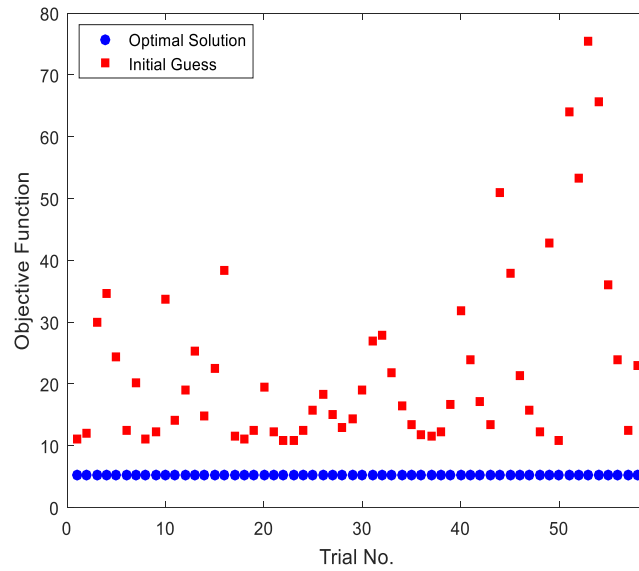


Figure 3.4 Value of the objective function for optimization trials (fall duration = 0.58 seconds)

Distinct initial guesses were provided to the optimization and the value of the objective function for each initial guess and the corresponding optimal solution are examined.

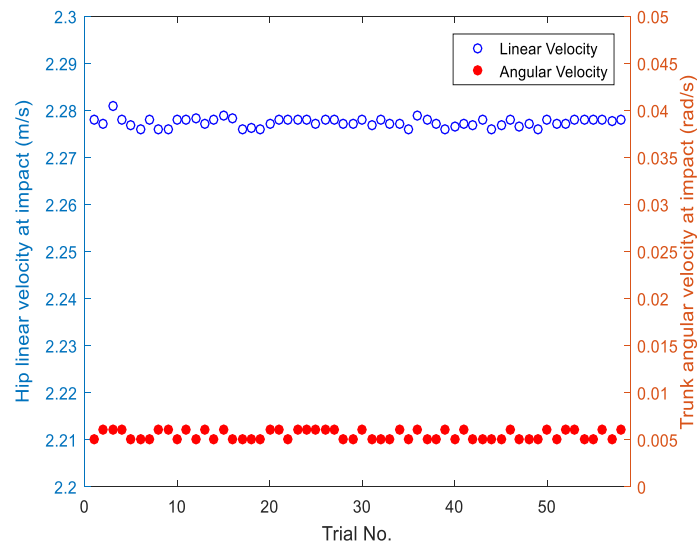


Figure 3.5 Hip linear velocity and trunk angular velocity at impact

Distinct initial guesses were provided to the optimization and the optimal value of the hip linear and trunk angular at impact were examined for each optimization trial.

As discussed in the previous section, the optimal solution is influenced by the choice of the fall duration. Further optimization trials were performed to examine whether the dependency of the optimal solution on the initial guess is affected by the fall duration or not. To take into account the effect of the fall duration, ten optimization trials with exactly the same conditions as some of the previous trials, and with a fall duration equal to 0.56 sec were performed. The results of these trials are shown in Figure 3.6.

The results of this study reveal that despite the diversity in the value of the objective function for each initial guess that was provided to the optimization, the objective function for all the cases converged to similar values, with an average equal to 5.19 ± 0.00 and 5.16 ± 0.00 for the case of fall duration equal to 0.58 sec and 0.55 sec, respectively (Figure 3.4). It was also observed that the average hip linear velocity and the trunk angular velocity at impact were equal to 2.28 ± 0.00 and 0.005 ± 0.000 m/s, respectively (fall duration equal to 0.58 sec).

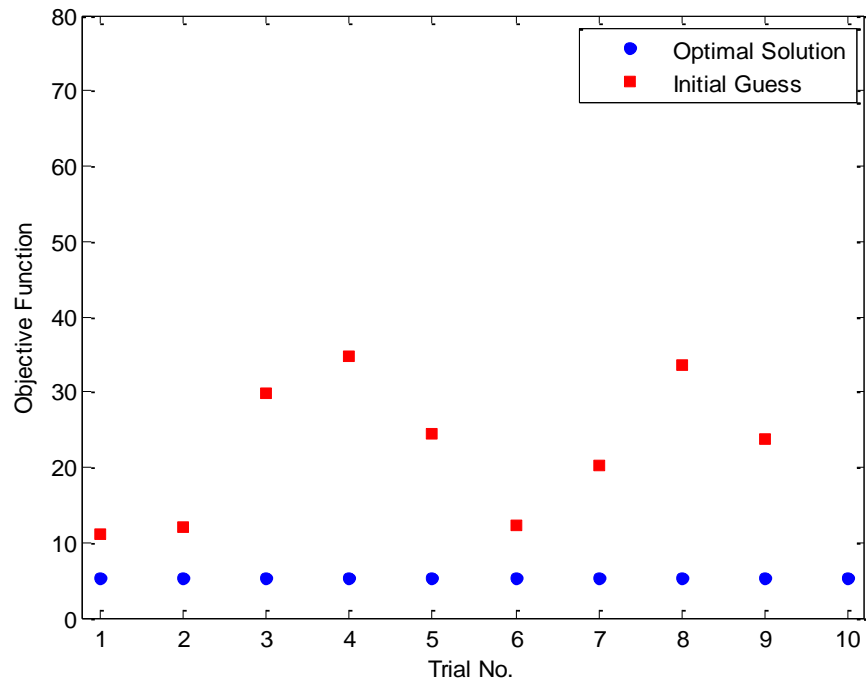


Figure 3.6 Value of the objective function for optimization trials (fall duration = 0.55 seconds)

Distinct initial guesses were provided to the optimization, and the value of the objective function for each initial guess and the corresponding optimal solution are shown.

The motions of the trajectories following two different initial guesses as well as the optimal solution when these initial guesses were provided to the optimization were examined at specific instants during the fall (Figure 3.7). To further investigate the dynamic characteristics of the optimal solutions in the case where the two above-mentioned initial guesses were provided to the optimization, the trajectories of the joint angles throughout the fall were plotted and examined (Figure 3.8).

To confirm that the initial guesses had dissimilar characteristics, the resultant motion of two initial guesses were examined in detail. Initial guess 1 was generated in the case where no torque was applied at the hip joint and -8 Nm was applied to the knee joint. Initial guess 2 was

generated in the case where 9 Nm and -16 Nm torque were applied at the hip and knee joints, respectively. The falling strategy and more specifically the joint trajectories throughout the fall were different in both cases. The orientation of the trunk throughout the fall is a clear example of this difference (Figure 3.7). Despite the fact that dissimilar initial guesses were provided to the optimization, similar joint characteristics were obtained when the optimization was performed with each initial guess. This was also confirmed by the examination of the joint angles throughout the fall (Figure 3.8).

Examination of the results reveals that very little difference exists in the results of the optimizations in the case where two different initial guesses were provided to the optimization. This finding reveals that the joint trajectories in both cases have similar patterns throughout the fall duration.



















Initial Guess 1	Time (s)	0	0.18	0.26	0.32	0.35	0.43
	TH = 0 TK = -8 Nm						
Initial Guess 2	Time (s)	0	0.18	0.36	0.44	0.47	0.55
	TH = 9 Nm TK = -16 Nm						
Optimal Solution	Time (s)	0	0.10	0.15	0.21	0.50	0.58
	Optimal Solution						

Figure 3.7 Body configurations at specific instants during the fall

The first two rows show the fall characteristics of initial guess 1, in which joint trajectories were generated in the case where no torque was applied at the hip joint and -8 Nm was applied at the knee joint. The second two rows show the fall characteristics of the second initial guess, which was generated in the case where 9 Nm torque was applied at the hip joint and -16 Nm was applied at the knee joint. The last two rows depict the motion characteristics of an optimal solution when each of the mentioned initial guesses was provided to the optimization.

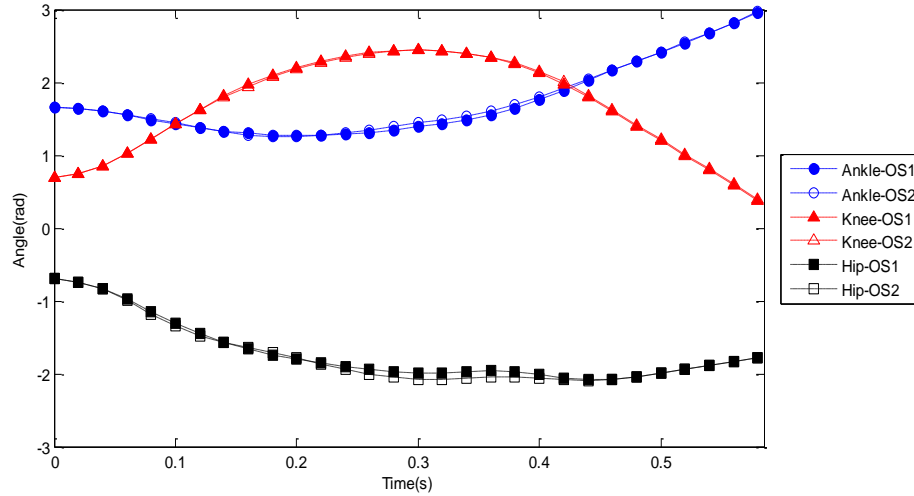


Figure 3.8 Joint trajectories of optimal solutions

The joint trajectories of an optimal solution when two different initial guesses are provided to the optimization are compared against each other. The optimal solutions that correspond to initial guesses 1 and 2 are drawn and labelled with suffixes OS1 and OS2, respectively.

3.3.3.3 Effects of the Initial Condition on the Optimal Solution

The effectiveness of a protective safe fall strategy in healthy individuals was shown to be affected by the stage of fall at which the strategy is employed. In this work, the relation between the effectiveness of the safe fall strategy and the time at which it is activated was examined by initiating the fall from different initial conditions, which were achieved by varying the initial ankle angle from 93° to 101° . In other words, slower times to initiate a fall strategy correspond to higher initial ankle angles from which a fall strategy begins. To generate the initial guess for the optimization, -16 Nm and 9 Nm torque were applied to the knee and hip joints, respectively.

As discussed earlier, an optimal solution for different fall conditions is influenced by the fall duration. In the current case, various optimization trials were performed to find the optimal fall duration for each case of different initial conditions. The optimal values of the objective function and optimal fall duration were computed for each case of an initial ankle angle, and the

results are shown in Figure 3.9. The results clearly show that the sooner the safe fall strategy is employed, the lower the resulting objective function. That is, hip linear velocity and the trunk angular velocity at impact would be lower when a safe fall strategy is started earlier.

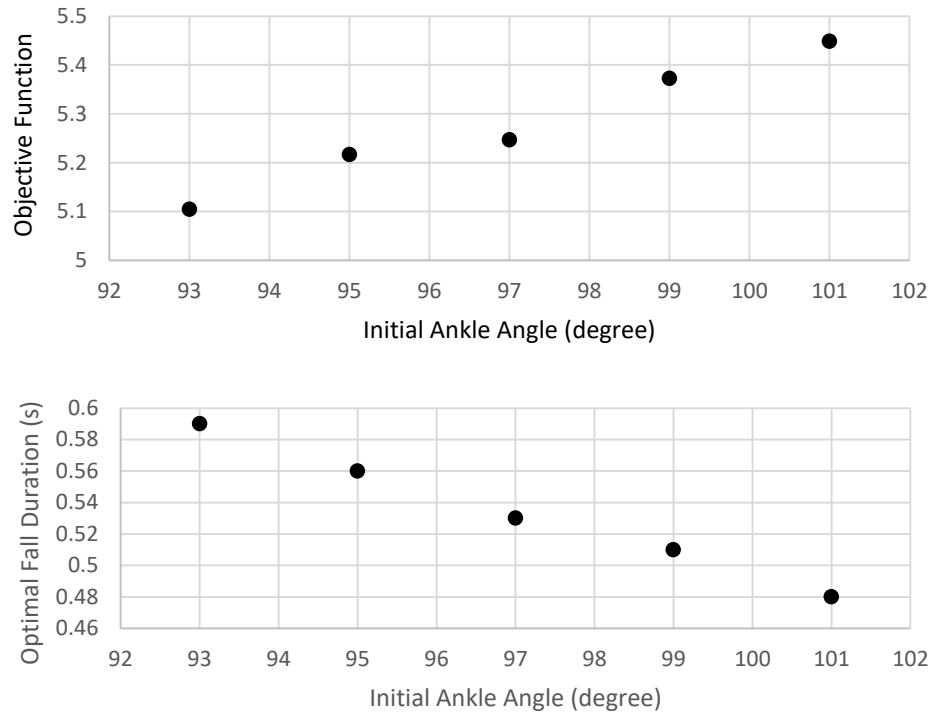


Figure 3.9 Effects of the initial ankle angle on the optimal solution

Examining the effects of the initial ankle angle on the objective function and the optimal fall duration.

3.3.4 Joint Characteristics of an Optimal Solution

In this section the joint characteristics of the three-link model, when an optimal fall strategy is employed, are examined. The kinematics and dynamics characteristics of the ankle, knee, and hip joints are shown in Figure 3.10, Figure 3.11, and Figure 3.12. The profiles of the joints angular velocity as well as the profile of the linear velocity of hip throughout the fall were examined, and the corresponding results are shown in Figure 3.13 and Figure 3.14, respectively.

To better illustrate the characteristics of the optimal fall strategy, diagrams of body position at specific instants in the fall (0.10, 0.20, 0.30, 0.40, 0.50, 0.55 sec) are depicted in each figure.

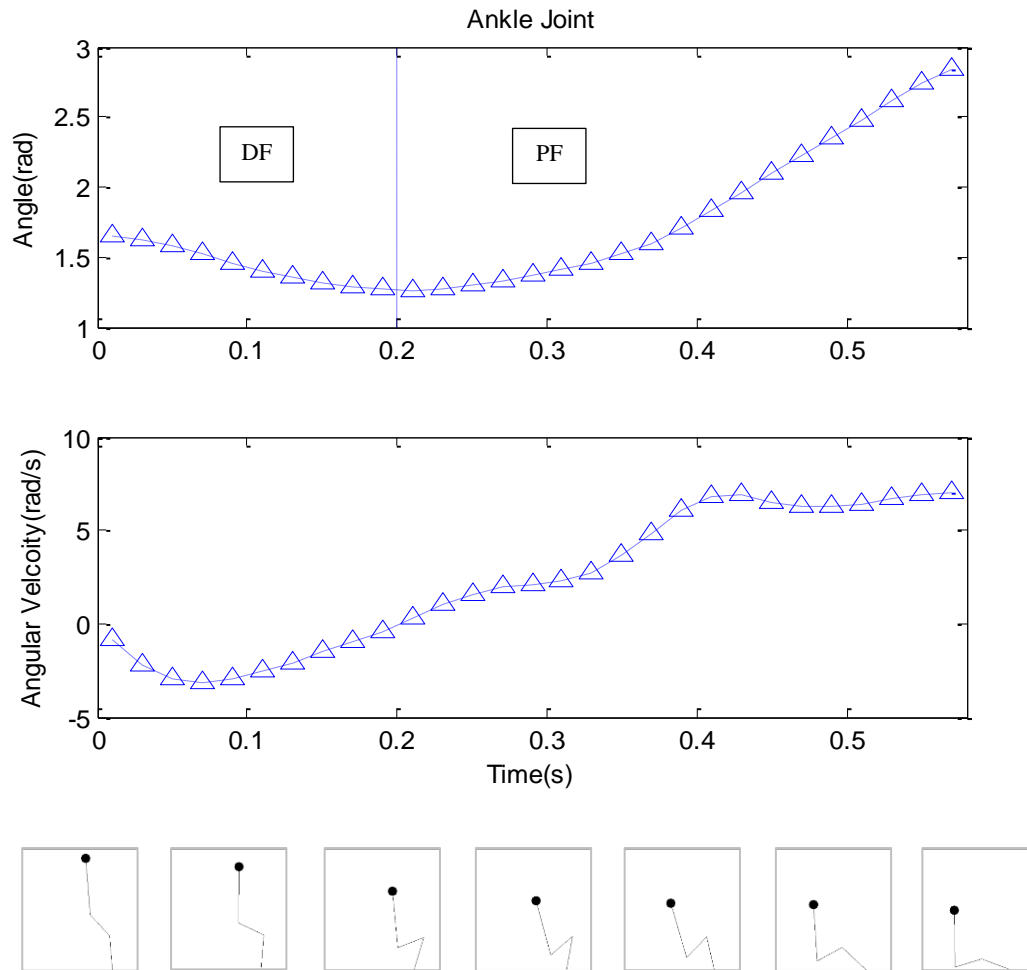


Figure 3.10 Optimized kinematics and dynamics characteristics of ankle joint

The profiles of the optimal ankle angle and angular velocity throughout the fall are shown.

The ankle joint is moving in the plantarflexion (PF) direction if increasing and is moving in the dorsiflexion (DF) direction if decreasing. The regions regarding the plantarflexion and dorsiflexion motion of the ankle are separated by the dashed line on the joint angle graph and corresponding areas to these motions are indicated by PF and DF labels, respectively.

Figure 3.10 shows that the fall was initiated from an ankle angle at which the shin segment was oriented posteriorly to the ankle joint. After the initiation of the fall, the ankle performed a dorsiflexion movement that resulted in an anterior rotation of the shin segment with respect to the ankle joint. The ankle rotation changed direction at 0.2 sec, and a plantarflexion motion was performed that continued up to the end of the fall duration.

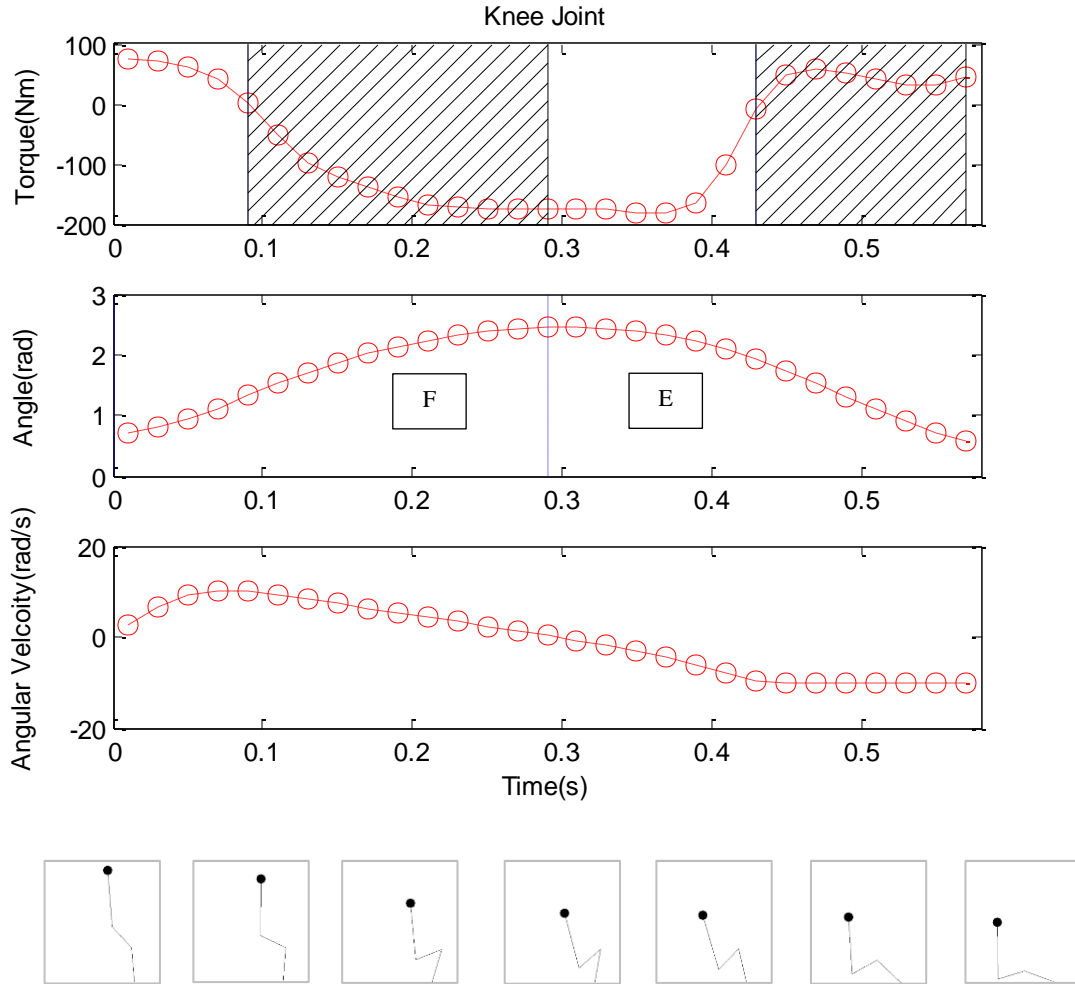


Figure 3.11 Optimized dynamic and kinematic characteristics of the knee joint

In these figures, the characteristics of the knee joint are plotted in the local reference frame of the joint. Knee torque is positive if applied in the flexion (F) direction and negative if applied in the extension (E) direction. Associated regions depicting an analogy with the application of eccentric and concentric torques at the knee joint are also shown, with hatched lines in the eccentric phases. Knee joint angle is increasing when moving in the flexion direction and decreasing when moving in the extension direction. Corresponding regions of extension and flexion are specified by E and F indices, respectively.

Examining the optimal profile of the knee torque, shown in Figure 3.11, determines that the maximum available flexion torque was applied at the knee joint at the initiation of the fall, and was then decreased with the continuation of the fall. The application of the flexion torque at the knee joint corresponded to the quick bending of the knee joint. The knee torque then changed direction rapidly and reached the maximum available extension torque to resist the downward motion of the body. Despite the fact that the torque was applied in a direction to resist the fall, the knee joint was performing a flexion motion. This is due to the fact that the available torque at the joint was not adequate to completely resist the downward motion of the body. The case where the direction of the applied torque and the rotation of the joint are in opposite direction represents an eccentric muscle contraction. The area corresponding to the eccentric contraction of the knee muscles, when extension torque is applied to the joint, is shown with hatched lines. With the continuation of the application of the extension torque at the knee joint, the motion of the joint changed direction. During this concentric muscle contraction, the thigh segment moved in an extension direction, which resulted in the horizontal displacement of the upper body. However, at the last stage of the fall, the knee torque changed direction, and the eccentric contraction of muscles at this joint prevented the risk of hyperextension of the knee.

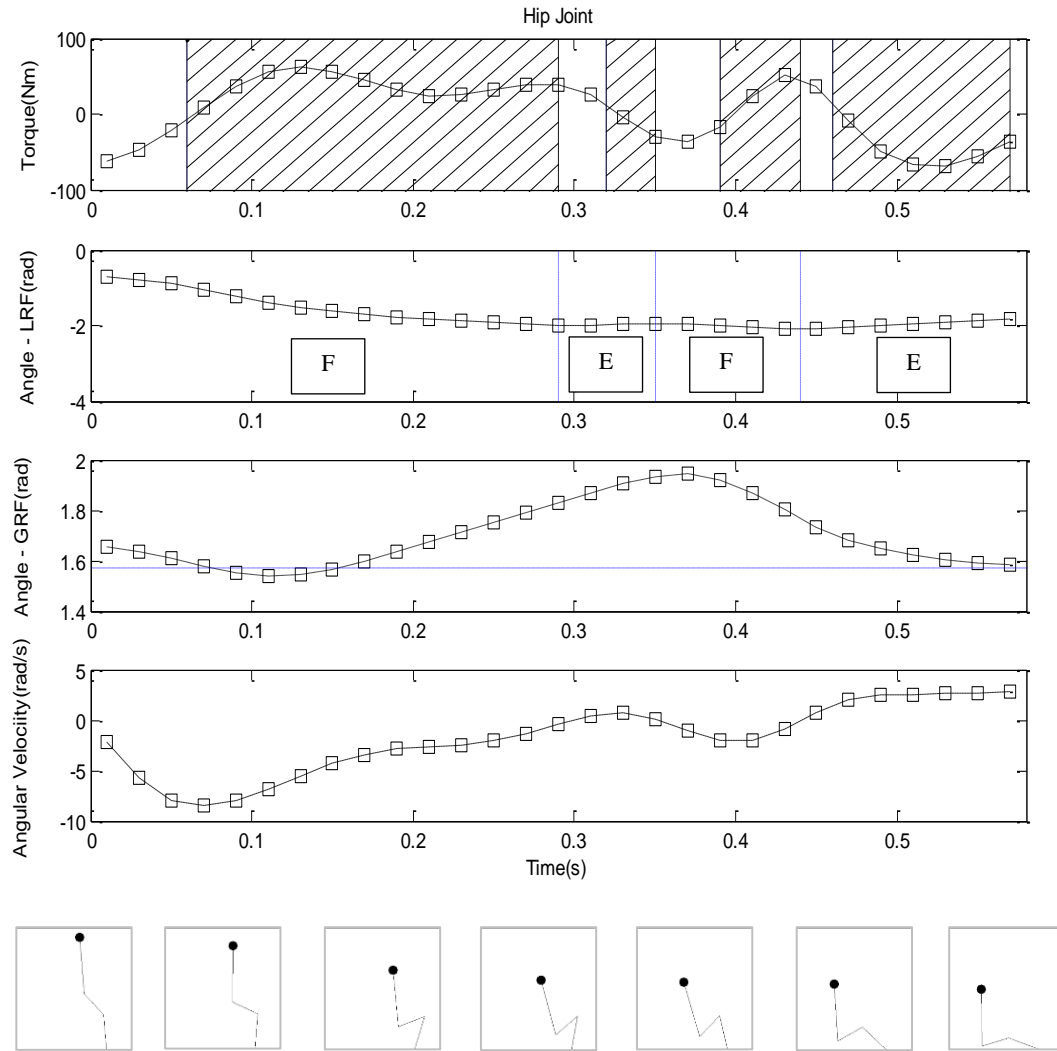


Figure 3.12 Optimized dynamics and kinematics characteristics of the hip joint

The hip angle is plotted both in the local reference frame of the joint (LRF), and the global reference frame (GRF).

Other joint characteristics are plotted in the local reference frame of the joint. Hip torque is positive if applied in the extension (E) direction and is negative if applied in the flexion (F) direction.

Hip joint angle is increasing when moving in the extension direction and decreasing when moving in the flexion direction. Associated regions depicting an analogy with the application of eccentric and concentric torques at the hip joint are also shown, with hatched lines in the eccentric phases.

The horizontal dashed line in the graph of the joint angle – GRF, shows the vertical axis in the global reference frame.

When examining the characteristics of the hip joint, it could be observed that at the onset of the fall, the maximum available flexion torque was applied at the hip joint that corresponded to the forward inclination of the trunk. As can be seen in the torque graph, the pattern of the application of the hip torque kept changing over the course of the fall. The application of this pattern of torque profile at the hip joint resulted in the near vertical orientation of the trunk throughout the fall, and more specifically at the moment of ground contact. The optimal hip trajectory confirmed head impact avoidance and resulted in the minimization of the deviation of the centre of mass from the base of support, which prevented the application of a high destabilizing torque.

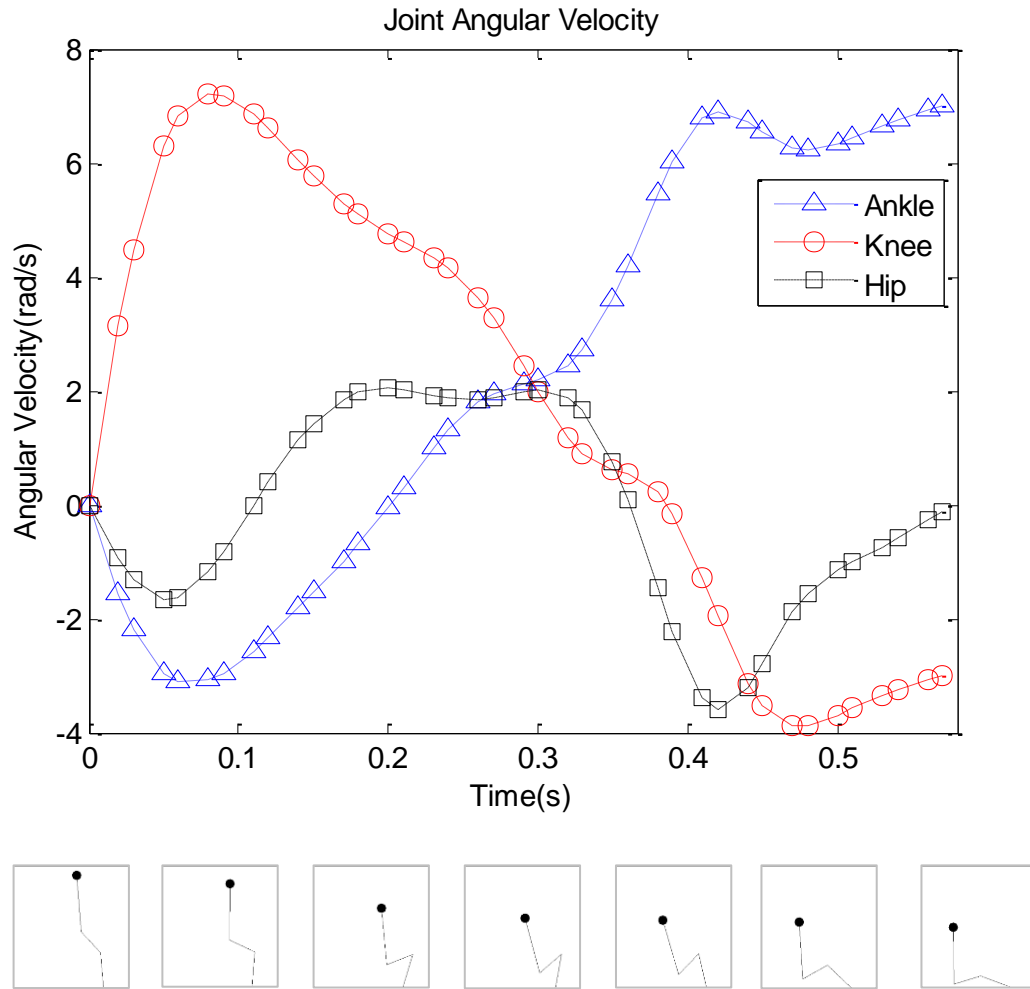


Figure 3.13 Optimized angular velocity of the joints plotted in the global reference frame

When examining the joint angular velocity profiles in the global reference frame (Figure 3.13), it could be observed that the angular velocity of the hip at the moment of ground contact is nearly zero. This confirms that the required objective regarding the minimization of the trunk angular velocity was successfully satisfied and head impact avoidance is achieved.

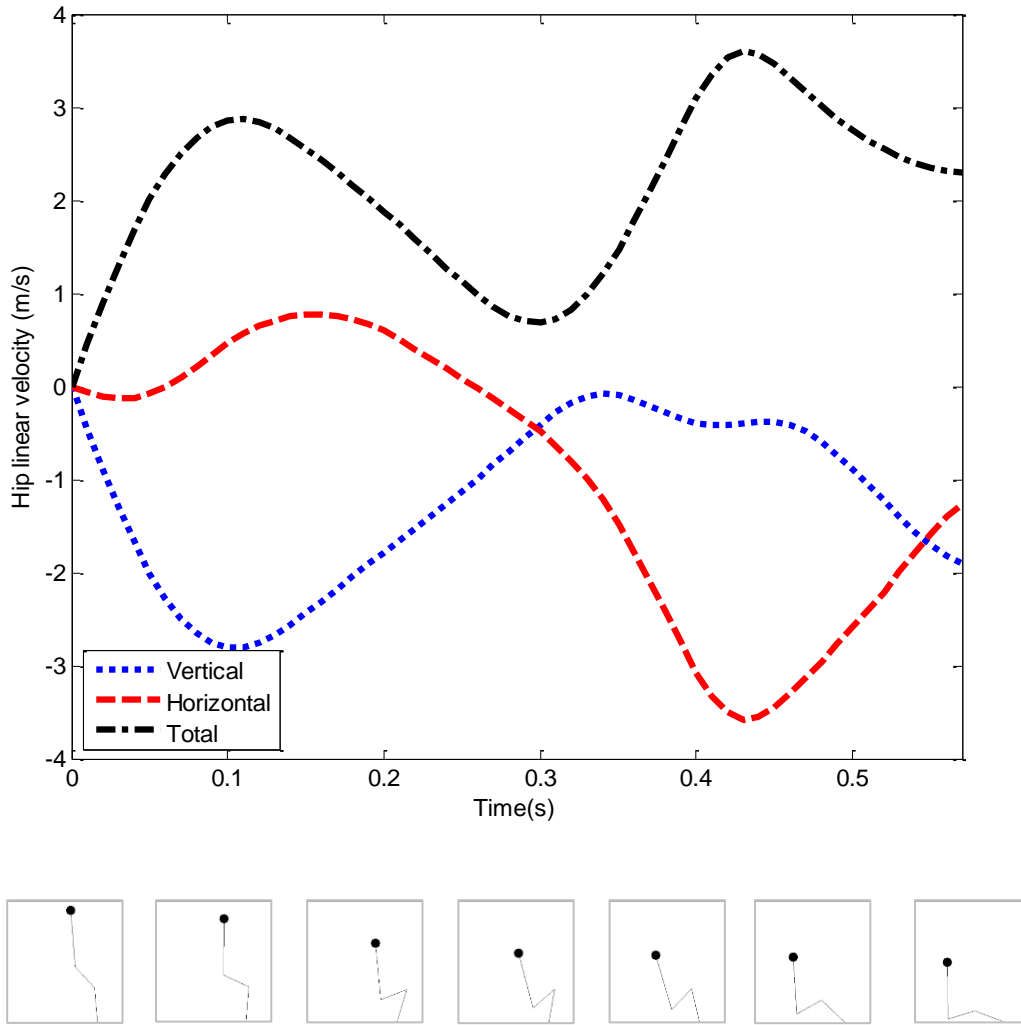


Figure 3.14 Optimized hip linear velocity

The profiles of the hip vertical, horizontal, and total linear velocity for the fall duration are plotted and examined separately.

Figure 3.14 shows the time history of the hip linear velocity throughout the fall, in which profiles of the hip vertical, horizontal, and total linear velocity are plotted separately. It is observed that the vertical component of the hip linear velocity started increasing with the initiation of fall and rapidly reached its maximum. This was due to the application of the flexion torque and the quick bending of the knee at the early stage of the fall. The vertical velocity of the

hip then started to decrease, which was concurrent with the application of the extension torque at the knee joint. The value of the hip vertical velocity decreased until the moment where the first link, representing the shin segment, moved posteriorly to the ankle joint. Afterward, the value of the hip vertical velocity kept increasing, up to the end of the fall duration. When the profile of the horizontal component of the hip linear velocity was examined, it was observed that this velocity reached its maximum value with the application of the extension torque at the knee joint at the last stage of the fall. The application of the extension torque led to the transformation of vertical kinetic energy to horizontal kinetic energy and consequently increased the horizontal linear velocity of the hip.

3.4 Discussion

The purpose of this study was to develop a safe fall strategy in the case of a human backward fall and to investigate the characteristics of the lower limb joints throughout the fall and at the moment of ground impact. After the establishment of the optimization technique for the one- and two-link models, the optimization methodology was developed for the three-link model and detailed investigations were performed to analyze the characteristics of this technique.

3.4.1 Optimization Validation

The results of the optimization methodology validation show that the initial guesses have little if any effects on the optimal solution. However, the results reveal that when performing an optimization under specific conditions, the fall duration should be optimized for that specific case. This means that the safe fall strategy should be optimized with respect to the fall duration as well as the previously defined objectives.

After the examination of previous studies on human falls, it was found that the optimal fall duration obtained in the current study is very similar to the cases of real-life falls among older

adults (593 ± 255 ms) [38], and it is lower but within one standard deviation of the laboratory falls performed by young adults (715 ± 160 ms) [23].

Activation of a safe fall strategy at different stages of loss of balance was studied by initializing the fall from different initial ankle angles. Examining the results of the optimization, in the cases where optimal fall strategy was applied at different stages of fall, reveal that the sooner the safe fall strategy is employed, the lower the hip linear velocity and the trunk angular velocity at impact would be. This finding is in agreement with previous findings that the effectiveness of the optimal safe fall strategy is higher if it is activated at an early stage of loss of balance [49].

3.4.2 Examining the Characteristics of an Optimized Fall Strategy

When examining the optimal fall strategy, specific characteristics were identified in the developed strategy. First, it was observed that the model underwent a quick squat motion, which led to the rapid reduction of the existing potential energy that would ultimately have been converted to kinetic energy at the moment of ground impact. Next, at the last stage of the fall, a quick knee extension was observed that led to the conversion of the vertical kinetic energy to horizontal kinetic energy. The calculated optimal trajectory of the knee joint throughout the fall was found to be similar to the results of a previous study on human falls [40]. The same falling technique was observed when optimal safe fall strategies were implemented in humanoid robot [55]. The kinematic and dynamic results observed at the hip joint are also in agreement with the results of previous work [22],[40].

To quantify the effectiveness of the safe fall strategy developed, the optimized hip linear velocity at impact for the three-link model was compared with the hip linear velocity at impact

for the three- and one-link models in the case of a free-fall⁴. It was observed that the hip linear velocity at impact, when the optimal fall strategy was employed in the three-link model, was reduced by 31% and 42%, compared to the cases of a free fall of the three- and one-link models, respectively⁵. These results reveal that the severity of fall could be minimized if the fall is modelled with the three-link model and in the case where an optimal control strategy is employed. These findings support the previously proposed concept of the activation of actuators at the joints of the exoskeleton in the case of a fall. However, this is in contrast with the currently used methods in which an exoskeleton falls in such a way that is represented with the one-link model of a free fall.

To validate the value of the impact velocity, the results of this work were compared to the findings of previous studies. The results of one study, in which real-life falls were examined among older adults, revealed that the average hip linear velocity was equal to 2.30 ± 0.63 m/s at the moment of ground contact. In this case, the average hip height at the initiation of the fall was reported to be 78.12 ± 14 cm. In the current study, where the hip height at the onset of fall was 73 cm, the average hip impact velocity was found to be 2.28 ± 0.00 m/s, which is very similar to the findings of the abovementioned study. In another study, participants were asked to perform a safe fall after they were released from an inclined position. The hip impact velocity was found to be 41% lower than the impact velocity of an equivalent mass of the human body, falling from the same height as the centre of mass of the participants' body at the onset of the fall [40]. When performing the same calculation for the case of the current study, this value was found to be

⁴ The case of a free-fall is when no torque is applied to the joints.

⁵ The one- and three-link models had the same potential energy at the onset of fall.

42%, which is very similar to the result of the previous study. This finding also verifies the effectiveness of the calculated optimal fall strategy.

Comparing the outcome of this study with the results of related studies on human falls reveals that the hip impact velocity obtained is within safe limits for healthy individuals and would not cause bone fracture in the case where the fall is performed over a protected ground surface [40],[48],[47].

3.4.3 Limitations

Several assumptions were made throughout the development of the optimal safe fall strategy that could have had a direct influence on the results of this work. First, not all real-life backward falls are symmetric, which means that body motion is not always restricted to the sagittal plane. Taking this factor into account would make the study of the dynamics of the fall, and consequently the development of a safe fall strategy, more complex. Another limitation of this study was the use of a simplified model of the human body in which the effect of friction, damping, and the passive effects of ligaments at the joints were neglected. It is worth noting that considering the effects of all these factors would directly influence the dynamics of the fall, and accordingly the optimal characteristics of the joints. Neglecting the effect of time in torque generation at the joints was another limitation of the optimization technique developed. However, this limitation will be addressed in Chapter 4 of this thesis, when developing the optimization technique for the case of a human-exoskeleton fall.

3.5 Summary

In summary, this chapter presented an optimization methodology that was developed to examine the biomechanics of an optimal human fall strategy. The main goals of this work were to develop a safe fall strategy to mitigate the severity of injury in the case of a backward fall by

avoiding head impact and minimizing the hip linear velocity at the moment of ground contact.

The results of this study confirmed that the severity of a fall could be significantly reduced if the optimal fall strategy is employed. The similarities in results between this study and previous studies on human falls have verified the validity of the safe fall strategy I developed.

The next chapter presents the details regarding the development, implementation, and corresponding outcomes of using this optimization technique to generate a control strategy for the case of a human-exoskeleton backward fall to mitigate the risk and severity of an injury.

Chapter 4: Human-Exoskeleton Falls Modelling and Optimization

4.1 Introduction

In the previous chapter, an optimization methodology was developed to study kinematics and dynamics characteristics of the lower limb joints during a “safe” human backward fall. This optimal strategy was designed to minimize the risk and severity of injury to the human body. The validity of the optimization methodology was confirmed by comparing the optimal solution obtained to the results of previous studies on human falls. Due to the similarities between the model of a human and a human-exoskeleton fall, the same optimization strategy could be used to develop a safe-fall control strategy in the case of a human-exoskeleton backward fall. First of all, except for the mass distribution, the governing dynamics of a fall is similar for both the human and human-exoskeleton when modelled with a three-link inverted pendulum. Secondly, the available torque at the actuated joints of the exoskeleton could be regarded as the muscle-generated torques at the human body joints, albeit with different limits. The optimization developed for the case of a human fall was therefore modified to take into account the distinctions between the human and human-exoskeleton models of a fall. Details regarding the establishment of the safe-fall control strategy for a model of a human-exoskeleton fall are described in the following sections of this chapter.

4.1.1 Methods

4.1.2 Dynamic Modelling of a Backward Fall with an Exoskeleton

The same procedure as discussed in the previous chapter was followed to develop the human-exoskeleton model in the simulation environment. The characteristics of a hypothetical exoskeleton including the mass, centre of mass, mass moment of inertia, length of each segment, and the actuators’ specifications were added to the already-existing, half-plane, three-link model

of a human fall. The total mass of the exoskeleton was assumed to be equal to 12 kg (Refer to Appendix E for more details regarding the characteristics of the exoskeleton model).

It was assumed that the lower limb joints of the human body were following the corresponding joint motions of the exoskeleton model. In other words, the kinematic and dynamic characteristics of the knee and hip joints of the human-exoskeleton model were governed by the characteristics of the actuators at the joints of the exoskeleton and the user had no control over changing characteristics. In the model, the hip and knee joints of the exoskeleton were assumed to be actuated, whereas the ankle joint was considered to be passive and locked throughout the motion of the exoskeleton. These assumptions are in agreement with the design of most of the currently used exoskeletons.

4.1.3 Optimizing a Human-Exoskeleton Backward Fall

4.1.3.1 Design Variables

The design variables, which have the similar format as previously discussed in Chapter 3 of this thesis, are defined in (4.1). Θ_{Ankle} is the angle between the shank segment of the device and the horizontal axis⁶, Θ_{Knee} is the angle between the shank and the thigh segment of the exoskeleton, and Θ_{Hip} is the joint angle between the thigh segment and the trunk segment of the exoskeleton. It is worth recalling that the lower limb joint angles of the human body were assumed to have equal values to the corresponding joint angles of the exoskeleton model. $\dot{\Theta}_{Ankle}$, $\dot{\Theta}_{Knee}$, and $\dot{\Theta}_{Hip}$ are the angular velocities of the ankle, knee, and hip joints of the exoskeleton,

⁶ The ankle joint of exoskeletons are mostly passive and are locked or have a very high stiffness. In the current model of a human-exoskeleton fall, again with no effect on the results, the angle between the shank segment of the exoskeleton and the horizontal axis is labelled as the ankle angle.

respectively. T_{Knee} and T_{Hip} are the actuator torques applied at the knee and hip joints, respectively.

$$\left[\Theta_{Ankle}, \Theta_{Knee}, \Theta_{Hip}, \dot{\Theta}_{Ankle}, \dot{\Theta}_{Knee}, \dot{\Theta}_{Hip}, T_{Knee}, T_{Hip} \right] \quad (4.1)$$

4.1.3.2 Constraints

In the model of a human fall, the biomechanical characteristics of the human body determined the upper and lower limits of the design variables. In the human-exoskeleton model, both the biomechanical characteristics of the human body and the functional characteristics of the actuators at the active joints of the exoskeleton determined the bounds on the design variables.

As discussed before, the joint angles from which the fall is initiated and the initial joint angular velocities are other types of constraints that had to be satisfied when developing the safe fall strategy. In the model of a human-exoskeleton, it was assumed that the fall is initiated from an initial position similar to the case of standing still (i.e., with the trunk, thighs, and shank relatively aligned) yet with a little backwards leaning deviation from a balanced posture. The initial joint angles from which the fall is in all the optimization trials were equal to 10° , 1° , and -1° at the ankle, knee, and hip joints, respectively. This is markedly different from the previous human-only falls described in Chapter 3, which were initiated from a partial squatting position with knee and hip angles equal to 40° and -40° , respectively.

As previously discussed, the same nonlinear constraints regarding the dynamics of the fall were used to define the characteristics of the fall throughout the fall. In the model of a human fall, only the vertical component of the ground reaction force was limited to gain a nonnegative value for the fall duration. However, in the model of a human-exoskeleton fall, it was assumed

that the ground surface condition (dry vs. wet floor) would influence the characteristics of the fall. To address this effect, a constraint regarding the limits on the coefficient of friction of the ground surface was added to the existing constraints. This parameter was specifically included in the optimization to create a more realistic model of a fall.

4.1.3.3 Objective Function

The objective function for the model of a human-exoskeleton fall was defined similar to the case of a human fall, which was to minimize the angular velocity of the trunk and the hip linear velocity at impact.

4.1.3.4 Optimization Technique

The optimization technique for the human-exoskeleton model of a fall remained unchanged and was similar to the case of a human fall (see Section 3.2.2.4).

4.1.3.5 Initial Guess

Similar to the model of a human fall, a pair of constant torques was applied at the hip and knee joints of the human-exoskeleton model. Then the resultant joints angle and angular velocities for the fall duration, computed by the forward dynamics analysis, were used as an initial guess for the optimization.

4.1.4 Development and Analysis of Optimized Human-Exoskeleton Falls

The same assumptions as the previous three-link model of a human fall were made for the human-exoskeleton model. First, the effects of both the fall duration and the choice of initial guess on the optimal value of the objective function were examined. Additionally, the effects of falling on different floor conditions on the optimal value of the objective function were examined. Lastly, the effects of actuator characteristics on the value of the objective function and

falling conditions were studied. Actuators that are used at the hip and knee joints of the exoskeleton impose specific operational constraints to the model of a human-exoskeleton fall.

4.2 Results

4.2.1 Effects of Fall Duration and Initial Guess on the Value of the Objective Function

In the previous chapter, for the model of a human fall, it was shown that the optimal solution is directly influenced by the predetermined value of the fall duration; however, it is minimally affected by the choice of the initial guess. In this section, optimizations were performed to determine both the effects of the fall duration and the initial guess on the optimal solution of a human-exoskeleton fall. The value of the objective function was examined for two different initial guesses and for fall durations ranging between 0.67 sec and 0.81 sec. The limits of available torque at the hip and knee joints were set equal to $[-50, 50]$ Nm. It was assumed that the actuators could provide equal maximum torques in both directions. The results of this study are presented in Figure 4.1.

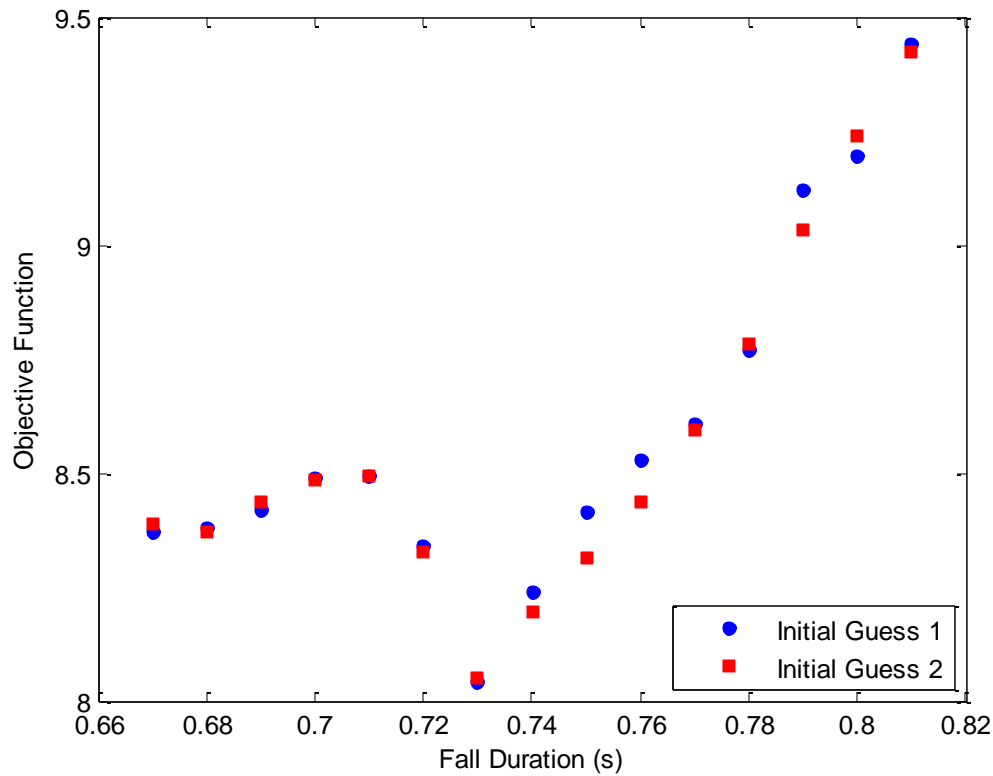


Figure 4.1 Value of the objective function for different fall durations and two initial guesses

The value of the objective function for two different initial guesses and for a range of different fall durations was examined in this study. Initial guess 1 corresponds to the characteristics of a fall where -1 Nm torque was applied at the hip and knee joints of the exoskeleton. Initial guess 2 corresponds to the characteristics of a fall where no torque was applied at the hip and knee joints of the exoskeleton. No feasible solution existed when the fall duration was shorter than 0.67 sec. For optimizations with longer than 0.81 sec fall duration, the value of the objective function continued to increase with an increase in fall duration.

In Figure 4.1, it could be observed that the value of the objective function, for both initial guesses, reached its lowest value when the fall duration was equal to 0.73 sec. The results of this study confirmed that there is a very low difference between the values of the objective function when different initial guesses are provided to the optimization.

4.2.2 Effects of Coefficient of Friction Constraint on the Value of the Objective Function

The ground surface condition has an influence on the ground reaction forces throughout the fall and consequently the optimal falling strategy. A range of different coefficients of friction was used to quantify the effects of different ground surface conditions. It was assumed that the exoskeleton's foot or the user's shoe has a rubber sole. It was shown before that in the case of walking on a wet or dry asphalt, the coefficient of friction would vary from 0.25 to 0.75 [68]. In this study, the effects of coefficient of friction on the value of the objective function were examined; the results of this study are shown in Figure 4.2. The limits of available torque at the hip and knee joints were both set to $[-50, 50]$ Nm, and the fall duration was set equal to 0.73 sec. The initial guess provided to the optimization was the joint characteristics of a fall in which a constant -1 Nm torque was applied at the hip and the knee joints.

Schematic diagrams of body position at specific instants of falling are shown in Fig. 4.3 to compare the optimal falling strategy in the case of a fall on a more slippery floor (coefficient of friction = 0.25) with the case of a fall on a less slippery floor (coefficient of friction = 0.75).

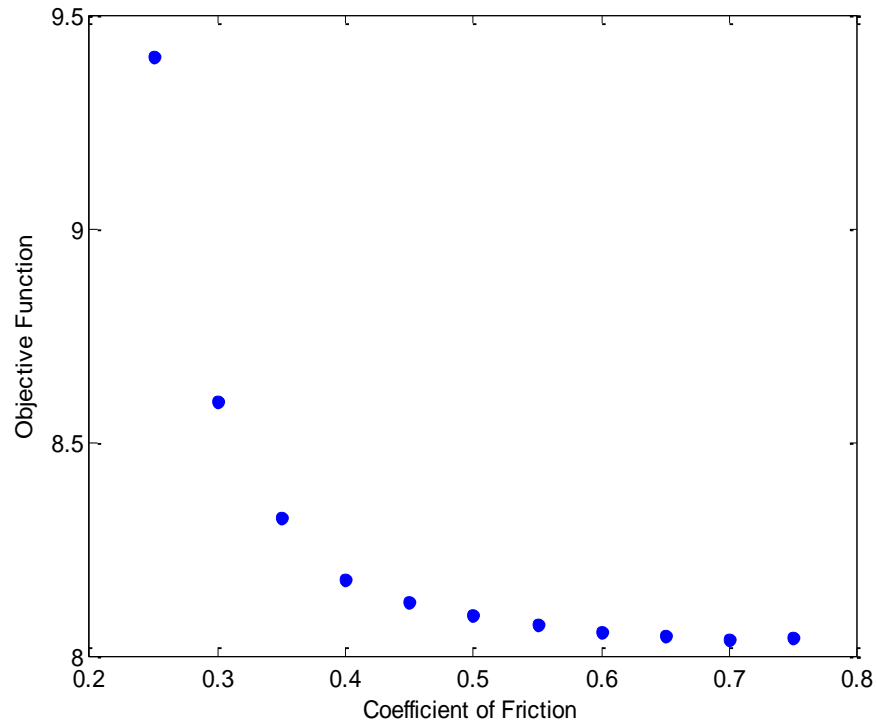


Figure 4.2 Value of the objective function for different ground surface conditions

The value of the coefficient of friction was varied from 0.25 to 0.75 to represent different ground surface conditions.

Time (s)	0	0.18	0.35	0.53	0.59	0.73
Optimal Solution CoF = 0.25						
Optimal Solution CoF = 0.75						

Figure 4.3 Body configuration at specific instants of optimal falls with different coefficients of friction (CoF)

Optimal fall strategies for different ground surface conditions were examined in this study. Constraints regarding different coefficients of friction were used to represent falling on different ground surface conditions.

The results of this study reveal that the falling strategy is slightly affected by the condition of the floor (Figure 4.3). It was also found that the value of the objective function is higher in the cases where the coefficient of friction is lower. These results suggest that falling on a more slippery floor would result in a more severe injury even if the optimal fall strategy is being employed.

4.2.3 Effects of Acceleration/Deceleration Time Constraint on the Value of the Objective Function

Including a constraint regarding the acceleration/deceleration specifications of the actuator would result in the development of a more realistic optimal safe-fall strategy in the case of falling with an exoskeleton. The specifications of a specific actuator were used to calculate the acceleration and deceleration time, as described in Appendix F [69]. For the case of the current model of a human-exoskeleton fall, and considering the specific characteristics of the actuator used in our validation experiments (see Chapter 5), the acceleration time was found to be the limiting constraint. The value of the actual acceleration limit was equal to 0.26 rad/s^2 , and it was defined as a constraint for the actuators at the knee and hip joints. The value of the objective function for different fall durations when this constraint was applied to the optimization were examined and compared to the case where no such constraint was considered in the optimization. As before, the joints characteristics of a fall when -1 Nm torque was applied to the hip and knee joints of the human-exoskeleton model were used as an initial guess to the optimization and the limits of torque at the hip and knee joints were set to [-50, 50] Nm. The coefficient of friction was set equal to 0.60. The results of this study are shown in Figure 4.4.

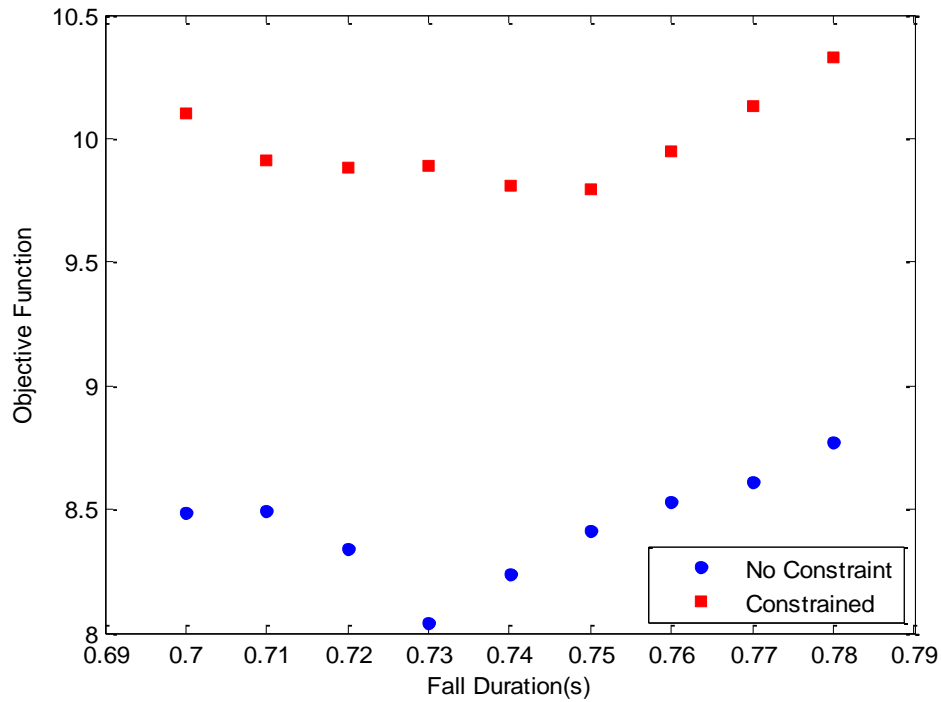


Figure 4.4 Value of the objective function for different fall durations with different actuator constraints

The optimal value of the objective function was examined for different fall durations in the case where an acceleration time constraint was applied to the optimization. The results were compared to the case where no constraint was placed on this value.

The outcome of this study reveals that having a constraint regarding the acceleration limit of the actuators, or in other words, the responsiveness of the actuators, will influence the results of the optimization. It was found that the value of the objective function is higher in the case where actuator performance limits are included in the optimization. It was also found that the value of the optimal fall duration is different in the case where these limits were considered. In the case of having a constraint on the responsiveness of the actuators, the optimal fall duration was found to be slightly longer (0.75 sec) than the case where no constraint was imposed on the responsiveness of the actuators (0.73 sec).

4.2.4 Joint Characteristics of an Optimal Human-Exoskeleton Fall

This section examines the joint characteristics of the human-exoskeleton model, when an optimal safe-fall strategy is employed. The results correspond to the case of human-exoskeleton fall, with fall duration of 0.75 sec while an acceleration limit was included. The limits of torque at the hip and knee joints were equal to $[-50, 50]$ Nm, and the coefficient of friction was set equal to 0.60. The kinematic and dynamic characteristics of the ankle, knee, and hip joints are shown in Figure 4.5, Figure 4.6, and Figure 4.7. The profiles of the joint angular velocities, as well as the profile of the linear velocity of the hip throughout the fall, were examined and the corresponding results are shown in Figure 4.8 and Figure 4.9, respectively. To better illustrate the characteristics of the optimal fall strategy, diagrams of human-exoskeleton model positions at specific instants of fall are depicted in each figure. The same terminology as what was used to describe the characteristics of the human fall is also used for the case of a human-exoskeleton model of a fall.

Figure 4.5 shows that the fall was initiated from an ankle angle at which the shin segment was oriented posteriorly to the ankle joint. After the initiation of fall, the shin segment moved with respect to the ankle joint. The ankle rotation changed direction at 0.3 sec, and a plantarflexion motion was performed that continued up to the end of the fall duration.

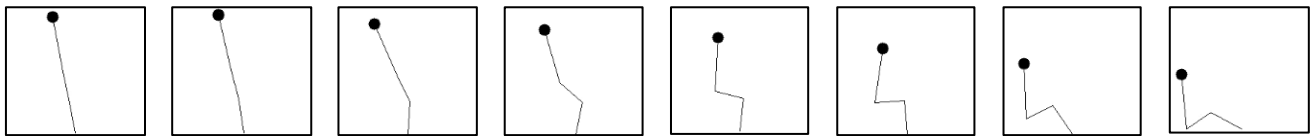
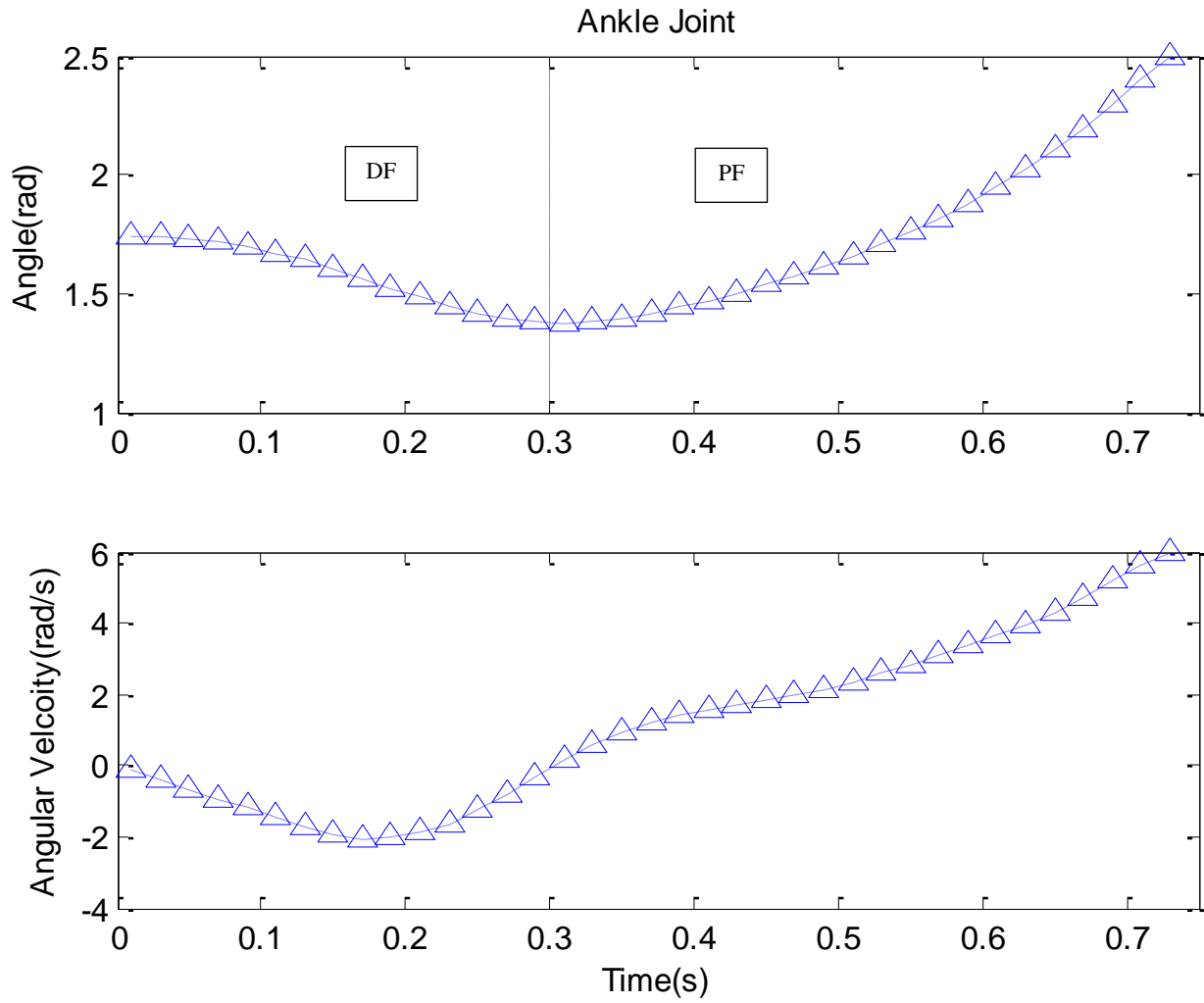


Figure 4.5 Optimized kinematics and dynamics characteristics of ankle joint (human-exoskeleton fall)

The profiles of the optimal ankle angle and angular velocity throughout the fall are shown. The ankle joint is moving in the plantarflexion (PF) direction if increasing and is moving in the dorsiflexion (DF) direction if decreasing. The regions regarding the plantarflexion and dorsiflexion motion of the ankle are separated by the dashed vertical line on the joint angle graph and corresponding areas to these motions are indicated by PF and DF labels, respectively.

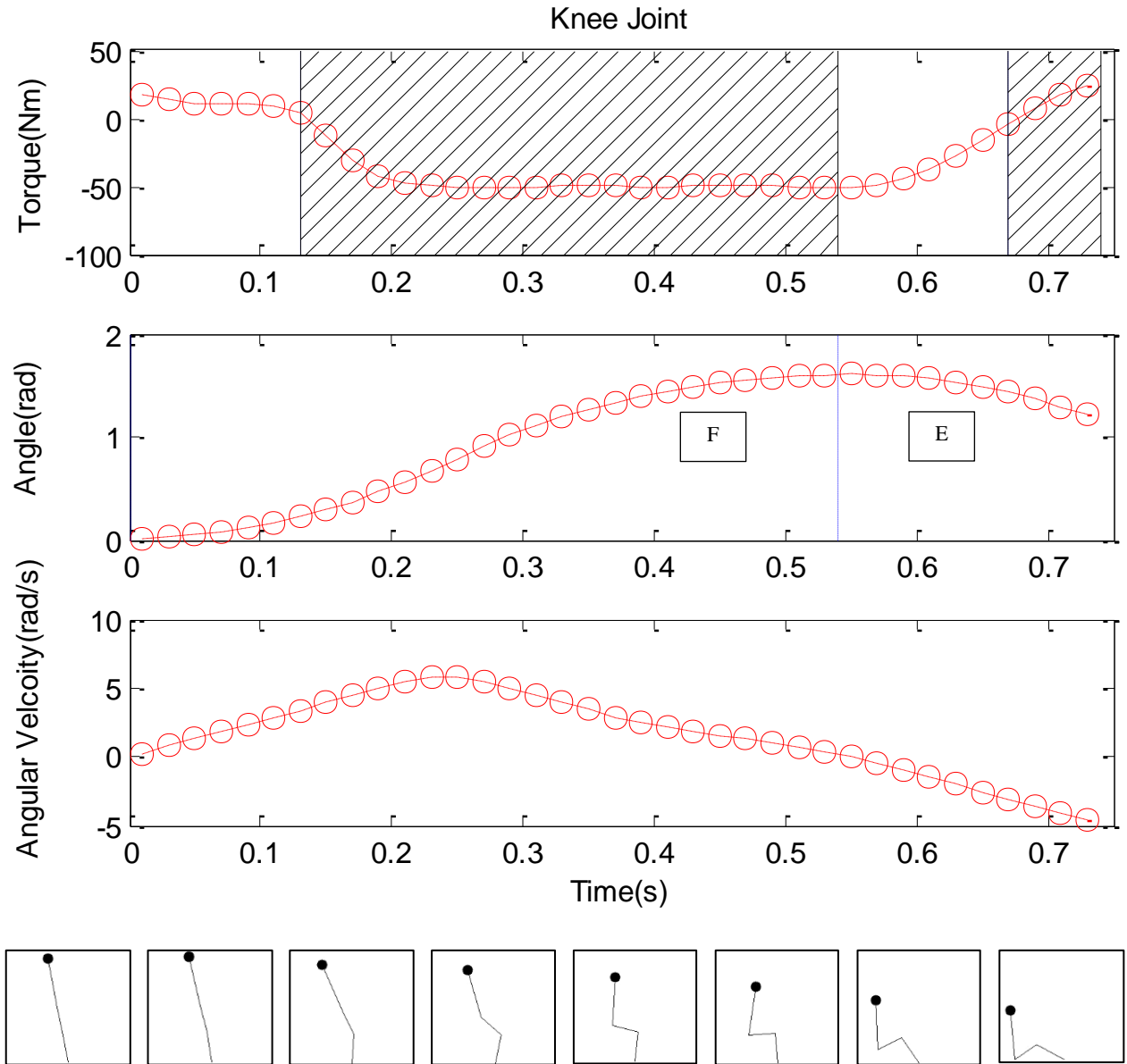


Figure 4.6 Optimized dynamic and kinematic characteristics of the knee joint (human-exoskeleton fall)

In these figures, the characteristics of the knee joint are plotted in the local reference frame of the joint. Knee torque is positive if applied in the flexion (F) direction and is negative if applied in the extension (E) direction. Associated regions depicting an analogy with the application of eccentric and concentric torques at the knee joint are also shown, with hatched lines in the eccentric phases. Knee joint angle is increasing when moving in the flexion direction and decreasing when moving in the extension direction. Corresponding regions of extension and flexion are specified by E and F indices, respectively.

When examining the results in Figure 4.6, it is observed that flexion torque was applied at the knee joint at the very beginning of the fall. The torque applied at the knee joint then changed direction and acted in extension, which lasted for almost the rest of the fall duration. Although extension torque was applied at the joint, the direction of knee motion was in the flexion direction. When compared to the characteristics of a human fall, this could be regarded as the application of eccentric torque at the knee joint during that period. This is the case where the applied torque at the joint and the joint's motion are in opposite directions. The area corresponding to the application of eccentric torque is shown in hatched lines. Throughout the last stage of the fall, the motion of the knee joint changed direction and was in extension. At the very last stage of the fall, the torque applied at the knee joint changed to flexion. Again this period could be regarded as the application of eccentric torque when compared to the case of a human fall. The application of eccentric torque at the joints corresponds to the case of applying braking torques at the joints such to resist the motion in the current direction of the joint's motion.

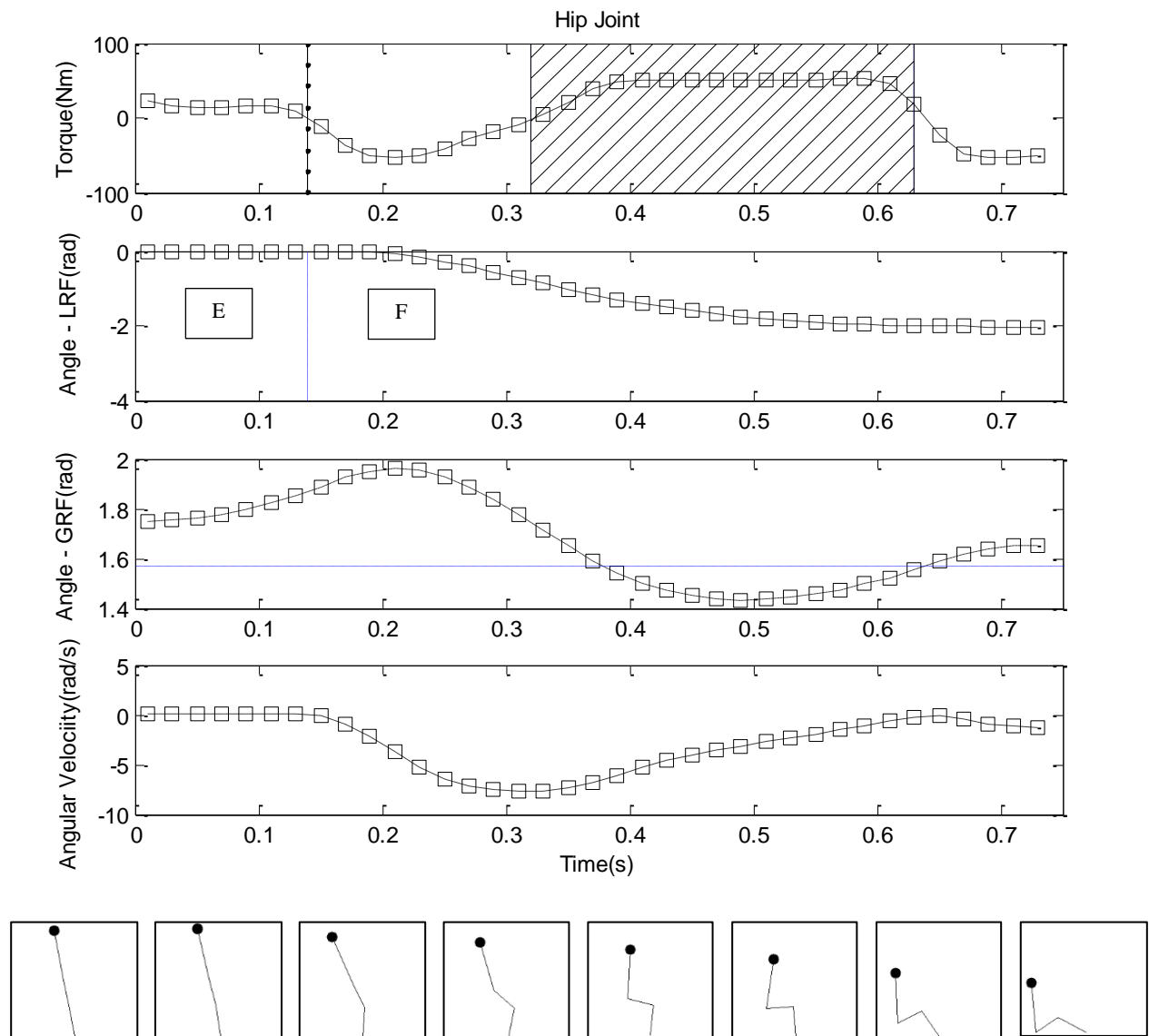


Figure 4.7 Optimized dynamic and kinematic characteristics of the hip joint (human-exoskeleton fall)

The hip angle is plotted both in the local reference frame of the joint (LRF) and the global reference frame (GRF). Other joint characteristics are plotted in the local reference frame of the joint. Hip torque is positive if applied in the extension (E) direction and is negative if applied in the flexion (F) direction. Hip joint angle is increasing when moving in the extension direction and decreasing when moving in the flexion direction. Associated regions depicting an analogy with the application of eccentric and concentric torques at the hip joint are also shown, with hatched lines in the eccentric phases. The horizontal dashed line in the graph of the joint angle – GRF, shows the vertical axis in the global reference frame.

When examining the characteristics of the hip joint (Figure 4.7), it could be observed that at the onset of the fall, extension torque was applied at the hip joint that corresponded to the extension of the trunk. Then exactly at the same moment (0.14 sec), the direction of application of torque and rotation of the hip joint both changed direction simultaneously. As flexion torque was applied to the hip joint, the trunk moved in the flexion direction. The joint's motion in the flexion direction lasted until the end of the fall. However, the hip torque changed direction with the continuation of the fall and was applied in the extension direction. At the very last stage of the fall, the hip torque changed direction again and was applied in the flexion direction.

As can be seen in the torque graph, the pattern of the application of the hip torque kept changing over the course of the fall. The application of this pattern of torque profile at the hip joint resulted in the near vertical orientation of the trunk throughout the last half of the fall duration, and specifically at the moment of ground contact. The resulting optimal hip trajectory confirmed the success of the head impact avoidance.

When examining the profile of joint angular velocities in the global reference frame (Figure 4.8), it could be observed that the angular velocity of the hip at the moment of ground contact is nearly zero.

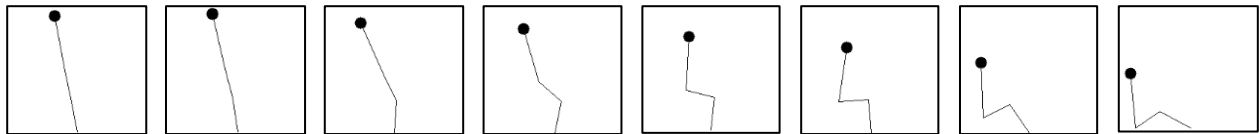
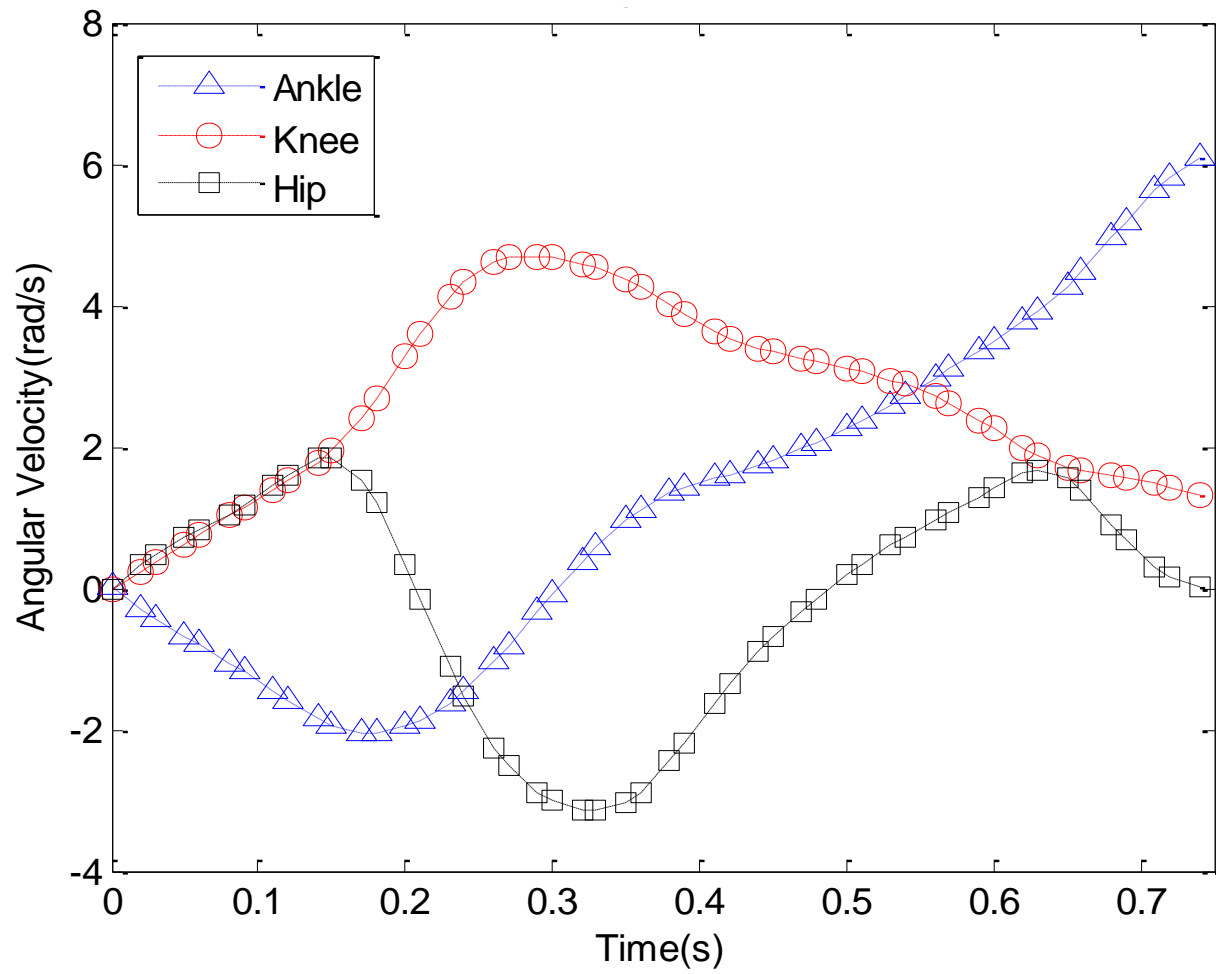


Figure 4.8 Optimized angular velocity of the joints plotted in the global reference frame (human-exoskeleton fall)

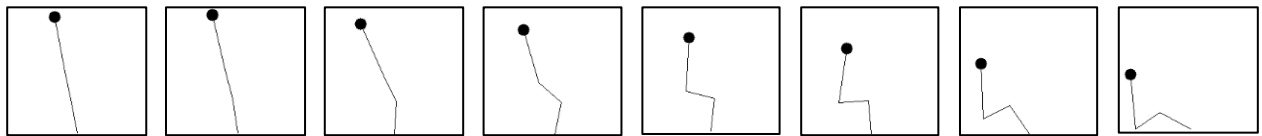
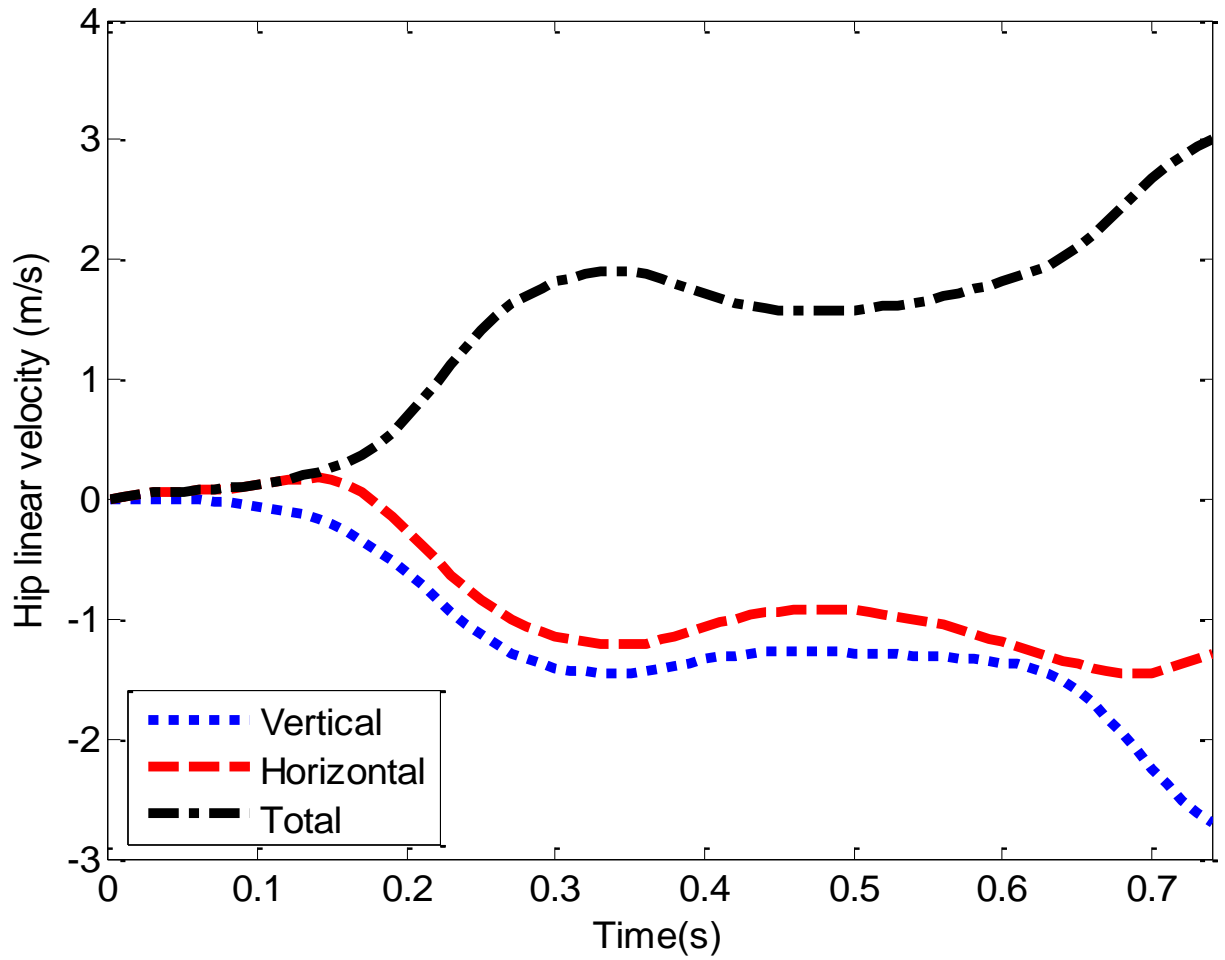


Figure 4.9 Optimized hip linear velocity (human-exoskeleton fall)

The profiles of the hip vertical, horizontal, and total linear velocity for the fall duration are plotted and examined separately.

Figure 4.9 shows the time history of the hip linear velocity, and profiles of the hip vertical, horizontal, and total linear velocity plotted separately, for the duration of the fall. It is observed that the total hip linear velocity started increasing with the initiation of fall, reached a maximum

and remained almost unchanged for most of the fall duration. However, at the last stage of the fall, this value started to increase and reached its maximum at the moment of ground contact. The value of the total hip impact velocity was equal to 3.00 m/s in this case.

4.3 Discussion

The purpose of this study was to develop a safe fall control strategy in the case of a human-exoskeleton backward fall. To achieve this goal, the previously developed optimization methodology (described in Chapter 3), was expanded to include the characteristics of an exoskeleton.

First, the effect of fall duration and initial guess on the value of the objective function were examined. The results of this study reveal that the choice of the initial guess has little effect on the optimal solution. However, the results showed that the value of the objective function is directly influenced by the fall duration. In other words, for specific optimization conditions, there exists an optimal fall duration with which the value of the objective function is minimum. These results are similar to the findings of the previous study on the optimization of the human backward fall (see Chapter 3).

As shown previously in this thesis, the optimal fall duration is directly affected by the fall conditions. As an example, the initial condition from which the fall is started would have an impact on the actual fall duration that is required to follow an optimal fall strategy. In the current case of a human-exoskeleton fall strategy, it was also found that the actuator's performance specifications would influence the optimal fall duration.

As mentioned previously, it was assumed that the feet remain in contact with the ground throughout the fall. To guarantee the validity of this assumption, two constraints were included in the development of the optimization. First, the value of the vertical ground reaction force was

constrained to obtain non-negative values, i.e., no loss of contact with the ground. Secondly, the static coefficient of friction was defined so as to limit the ratio of the vertical and horizontal ground reaction forces. The results of this study reveal that the floor surface slipperiness does impact the optimal safe fall strategy. In other words, an optimal fall strategy while falling on a more slippery floor is different from an optimal fall strategy when falling on a less slippery floor. Also, the results showed that the severity of fall is higher in the case of falling on a more slippery floor. This finding is in agreement with the result of previous studies on human falls. It was shown previously that the risk of fall-related fractures was higher in colder seasons, which is associated with more slippery (e.g., wet, icy) conditions [70]. It is worth noting that for these optimizations, the fall duration may have an effect on the value of the objective function, but according to previous results it is unlikely to have an influence on the optimal fall strategy.

Electrical actuators have particular specifications that should be taken into account when an actuator is selected for a specific task. Since the entire fall duration is less than one second, the responsiveness of the actuators being used at the joints of the exoskeleton in the case of a fall would become a critical characteristic to consider. In this work, the responsiveness of an actuator was associated with the acceleration/deceleration limit of the actuator. Ideally, in the case of the current work, this value should be as high as possible. However, clearly, due to the mechanical limitations, the acceleration/deceleration time of an actuator is a nonzero parameter. This constraint was included in the optimization methodology to obtain a more realistic optimal safe fall strategy. The results of this examination reveal that the severity of fall would be higher in the case where the acceleration/deceleration time constraint was considered in the optimization. However, the risk or severity of fall-related injury could be reduced with the use of highly responsive actuators.

When examining the optimal human-exoskeleton fall strategy, characteristics similar to those of the optimal human fall strategy were observed. The pattern of ankle movement was similar in both models. When examining the optimal knee torque profile in the case of a human and human-exoskeleton optimal fall strategy, the same regions corresponding to the application of eccentric and concentric torques were observed. Similar to the optimal model of a human fall, the human-exoskeleton model underwent a squat motion but with a time delay. In the optimal model of a human fall, the knee angle reached its minimum (corresponding to flexion motion) at nearly 0.3 sec after the initiation of the fall. However, due to the existing distinctions between the two models, some dissimilarity was detected as well. This time was equal to 0.54 sec in the case of an optimal human-exoskeleton fall. This is partly due to the difference in the initial condition from which the fall was started in the two models. Moreover, the observed differences were probably also due to the actuator characteristics and performance limitations. Similar to the optimal human fall strategy, the knee joint of the human-exoskeleton model was extended at the last stage of the fall. However, due to the angular velocity constraints imposed, the angular velocities of the joints were found to be lower in the model of a human-exoskeleton fall, compared to the model of a human fall. The pattern of the optimal torque applied at the hip joints of the human and human-exoskeleton models had more dissimilarity. Less abrupt changes were observed in the profile of the hip torque in the model of a human-exoskeleton fall, compared to the optimal human fall strategy.

To quantify the effectiveness of the safe fall strategy, the optimized hip linear velocity at impact for the three-link model of a human-exoskeleton fall was compared with the hip linear

velocity at impact for the one-link model of a human-exoskeleton free fall⁷ (the current commercial exoskeleton fall “strategy”). It was observed that the hip linear velocity at impact, when the optimal fall strategy was employed in the three-link model, was reduced by 58% compared to the case of a free fall of the one-link model⁸. The near-zero angular velocity of trunk and the upright inclination of the trunk at impact confirm that the required objective regarding the head impact avoidance is achieved. These results reveal that the severity of fall could be minimized if the optimal control strategy is employed and support the previously proposed concept of the activation of actuators at the joints of the exoskeleton in the case of a fall.

To reiterate, the value obtained for the hip impact velocity is within the safe range of hip impact velocity to avoid bone fracture for healthy individuals. However, users of exoskeletons are usually individuals with some form of lower limb disability that might have low bone density, low muscle tone, and skin problems. All these conditions increase the risk and severity of injury for this user group. To address this issue, additional protection strategies or mechanisms should be utilized, such as airbags, shock absorbers, and paddings, in conjunction with the safe fall strategy developed in this thesis.

4.3.1 Limitations

As discussed before, several assumptions were made throughout the development of the optimal safe fall strategy that might have influenced the results of this work. First, not all backward falls are symmetric, which means that the body motion is not restricted to the sagittal plane. However, in this thesis, the development of the optimal fall strategy was done for a more

⁷ The case of a free fall is when no torque is applied to the joints and joints are locked relatively straight.

⁸ Both models had the same potential energy at the onset of fall.

simplified case of a human-exoskeleton fall. Now that the optimal fall strategy has revealed its efficacy for the current model of a human-exoskeleton backward fall, it could be further developed for more complex cases of falls in future. Although constraints regarding one of the performance characteristics of the actuators were included in the model of a human-exoskeleton fall, other characteristics such as the effect of friction and damping were neglected, as were real-time software parameters such as control loop rate and delays.

4.4 Summary

In summary, this chapter presented an optimization methodology that was developed to reduce the risk and severity of injury in the case of a backward fall while using a lower-limb exoskeleton. The main goals of this work were to avoid head impact and minimize the hip linear velocity at the moment of ground contact. The results of this study confirmed that the severity of fall could be significantly reduced if the optimal fall strategy is employed. The similarities in results between this study and the previously developed optimal safe fall strategy for a human model support the validity of the developed safe fall strategy.

Chapter 5: Numerical and Experimental Validations

The optimization methodology, detailed in Chapter 3 and 4, resulted in the development of a safe fall strategy that significantly reduces the severity of an unintentional backwards fall. Low trunk angular velocity and hip linear velocity at ground impact were shown to be indicators of a safe landing technique. Results of the optimization, including the joints' characteristics during the fall and at impact, were in line with results of previous studies on human and humanoid robot falls. Moreover, the optimization methodology was validated by examining the effects of different parameters (i.e., the choice of the initial guess and initial conditions of the fall) on the optimal results. However, in order to be confident in using these results for design recommendations and/or implementation of safe falling behaviours, more rigorous numerical and physical validations are needed. The results of numerical and experimental validations of the optimization methodology are presented in this chapter.

5.1 Numerical Validation Methods

To better understand the numerical validation methods, first the development of the optimization technique is reviewed in this section. Next, the numerical validation methods are described and the corresponding results are presented.

As mentioned previously in Chapter 3, the governing dynamic of the three-link model of a fall is the solution of a system of three nonlinear second-order differential equations. First, substitutions were made to transform the second-order equations into first-order equations. A forward difference discretization technique was then used to formulate the first-order differential equations. To ensure that the governing dynamics of motion are valid during the entire fall, the derived equations of motion were defined as non-linear constraints that had to be satisfied at each moment of the fall. Subsequent to performing the optimization, optimal joint

characteristics, including the joint angles, angular velocities, and torque profiles, at the actuated joints, were obtained.

To investigate the validity of the results, a forward dynamic analysis was performed to examine whether or not the defined constraints regarding the governing dynamics of the fall were satisfied for the entire fall duration. To test this, the corresponding optimal torque profiles were applied to the hip and knee joints. First, by using the same forward difference discretization technique that was used in the development of the optimization, the joint angles and angular velocities were calculated for all the joints. The results of this investigation reveal that the joint trajectories obtained from the forward dynamic analysis matched the corresponding joint trajectories obtained from the optimization (Figure 5.1). This confirms that the results obtained from the optimization do comply with the governing dynamics of the fall.

In order to verify the results obtained by using a numerical technique, one can solve the same problem with a different numerical method. If the problem is properly formulated, similar results should be obtained when using different numerical methods [71]. In this work, a forward dynamic analysis was next performed by using the MATLAB ode45 solver. Similar to the previous analysis, optimal torque profiles were applied to the hip and knee joints and all the joint angles and angular velocities were calculated. The results of this analysis reveal that the joint trajectories obtained when using the ode45 solver and the optimal joint trajectories obtained from the optimization have similar characteristics (Figure 5.2).

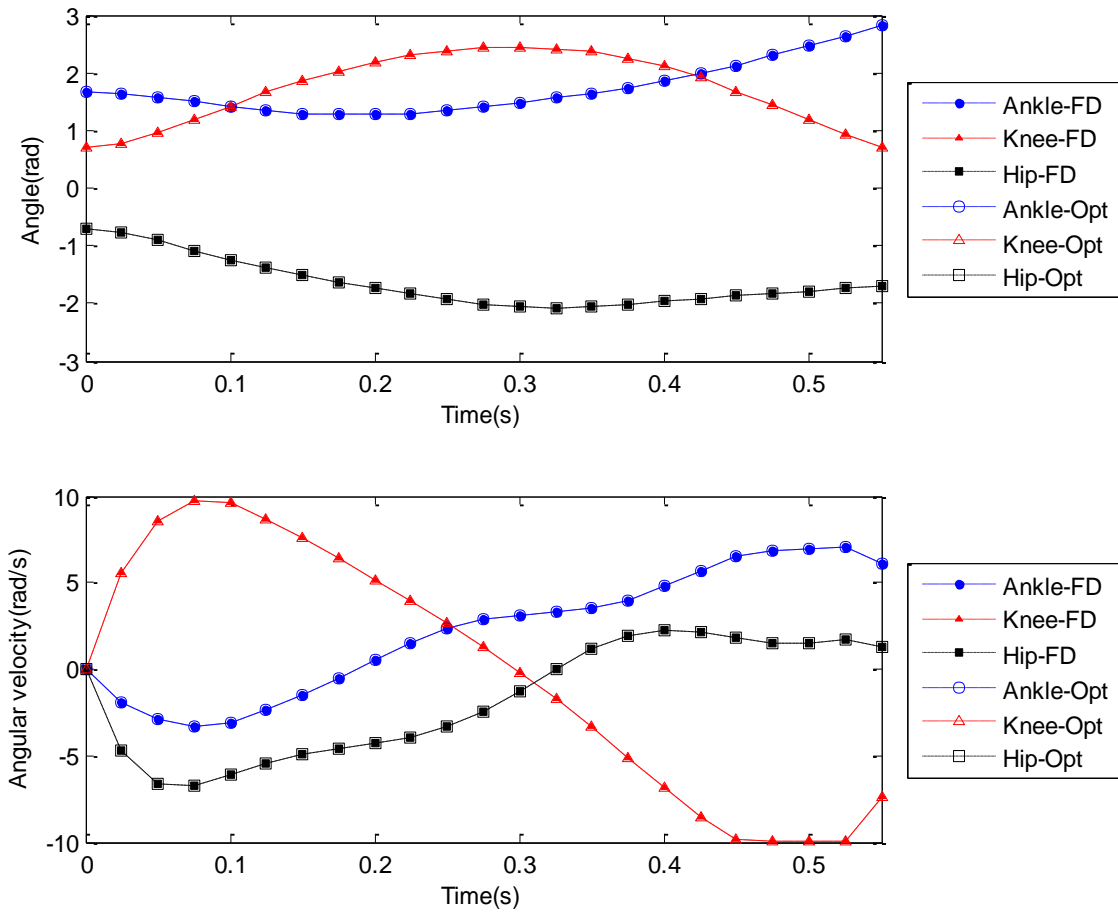


Figure 5.1 Comparing joint trajectories obtained from forward difference analysis and optimization

A forward dynamic analysis was performed to generate joint trajectories when the optimal torque profiles were applied to the hip and knee joints. A forward difference (FD) discretization technique was used to solve the governing equations of motion in this case. Results of this analysis were compared with the optimal (Opt) joint trajectories obtained from the optimization.

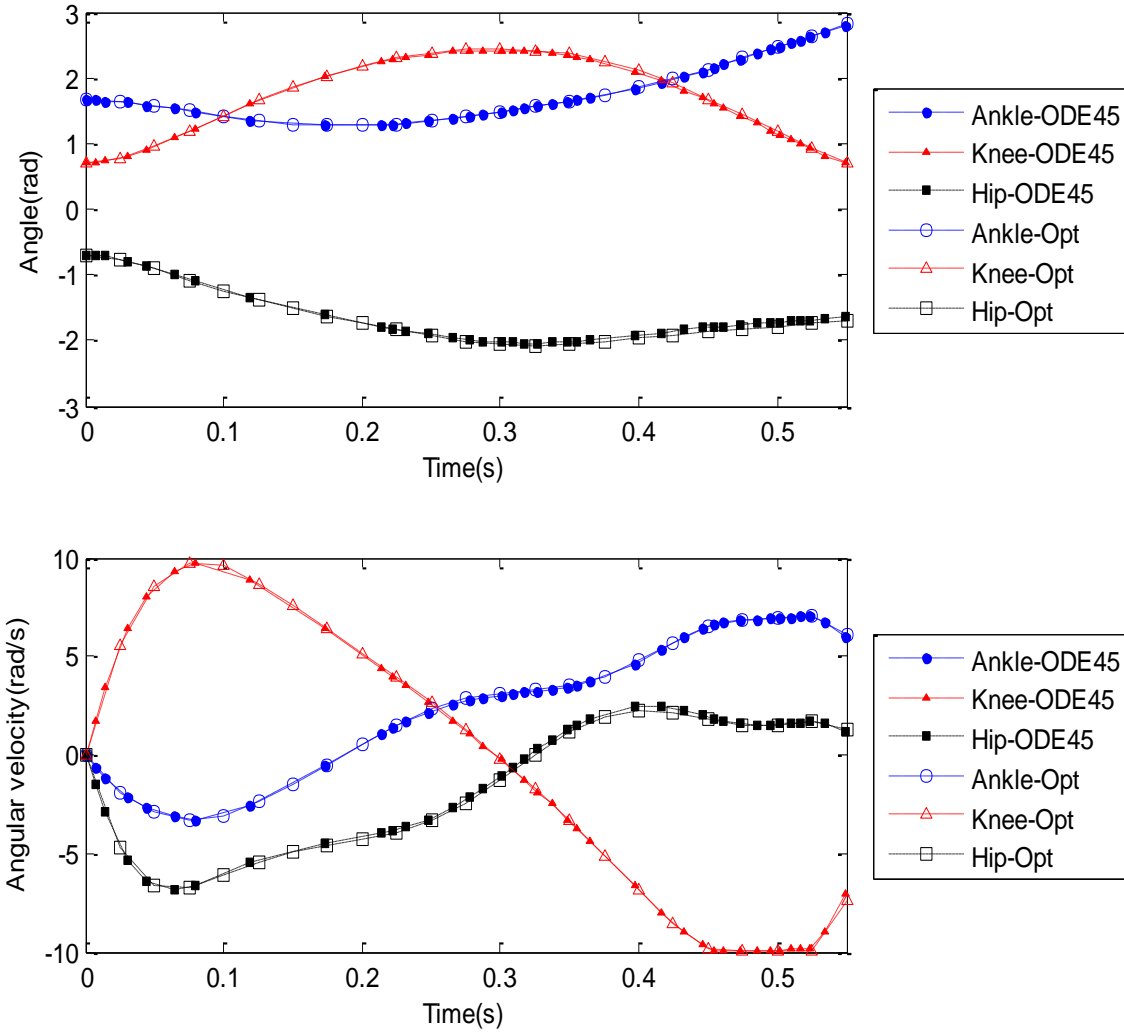


Figure 5.2 Comparing joint trajectories obtained using ode45 solver and optimization

A forward dynamic analysis was performed to generate joint trajectories when the optimal torque profiles were applied to the hip and knee joints. ODE45 solver was used to solve the governing equations of motion in this case. Results of this analysis were compared with the optimal (Opt) joint trajectories obtained from the optimization.

5.2 Experimental Validation

5.2.1 Introduction

Any developed optimization methodology needs to be validated physically before being implemented in an actual exoskeleton and tested with human subjects. Also, due to access limitations to commercially available lower limb exoskeletons, the implementation of the developed safe fall strategy in any of these devices was not feasible. Thus, in this work, a simplified test setup was designed and built to validate the calculated optimal fall strategy.

5.2.2 Test Bed Design

The test setup consisted of a model of a triple-link inverted pendulum, a control system, and a power supply, designed and fabricated by an undergraduate engineering team (Figure 5.3). As mentioned before, when developing the optimization, it was assumed that the characteristics of the human body are symmetrical and the dynamics of the fall were studied only in the sagittal plane. The mechanical test setup characterized a half-plane model of a human body. Because of safety considerations and design challenges, it was decided to build a half-scale length model of a human body. In addition, the mass distribution of the model represented a 1/32-scale mass of a human body, which was used in the development of the optimal human fall strategy. Three joints of the triple-link inverted pendulum replicated the motion of the hip, knee, and ankle joints. Similar to the three-link model of a human fall, the hip and knee joints of the inverted pendulum were actuated and the ankle was a passive joint. The hip and knee joint angles were read through the actuator's encoder and the ankle joint angle was read by a potentiometer that was installed at the joint. Joint angle readings were made in real-time (at approximately 500 Hz) and corresponding data were then sent to the control system.

The optimization routine described in Chapter 3 was modified for the physical characteristics of the actual mechanical test setup. The optimization was performed and the optimal trajectories of the hip and knee joints were calculated. These time-series data were then provided to the control system in the form of a lookup table.

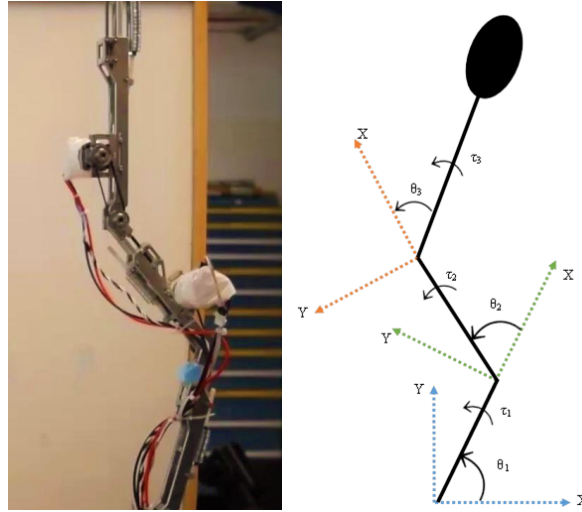


Figure 5.3 Mechanical test setup

In the control system, and for each loop iteration, the time from the start of the fall was calculated and the appropriate desired joint angles were interpolated from the precomputed lookup table. These parameters were then passed to the control algorithm to generate appropriate motor commands. Real-time joint angles were read through the hip and knee encoders and were sent to the control algorithm. A position control strategy was used to control the hip and knee joint trajectories throughout the fall duration [72].

5.2.3 Experimental Procedure

5.2.3.1 Data Collection

Several steps had to be taken to prepare the setup prior to performing the experiments. First, the mechanical test setup was calibrated to initialize the joint angles. The encoder and potentiometer values, when the device is held horizontally, were used to establish a reference point for the angular measurements. Next, the optimal time-stamped hip and knee trajectories for the fall duration were loaded into the control system. These data were then interpolated to artificially increase the resolution. A position control algorithm was used to set the hip and knee joint angles to their initial values, which were specified by the time-series data set. Since there is no actuation at the ankle joint, the setup had to be held upright to prevent the device from falling.

The controller was programmed to start the safe fall control strategy once the ankle angle passed beyond a specified angle. Therefore, the ankle angle sensor was constantly monitored subsequent to the initialization of the hip and knee joints. When the ankle angle exceeded the specified limit, the position control strategy was activated to control the hip and knee joint angles throughout the fall. The time from the start of the fall was calculated and the desired joint angles were interpolated from the precomputed lookup table. Online readings of the potentiometer and encoders were passed through the control algorithm to generate control commands for the actuators. This process continued until the pre-computed fall time was reached. The actuators were shut off after the completion of the fall duration.

5.2.3.2 Data Analysis

The collected data included the time series of the hip, knee, and ankle joint angles. Custom-developed MATLABTM scripts were used to process these data. The forward difference method was used to calculate the joints' angular velocities for the fall duration using the joints' angle

data. Next, a low-pass, fourth-order Butterworth filter was used to filter data. A residual analysis was performed in order to determine a reasonable cutoff frequency for the filter.

5.2.4 Results

Different fall strategies were implemented with the device and experiments were performed in order to assess the functional performance of the test setup. In this section, the results of one experiment, in which an optimal safe fall strategy was implemented with the device, are presented. The initial joint angles from which the fall initiated were 90° , 40° , and -40° at the ankle, knee, and the hip joints, respectively. The initial guess for the optimization was generated using a forward kinematic analysis when -0.6 and 0.3 Nm were applied at the knee and hip joints, respectively. The optimization was performed for different fall durations and the optimal fall duration was found to be equal to 0.47 sec.

As shown in Figure 5.4, a delay in the knee and hip joint trajectories response was observed at the beginning of the fall. The joint angle trajectories closely followed the target trajectories throughout the terminal phase of the fall. Several experiments were performed to tune the system, whereby it was discovered that the test system actuators did not have the necessary response time to accurately follow the target trajectory. Several attempts were made to tune the PID controller gains in order to improve the response time of the system. However, due to the inherent limitations of the hardware and software design, the response time of the actuators could not be increased any further.

Large deviations were observed between the experimental and optimal values of the joints angular velocity throughout the fall duration (Figure 5.5). As mentioned before, this was due to hardware and software limitations. Specifically, some issues were observed regarding the real-time controller that was used to implement the optimal control strategy.

Similar deviations were observed in the profile of the hip linear velocity for the experimental and simulation results during the fall (Figure 5.6). However, the hip linear velocity at impact was found to have similar values in both the experimental (2.045 m/s) and simulation results (2.097 m/s). For this metric, the observed error between the experimental and simulation was less than 3%.

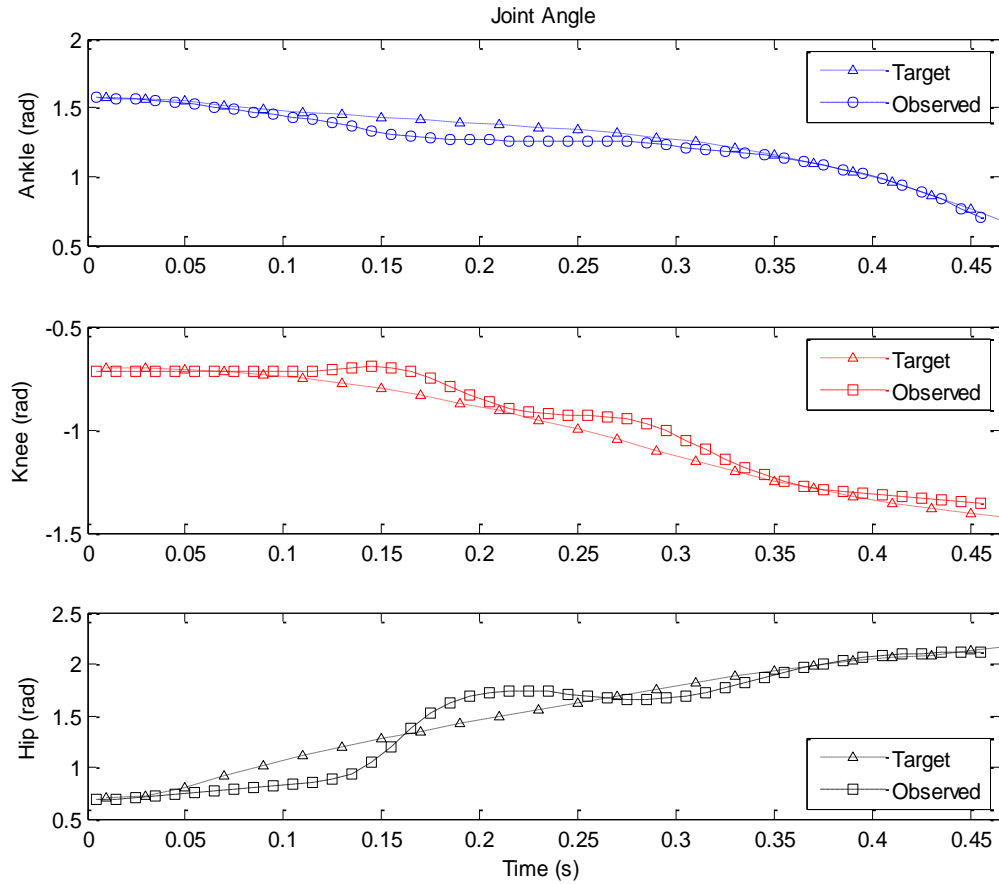


Figure 5.4 Comparison of joint angles between the simulation and experimental results

The recorded joints angles in the experiment (labeled as *Observed*) are compared to the optimal target trajectories (labeled as *Target*).

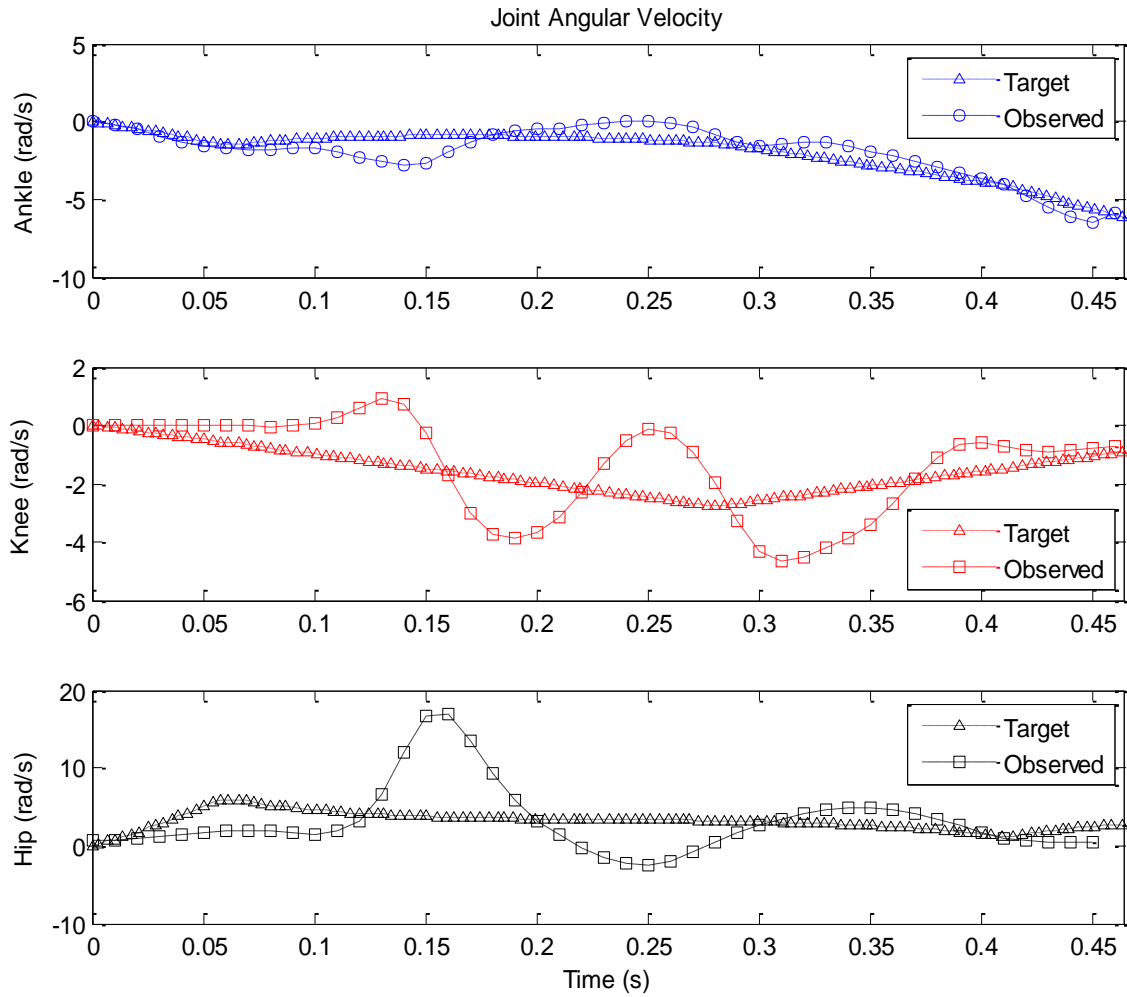


Figure 5.5 Comparison of joint angular velocity between the simulation and experimental results

The computed joints angular velocity using experimental data (labeled as *Observed*) is compared to the optimal trajectories of joints angular velocity (labeled as *Target*).

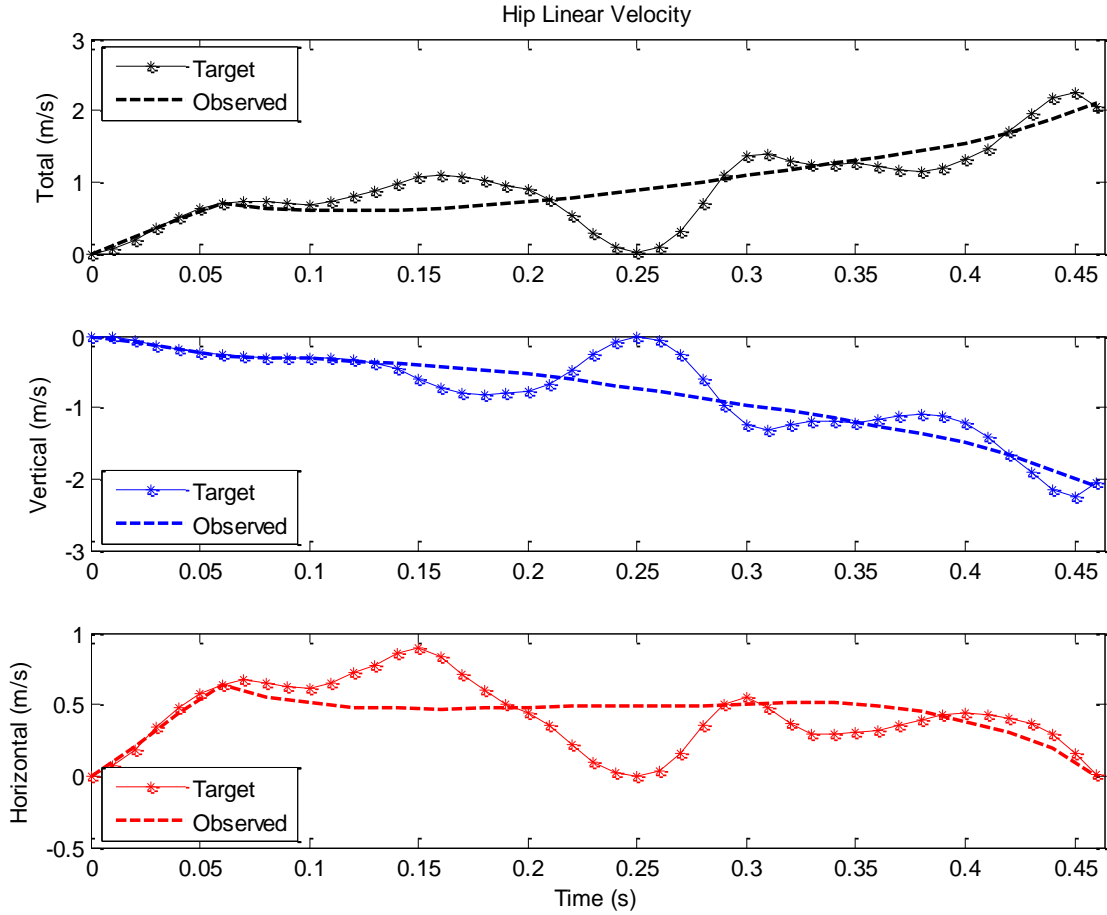


Figure 5.6 Comparison of hip linear velocity between the simulation and experimental results

The time series of hip linear velocity in the experiment (labeled as *Observed*) is compared to the results of the optimization (labeled as *Target*).

5.3 Discussion

Numerical and experimental validations were conducted to verify the results of the optimization methodology presented in Chapter 3. The numerical validation method included performing a forward dynamic analysis and comparing the results when two different numerical techniques were used to solve the differential equation. Similar results were obtained when differential equations were solved MATLAB's ode45 solver and forward difference

discretization technique. The outcomes of the numerical validation support the robustness of the optimization algorithm developed in this thesis.

A mechanical test setup was built for the purpose of validating the results of the previously developed optimization methodology. This optimization methodology was adapted to take into account the characteristics of the scaled mechanical test setup. Optimization was performed and the optimal joint trajectories were generated for a specific falling condition. Optimal joint trajectories were then implemented in the system and experiments were performed to assess the outcome. The primary results of the experiment confirmed that an optimal fall strategy could be implemented in the mechanical test setup. Further investigations should be made to assure the repeatability of the results by performing additional experiments. However, due to some fundamental hardware and software limitations, further experiments could not be conducted with the current experimental test setup. Some of the major existing limitations are listed below:

- Actuators at the hip and knee joints were not powerful and responsive enough to provide the torque at the required speed and within the desired response time.
- The design of the ankle joint and installation of the sensor led to faulty readings of the potentiometer that could not have been improved without making fundamental changes to the current design of the joint.
- The controller used to implement the control strategy could not implement true real-time control at a high enough closed-loop control rate. This was due to the limitations of the software being used that resulted in variations in the sampling rate.

To address the above-mentioned issues with the first prototype, a second prototype is currently under development.

Chapter 6: Conclusions

6.1 Summary of Contributions

Current exoskeleton designs are susceptible to falls and causing injury to their users. This thesis has presented an optimization methodology to develop a safe fall control strategy in the case of a human-exoskeleton backward fall. The motivation for this work is ultimately to improve the users' safety while wearing and using LLEs. To achieve this objective, the specific goals were defined as: reducing the risk of head impact/avoiding head impact and minimizing the hip linear velocity at the moment of ground contact.

The review of literature, presented in Chapter 2, suggests that healthy individuals employ protective responses to diminish the intensity of a fall and, subsequently, the severity of potential injuries to the human body. Also, some studies have established safe-fall strategies for bipedal humanoid robots. These strategies found that it was possible to reduce damage to the robot as a result of ground impact. In addition, proposed strategies to mitigate the risk of user injury in the case of a human-exoskeleton fall were reviewed. Chapter 2 ends with a description of relevant optimization methods to be used in the development of safe-fall strategies for human-exoskeleton falls.

Due to the availability of data on the biomechanics of human falls, safe-fall strategies were first examined for human-only falls. Human falls were modelled with one-, two-, and three-link inverted pendulum models (Chapter 3). For each model, the dynamics of the fall were derived and an optimization routine was developed to find the optimal joint trajectories that minimized an objective function and satisfied a set of constraints. In the case of a three-link model of a human fall, the objective function included a weighted function of the trunk angular velocity and hip linear velocity at impact. The results of the optimization confirm that employing an optimal

safe fall strategy may reduce the risk of injury in the case of a fall. These results revealed that the optimal coordination of lower limb joints would result in head impact avoidance and minimization of hip linear impact velocity. The results of this study were in agreement with previous experiments studying human falls. This helped to verify the validity and efficacy of the optimal safe-fall strategy developed.

The results presented in Chapter 3 contribute to a better understanding of the biomechanics of human falls. This knowledge not only is important in assessing the safe-fall strategies in human falls, it could also be used in the development of safe-fall strategies for human-exoskeleton falls. The author next extended the optimization methodology to include a model of an exoskeleton in the already existing model of a human fall (Chapter 4). The results of the optimization demonstrated that an exoskeleton's joint trajectories could be optimized to decrease the severity of a fall. In other words, the results of this study confirmed that employing a safe-fall control strategy would lead to a safe fall, in which the angular velocity of the trunk at impact is near zero and the linear hip impact velocity is minimized. To further enhance the safety of the user, it is suggested to use cushioning mechanisms such as hip and head protectors or airbag systems in adjunct with the application of the safe fall control strategy.

A safe fall control strategy was implemented in a mechanical test setup to evaluate the validity of the safe-fall strategy presented in Chapters 3 and 4. Experiments were performed to examine the kinematic and dynamic characteristics of the joints. The optimal joint trajectories, developed earlier in this work, were implemented in a model of a three-link inverted pendulum. The joint trajectories during the fall were recorded and then compared with the target optimal joint trajectories. The primary results of the experiments verified that the control strategy developed in this study could be implemented in a mechanical test setup.

The author believes this work is one of the first studies reporting the development of a safe-fall control strategy for a human-exoskeleton fall, and also the first study analyzing the characteristics of a human-exoskeleton fall using a mathematical model. The main scientific contributions of this thesis are the development of an optimization methodology and the application of this method that may lead to the improvement of exoskeleton safety in the case of a backward fall. It is worth recalling that none of the even most advanced LLEs that are currently used for rehabilitation purposes have any kind of safe-fall algorithm implemented in their control system. Illustrating the efficacy of an injury mitigation control strategy, developed in this project, may lead to future implementation in commercial exoskeleton systems. This would eventually help accelerate the transition of exoskeletons from research centres to be widely used in the community.

6.2 Recommendations and Future Work

This thesis developed an optimal fall strategy for a simplified model of a human-exoskeleton backward fall. First, not all backward falls are symmetric and the motion is not always limited to the sagittal plane. Modelling an asymmetric fall is more complex, and a more elaborate model of a human-exoskeleton system is needed to simulate the dynamics of the fall in this case. Additionally, the effects of the involvement of upper extremities during the fall were ignored in this study and should be investigated in future studies. Thirdly, several constraints including the joint characteristics of the human body, the effects of spasticity, and limits of joint angles and angular velocities for persons with an SCI should be considered in the development of future human-exoskeleton fall models. Moreover, more details regarding the dynamics of the actuators should be included in the constraint function. Finally, a more accurate objective function should be defined to better reflect the goal of avoiding the head impact. Currently, there

is no constraint and no penalty in the objective function regarding the orientation of the trunk at contact. This is a limitation of the developed optimization methodology that should be addressed in future models of a human-exoskeleton fall.

In the safe-fall strategy developed in this thesis, it is assumed that the actuators are shut down at the moment where the hip hits the ground, and no analysis is done to assess the dynamics of the system after impact. However, it is worth examining the dynamics of the fall after ground impact to investigate the stability of the system. This should be done to ensure that the head is not at risk of collision with the ground or other surrounding objects.

This thesis provides limited evidence regarding the implementation of the optimal safe-fall strategy in an actual mechanical test setup. The feasibility of executing the optimal strategy should be further investigated and the effectiveness of this method should be examined more thoroughly.

In summary, the results of this work reveal that the development and implementation of a safe fall control strategy is a challenging problem. Numerous parameters are involved in the development of a safe fall strategy, including the characteristics of the device itself and environmental conditions (e.g., floor surface characteristics). Moreover, executing a safe fall control strategy in a prototype or an actual exoskeleton would be a significant and complex challenge, and appropriate software and hardware platforms are needed to be able to successfully implement such a control strategy. It should be recalled that this thesis is among the first research studies that have modelled exoskeleton falls and provides the basis for future investigations in this field of research.

Bibliography

- [1] E. A. Courtney-Long, D. D. Carroll, Q. C. Zhang, A. C. Stevens, S. Griffin-Blake, B. S. Armour, and V. A. Campbell, "Prevalence of disability and disability type among adults — United States, 2013," *MMWR. Morb. Mortal. Wkly. Rep.*, vol. 64, no. 29, pp. 784–792, 2015.
- [2] "Disability in Canada: Initial findings from the Canadian survey on disability fact sheet," 2013. [Online]. Available: <http://www.statcan.gc.ca/pub/89-654-x/89-654-x2013002-eng.htm>.
- [3] D. E. Rosenberg, C. H. Bombardier, J. M. Hoffman, and B. Belza, "Physical activity among persons aging with mobility disabilities: shaping a research agenda.," *J. Aging Res.*, vol. 2011, p. 708510, 2011.
- [4] V. K. Noonan, M. Fingas, A. Farry, D. Baxter, A. Singh, M. G. Fehlings, and M. F. Dvorak, "Incidence and prevalence of spinal cord injury in Canada: A national perspective," *Neuroepidemiology*, vol. 38, no. 4, pp. 219–226, 2012.
- [5] "Spinal Cord Injury (SCI) Facts and Figures at a Glance." [Online]. Available: http://www.msktc.org/lib/docs/Data_Sheets_/SCI_Facts_and_Figures_2016.pdf. [Accessed: 27-Oct-2016].
- [6] "WHO | Assistive devices and technologies," *WHO*, 2016. [Online]. Available: <http://www.who.int/disabilities/technology/en/>. [Accessed: 27-Oct-2016].
- [7] "WHO | Personal Mobility - facilitating access to quality mobility aids and devices," *WHO*, 2016. [Online]. Available: http://www.who.int/disabilities/media/news/personal_mobility/en. [Accessed: 27-Oct-2016].
- [8] J. F. Borisoff, J. Mattie, and V. Rafer, "Concept proposal for a detachable exoskeleton-wheelchair to improve mobility and health," in *2013 IEEE 13th International Conference on Rehabilitation Robotics (ICORR)*, 2013, pp. 1–6.
- [9] J. Arva, G. Paleg, M. Lange, J. Lieberman, M. Schmeler, B. Dicianno, M. Babinec, and L. Rosen, "RESNA position on the application of wheelchair standing devices.," *Assist. Technol.*, vol. 21, no. 3, pp. 161–8–71, Jan. 2009.
- [10] M. T. Karimi, "Evidence-based evaluation of physiological effects of standing and

- walking in individuals with spinal cord injury,” *Iran. J. Med. Sci.*, vol. 36, no. 4, pp. 242–253, 2011.
- [11] A. M. Dollar and H. Herr, “Lower extremity exoskeletons and active orthoses: Challenges and state-of-the-art,” *IEEE Trans. Robot.*, vol. 24, no. 1, pp. 144–158, Feb. 2008.
 - [12] “FDA medical device classification.” [Online]. Available: <http://www.accessdata.fda.gov/scripts/cdrh/cfdocs/cfpdc/classification.cfm?id=phl>. [Accessed: 27-Oct-2016].
 - [13] “FDA news and events.” [Online]. Available: <http://www.fda.gov/NewsEvents/Newsroom/PressAnnouncements/ucm402970.htm>. [Accessed: 28-Oct-2016].
 - [14] G. Chen, C. K. Chan, Z. Guo, and H. Yu, “A review of lower extremity assistive robotic exoskeletons in rehabilitation therapy,” *Crit. Rev. Biomed. Eng.*, vol. 41, no. 4–5, pp. 343–363, 2013.
 - [15] R. J. Farris, H. A. Quintero, S. A. Murray, K. H. Ha, C. Hartigan, and M. Goldfarb, “A preliminary assessment of legged mobility provided by a lower limb exoskeleton for persons with paraplegia,” *IEEE Trans. Neural Syst. Rehabil. Eng.*, vol. 22, no. 3, pp. 482–90, May 2014.
 - [16] P. D. Neuhaus, J. H. Noorden, T. J. Craig, T. Torres, J. Kirschbaum, and J. E. Pratt, “Design and evaluation of Mina: A robotic orthosis for paraplegics,” *2011 IEEE Int. Conf. Rehabil. Robot.*, pp. 1–8, 2011.
 - [17] V. Lajeunesse, C. Vincent, F. Routhier, E. Careau, and F. Michaud, “Exoskeletons’ design and usefulness evidence according to a systematic review of lower limb exoskeletons used for functional mobility by people with spinal cord injury,” *Disabil. Rehabil. Assist. Technol.*, vol. 0, no. 0, pp. 1–13, 2015.
 - [18] “CFR - Code of federal regulations title 21.” [Online]. Available: <https://www.accessdata.fda.gov/scripts/cdrh/cfdocs/cfcfr/cfrsearch.cfm?fr=890.3480>. [Accessed: 29-Oct-2016].
 - [19] W. Bauman, M. Korsten, M. Radulovic, G. Schilero, J. Wech, and A. Spungen, “Secondary medical consequences of spinal cord injury,” *Top. Spinal Cord Inj. Rehabil.*, vol. 18, no. 4, pp. 354–378, 2012.

- [20] S. A. Kolakowsky-Hayner, J. Crew, S. Moran, and A. Shah, "Safety and feasibility of using the EksoTM Bionic exoskeleton to aid ambulation after spinal cord injury," *J. Spine*, 2013.
- [21] J. Wolff, C. Parker, J. Borisoff, B. W. Mortenson, and J. Mattie, "A survey of stakeholder perspectives on exoskeleton technology.," *J. Neuroeng. Rehabil.*, vol. 11, no. 1, p. 169, Dec. 2014.
- [22] S. N. Robinovitch, J. Chiu, R. Sandler, and Q. Liu, "Impact severity in self-initiated sits and falls associates with center-of-gravity excursion during descent," *J. Biomech.*, vol. 33, no. 7, pp. 863–870, Jul. 2000.
- [23] E. T. Hsiao and S. N. Robinovitch, "Common protective movements govern unexpected falls from standing height," *J. Biomech.*, vol. 31, no. 1, pp. 1–9, 1997.
- [24] D. A. Winter, "Human balance and posture standing and walking control during," *Gait Posture*, vol. 3, pp. 193–214, 1995.
- [25] M. C. Do, Y. Breniere, and P. Brenguier, "A biomechanical study of balance recovery during the fall forward," *J. Biomech.*, vol. 15, no. 12, pp. 933–939, 1982.
- [26] L. Currie, *Fall and Injury Prevention*, no. 8. 2008.
- [27] R. W. Sattin, D. A. Lambert Huber, C. A. DeVito, J. G. Rodriguez, A. Ros, S. Bacchelli, J. a Stevens, and R. J. Waxweiler, "The incidence of fall injury events among the elderly in a defined population.," *Am. J. Epidemiol.*, vol. 131, no. 6, pp. 1028–37, 1990.
- [28] "WISQARS Leading causes of nonfatal injury reports." [Online]. Available: <http://webappa.cdc.gov/sasweb/ncipc/nfilead2001.html>.
- [29] M. T. Do, V. C. Chang, N. Kuran, and W. Thompson, "Fall-related injuries among Canadian seniors , 2005 – 2013 : an analysis of the Canadian Community Health Survey," vol. 35, no. 7, pp. 2005–2013, 2015.
- [30] I. Gitajn and E. Rodriguez, "Biomechanics of musculoskeletal injury," in *Biomechanics in Applications*, vol. 33, no. 4, InTech, 2011, p. 378.
- [31] D. A. Sterling, J. A. O'Connor, and J. Bonadies, "Geriatric falls: injury severity is high and disproportionate to mechanism.," *J. Trauma*, vol. 50, no. 1, pp. 116–119, 2001.
- [32] J. Ruiz-del-Solar, R. Palma-Amestoy, R. Marchant, I. Parra-Tsunekawa, and P. Zegers, "Learning to fall: Designing low damage fall sequences for humanoid soccer robots," *Rob.*

- Auton. Syst.*, vol. 57, no. 8, pp. 796–807, 2009.
- [33] V. H. Frankel and J. W. Pugh, “Biomechanics of the hip,” in *Surgery of the Hip Joint*, vol. 92, New York, NY: Springer New York, 1984, pp. 115–131.
 - [34] M. C. Nevitt, S. R. Cummings, and E. S. Hudes, “Risk factors for injurious falls: a prospective study,” *J. Gerontol.*, vol. 46, no. 5, pp. M164–M170, 1991.
 - [35] C. I. Gryfe, A. Amies, and M. J. Ashley, “A longitudinal study of falls in an elderly population: I. Incidence and morbidity,” *Age Ageing*, vol. 6, no. 4, pp. 201–210, 1977.
 - [36] M. C. Nevitt, “Risk factors for recurrent nonsyncopal falls,” *Jama*, vol. 261, no. 18, p. 2663, 1989.
 - [37] J. B. Lauritzen and V. Askegaard, “Protection against hip fractures by energy absorption,” *Dan. Med. Bull.*, vol. 39, no. 1, pp. 91–93, 1992.
 - [38] W. J. Choi, J. M. Wakeling, and S. N. Robinovitch, “Kinematic analysis of video-captured falls experienced by older adults in long-term care,” *J. Biomech.*, vol. 48, no. 6, pp. 911–920, 2015.
 - [39] J. S. Tan, J. J. Eng, S. N. Robinovitch, and B. Warnick, “Wrist impact velocities are smaller in forward falls than backward falls from standing,” *J. Biomech.*, vol. 39, no. 10, pp. 1804–1811, 2006.
 - [40] S. N. Robinovitch, R. Brumer, and J. Maurer, “Effect of the ‘squat protective response’ on impact velocity during backward falls,” *J. Biomech.*, vol. 37, no. 9, pp. 1329–37, Sep. 2004.
 - [41] R. Sandler and S. Robinovitch, “An Analysis of the Effect of Lower Extremity Strength on Impact Severity During a Backward Fall,” *J. Biomech. Eng.*, vol. 123, no. 6, p. 590, 2001.
 - [42] L. A. Talbot, R. J. Musiol, E. K. Witham, and E. J. Metter, “Falls in young, middle-aged and older community dwelling adults: perceived cause, environmental factors and injury,” *BMC Public Health*, vol. 5, no. 1, p. 86, 2005.
 - [43] S. R. Cummings and M. C. Nevitt, “A hypothesis: the causes of hip fractures,” *J. Gerontol.*, vol. 44, no. 4, pp. M107–11, Jul. 1989.
 - [44] G. E. Stelmach and C. J. Worringham, “Sensorimotor deficits related to postural stability. Implications for falling in the elderly,” *Clin. Geriatr. Med.*, vol. 1, no. 3, pp. 679–94,

Aug. 1985.

- [45] A. J. van den Kroonenberg, W. C. Hayes, and T. A. McMahon, "Dynamic models for sideways falls from standing height," *J. Biomech. Eng.*, vol. 117, no. 3, pp. 309–318, 1995.
- [46] R. Schonnop, Y. Yang, F. Feldman, E. Robinson, M. Loughin, and S. N. Robinovitch, "Prevalence of and factors associated with head impact during falls in older adults in long-term care.," *CMAJ*, vol. 185, no. 17, pp. E803-10, 2013.
- [47] A. J. van den Kroonenberg, W. C. Hayes, and T. A. McMahon, "Hip impact velocities and body configurations for voluntary falls from standing height," *J. Biomech.*, vol. 29, no. 6, pp. 807–811, 1996.
- [48] F. Feldman and S. N. Robinovitch, "Reducing hip fracture risk during sideways falls: Evidence in young adults of the protective effects of impact to the hands and stepping," *J. Biomech.*, vol. 40, no. 12, pp. 2612–2618, 2007.
- [49] S. Robinovitch and R. Sandler, "Impact severity during a backward fall depends on the timing of the 'squat' protective response during descent," in *Bioengineering Conference ASME*, 2001, vol. 50, no. 2, pp. 881–882.
- [50] K. Ogata, K. T. K. Terada, and Y. K. Y. Kuniyoshi, "Falling motion control for humanoid robots while walking," *2007 7th IEEE-RAS Int. Conf. Humanoid Robot.*, pp. 306–311, 2007.
- [51] K. Fujiwara, F. Kanehiro, S. Kajita, and H. Hirukawa, "Safe knee landing of a human-size humanoid robot while falling forward," *2004 IEEE/RSJ Int. Conf. Intell. Robot. Syst. (IEEE Cat. No.04CH37566)*, vol. 1, pp. 503–508, 2004.
- [52] K. Fujiwara, F. Kanehiro, H. Saito, S. Kajita, K. Harada, and H. Hirukawa, "Falling motion control of a humanoid robot trained by virtual supplementary tests," *IEEE Int. Conf. Robot. Autom. 2004. Proceedings. ICRA '04. 2004*, vol. 2, no. April, pp. 1077–1082, 2004.
- [53] K. Fujiwara, F. Kanehiro, S. Kajita, K. Kaneko, K. Yokoi, and H. Hirukawa, "UKEMI: falling motion control to minimize damage to biped humanoid robot," *IEEE/RSJ Int. Conf. Intell. Robot. Syst.*, vol. 3, no. October, pp. 2521–2526, 2002.
- [54] S. Yun, A. Goswami, and Y. Sakagami, "Safe fall: Humanoid robot fall direction change

- through intelligent stepping and inertia shaping,” *2009 IEEE Int. Conf. Robot. Autom.*, pp. 781–787, 2009.
- [55] K. Fujiwara, F. Kanehiro, S. Kajita, K. Yokoi, H. Saito, K. Harada, K. Kaneko, and H. Hirukawa, “The first human-size humanoid that can fall over safely and stand-up again,” *Proc. 2003 IEEE/RSJ Int. Conf. Intell. Robot. Syst. (IROS 2003) (Cat. No.03CH37453)*, vol. 2, no. October, pp. 1920–1926, 2003.
 - [56] K. Fujiwara, S. Kajita, K. Harada, K. Kaneko, M. Morisawa, F. Kanehiro, S. Nakaoka, and H. Hirukawa, “Towards an optimal falling motion for a humanoid robot,” *Proc. 2006 6th IEEE-RAS Int. Conf. Humanoid Robot. HUMANOIDS*, pp. 524–529, 2006.
 - [57] K. Fujiwara, S. Kajita, K. Harada, K. Kaneko, M. Morisawa, F. Kanehiro, S. Nakaoka, and H. Hirukawa, “An Optimal planning of falling motions of a humanoid robot,” *IEEE Int. Conf. Intell. Robot. Syst.*, no. Table I, pp. 456–462, 2007.
 - [58] A. Goffer, “Enhanced safety of gait in powered exoskeletons,” *Dyn. Walk. Conf. Abstr. online.*, 2014.
 - [59] R. Angold, “Gait orthotic device and method for protecting gait orthotic device and user from damage,” 2014.
 - [60] M. McGrath, D. Howard, and R. Baker, “The strengths and weaknesses of inverted pendulum models of human walking,” *Gait Posture*, vol. 41, no. 2, pp. 389–94, 2015.
 - [61] L. L. Menegaldo, A. D. T. Fleury, and H. I. Weber, “Biomechanical modeling and optimal control of human posture,” *J. Biomech.*, vol. 36, no. 11, pp. 1701–1712, 2003.
 - [62] J. Angeles, *Fundamentals of robotic mechanical systems*. Boston, MA: Springer US, 2007.
 - [63] H. Josephs and R. Huston, *Dynamics of mechanical systems*. CRC Press, 2002.
 - [64] D. A. Winter, “Anthropometry,” in *Biomechanics and motor control of human movement*, 2009, pp. 82–106.
 - [65] M. R. Yeadon, M. A. King, and C. Wilson, “Modelling the maximum voluntary joint torque/angular velocity relationship in human movement,” *J. Biomech.*, vol. 39, no. 3, pp. 476–482, 2006.
 - [66] “Optimization toolbox™ User’s Guide R2015b,” 2015.
 - [67] “Simscape™ user’s guide R2016a,” 2016.

- [68] “Friction and friction coefficients,” 2016. [Online]. Available: http://www.engineeringtoolbox.com/friction-coefficients-d_778.html.
- [69] “AC servo actuator-SHA series manual.” .
- [70] M. Bulajic-kopjar, “Seasonal variations in incidence of fractures among elderly people,” *Inj. Prev.*, pp. 16–19, 2000.
- [71] R. Jauregui and F. Silva, “Numerical validation methods,” *Numer. Anal. - Theory Appl.*, pp. 155–174, 2011.
- [72] T. Darcie, B. Pawlina, O. Gadsby, and S. Shariat Jaffari, “Exoskeleton safe-fall system.” [Online]. Available: https://seelio.com/w/242j/exoskeleton-safe_fall-system. [Accessed: 19-Dec-2016].
- [73] S. Boyd and L. Vandenberghe, *Convex Optimization*, vol. 25, no. 3. 2010.
- [74] A. Antoniou and W. Lu, *Practical optimization: Algorithms and engineering applications*. Boston, MA: Springer US, 2007.

Appendices

Appendix A: Governing Equations of Motion of a One-link, Two-link, and Three-link Model

The Euler-Lagrange method was used to derive the equations of motion for all the three models and a system of second-order nonlinear ordinary differential equations were derived in the state space format. Governing equations of motion for the one-, two-, and three-link models of a human fall are described in Sections A.1, A.2, and A.3, respectively.

A.1 One-Link Model

According to the global reference frame ($[X_0, Y_0]$ - Figure A.1), ankle angle is increasing if the link is moving in the counter clockwise direction, and it is decreasing if moving in the clockwise direction. Joint torque is positive if applied in the dorsiflexion direction, and is negative if applied in the plantarflexion direction. The governing equation of motion for a one-link model is defined in (A.1). Corresponding description and value of each parameter is described in Table A-1.

$$\left[I_{COM} + M(r_{COM}l)^2 \right] \ddot{\theta} + Mgr_{COM}L \cos \theta = \tau \quad (\text{A.1})$$

Table A-1 Characteristics of a one-link model

Parameter	Description	Value
M	Total body mass (kg)	53.70
L	Total body height (m)	1.60
I_{COM}	Mass moment of inertia of human body about the center of mass (kgm^2)	7.97
r_{COM}	Proximal center of mass as a percent of the body height	0.552
θ	Ankle angle (rad)	Variable
τ	Ankle torque (Nm)	Variable

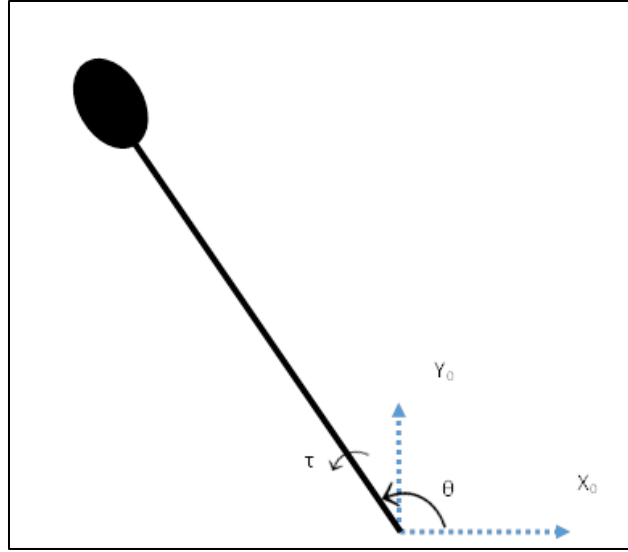


Figure A.1 One-link model of a human fall

A.2 Two-Link Model

According to the global reference frame ($[X_0, Y_0]$ - Figure A.2) and the local reference frame on the hip joint ($[X_1, Y_1]$ - Figure A.2), both ankle and hip angle are increasing if the links are moving in the counterclockwise direction and decreasing if moving in the clockwise direction. Joint torque is positive if applied in the plantarflexion and extension direction at the ankle and the hip joints, respectively. Joint torque is negative if applied in the dorsiflexion and flexion direction at the ankle and the hip joints, respectively. The governing equations of motion for a two-link model are defined in (A.2). Corresponding description and value of each parameter is described in Table A-2.

$$\begin{cases}
\left[I_{LE,ankle} + M_{HAT} \left((r_{G,hip} L_{TR})^2 + L_{LE}^2 + 2r_{COM,HAT} L_{TR} L_{LE} \cos \theta_2 \right) \right] \ddot{\theta}_1 + M_{HAT} \left[(r_{G,hip} L_{TR})^2 + r_{COM,HAT} L_{TR} L_{LE} \cos \theta_2 \right] \ddot{\theta}_2 \\
- 2M_{HAT} r_{COM,HAT} L_{TR} L_{LE} \sin \theta_2 \dot{\theta}_1 \dot{\theta}_2 - M_{HAT} r_{COM,HAT} L_{TR} L_{LE} \sin \theta_2 \dot{\theta}_2^2 + M_{LE} g r_{COM,LE} L_{ST} \cos \theta_1 \\
+ M_{HAT} g \left[r_{COM,HAT} L_{TR} \cos(\theta_1 + \theta_2) + L_{LE} \cos \theta_1 \right] = \tau_1 \\
\\
M_{HAT} \left((r_{G,hip} L_{TR})^2 + r_{COM,HAT} L_{TR} L_{LE} \cos \theta_2 \right) \ddot{\theta}_1 + M_{HAT} (r_{G,hip} L_{TR})^2 \ddot{\theta}_2 + M_{HAT} r_{COM,HAT} L_{TR} L_{LE} \sin \theta_2 \dot{\theta}_1^2 \\
+ M_{HAT} g r_{COM,HAT} L_{TR} \cos(\theta_1 + \theta_2) = \tau_2
\end{cases} \quad (A.2)$$

Table A-2 **Characteristics of a two-link model**

Parameter	Description	Value
M_{HAT}	Total mass of the upper extremity (kg)	36.41
M_{LE}	Total mass of the lower extremity (kg)	17.29
L_{TR}	Length of the trunk segment (m)	0.460
L_{LE}	Total length of the lower extremity (m)	0.848
L_{ST}	Sum of the length of the shank and thigh segments (m)	0.786
$I_{LE,ankle}$	Mass moment of inertia of the lower extremity about the ankle joint (kgm ²)	4.509
$r_{G,hip}$	Radius of gyration of the upper extremity about the hip joint, as a percent of the trunk length	0.798
$r_{COM,HAT}$	Proximal center of mass of the upper extremity as a percent of the upper extremity length	0.626
$r_{COM,LE}$	Proximal center of mass of the lower extremity as a percent of L_{ST}	0.553
θ_1	Ankle angle (rad)	Variable
θ_2	Hip angle (rad)	Variable
$\dot{\theta}_1$	Ankle angular velocity (rad/s)	Variable
$\dot{\theta}_2$	Hip angular velocity (rad/s)	Variable
$\ddot{\theta}_1$	Ankle angular acceleration (rad/s ²)	Variable
$\ddot{\theta}_2$	Hip angular acceleration (rad/s ²)	Variable
τ_1	Ankle torque (Nm)	Variable
τ_2	Hip torque (Nm)	Variable

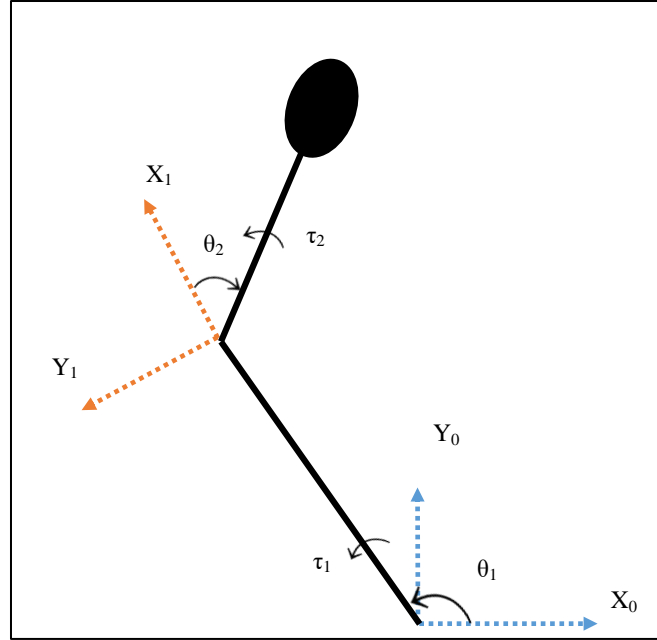


Figure A.2 Two-link model of a human fall

A.3 Three-Link Model

According to the global reference frame ($[X_0, Y_0]$ - Figure A.3) and the local reference frame on the knee and hip joint ($[X_1, Y_1], [X_2, Y_2]$ - Figure A.3), all the joint angles are increasing if the links are moving in the counter clockwise direction and decreasing if moving in the clockwise direction. Joint torque is positive if applied in the plantarflexion, flexion and extension direction at the ankle, knee, and the hip joints, respectively. Joint torque is negative if applied in the dorsiflexion, extension, and flexion direction at the ankle and the hip joints, respectively. The set of governing equations of motion, consisting of three nonlinear, second order differential equation, are defined in (A.3). Corresponding description and value of each parameter is described in Table A-3.

Equation No.1

$$\begin{aligned}
& \left\{ M_{HAT} \left[\left(r_{G,hip} L_{HAT} \right)^2 + L_{TH}^2 + (L_{SH} + L_F)^2 + 2r_{COM,HAT} L_{HAT} L_{TH} \cos \theta_3 + 2L_{TH} (L_{SH} + L_F) \cos \theta_2 + 2r_{COM,HAT} (L_{SH} + L_F) L_{HAT} \cos(\theta_2 + \theta_3) \right] \right\} \ddot{\theta}_1 \\
& + M_{SH} r_{G,ankle}^2 L_{SH}^2 + M_{TH} \left((L_{SH} + L_F)^2 + 2r_{COM,TH} L_{TH} (L_{SH} + L_F) \cos \theta_2 + r_{G,knee}^2 L_{TH}^2 \right) \\
& + \left\{ M_{HAT} \left[L_{TH}^2 + 2L_{COG,HAT} L_{HAT} L_{TH} \cos \theta_3 + L_{TH} (L_{SH} + L_F) \cos \theta_2 + L_{COG,HAT} (L_{SH} + L_F) L_{HAT} \cos(\theta_2 + \theta_3) + (r_{G,hip} L_{HAT})^2 \right] + M_{TH} (r_{G,knee}^2 L_{TH}^2 + L_{COG,TH} L_{TH} (L_{SH} + L_F) \cos \theta_2) \right\} \ddot{\theta}_2 \\
& + M_{HAT} \left\{ r_{COM,HAT} L_{HAT} L_{TH} \cos \theta_3 + r_{COM,HAT} L_{HAT} (L_{SH} + L_F) \cos(\theta_2 + \theta_3) + (r_{G,hip} L_{HAT})^2 \right\} \ddot{\theta}_3 \\
& - M_{HAT} \left\{ 2r_{COM,HAT} L_{HAT} L_{TH} \sin \theta_3 \dot{\theta}_3 + 2L_{TH} (L_{SH} + L_F) \sin \theta_2 \dot{\theta}_2 + 2r_{COM,HAT} (L_{SH} + L_F) L_{HAT} (\dot{\theta}_2 + \dot{\theta}_3) \sin(\theta_2 + \theta_3) \right\} \dot{\theta}_1 \\
& - M_{HAT} \left\{ 2r_{COM,HAT} L_{HAT} L_{TH} \sin \theta_3 \dot{\theta}_3 + L_{TH} (L_{SH} + L_F) \sin \theta_2 \dot{\theta}_2 + r_{COM,HAT} (L_{SH} + L_F) L_{HAT} (\dot{\theta}_2 + \dot{\theta}_3) \sin(\theta_2 + \theta_3) \right\} \dot{\theta}_2 \\
& - M_{HAT} \left\{ r_{COM,HAT} L_{HAT} L_{TH} \sin \theta_3 \dot{\theta}_3 + r_{COM,HAT} L_{HAT} (L_{SH} + L_F) (\dot{\theta}_2 + \dot{\theta}_3) \sin(\theta_2 + \theta_3) \right\} \dot{\theta}_3 \\
& - M_{TH} \left\{ 2r_{COM,TH} L_{TH} (L_{SH} + L_F) \sin \theta_2 \dot{\theta}_1 \dot{\theta}_2 + (r_{COM,TH} L_{TH} (L_{SH} + L_F) \sin \theta_2) \dot{\theta}_2^2 \right\} \\
& + [r_{COM,SH} M_{SH} L_{SH} g \cos \theta_A + (M_{TH} + M_{HAT}) (L_{SH} + L_F) g \cos \theta_A + (r_{COM,TH} M_{TH} + M_{HAT}) L_{TH} g \cos(\theta_A + \theta_K) + r_{COM,HAT} M_{HAT} g L_{HAT} \cos(\theta_A + \theta_K + \theta_H)] = \tau_1 \tag{A.3}
\end{aligned}$$

Equation No.2

$$\begin{aligned}
& \left\{ M_{HAT} \left[\left\{ L_{TH}^2 + 2r_{COM,HAT} L_{HAT} L_{TH} \cos \theta_3 + L_{TH} (L_{SH} + L_F) \cos \theta_2 + r_{COM,HAT} (L_{SH} + L_F) L_{HAT} \cos(\theta_2 + \theta_3) + (r_{G,hip} L_{HAT})^2 \right\} \right] \right\} \ddot{\theta}_1 \\
& + M_{TH} \left((r_{G,knee} L_{TH})^2 + r_{COM,TH} L_{TH} (L_{SH} + L_F) \cos \theta_2 \right) \\
& + \left\{ M_{HAT} \left[L_{TH}^2 + 2r_{COM,HAT} L_{HAT} L_{TH} \cos \theta_3 + (r_{G,hip} L_{HAT})^2 \right] + M_{TH} (r_{G,knee} L_{TH})^2 \right\} \ddot{\theta}_2 + M_{HAT} \left\{ r_{COM,HAT} L_{HAT} L_{TH} \cos \theta_3 + (r_{G,hip} L_{HAT})^2 \right\} \ddot{\theta}_3 \\
& - M_{HAT} \left\{ 2r_{COM,HAT} L_{HAT} L_{TH} \sin \theta_3 \dot{\theta}_3 \right\} \dot{\theta}_2 - M_{HAT} \left\{ 2r_{COM,HAT} L_{HAT} L_{TH} \sin \theta_3 \dot{\theta}_3 + L_{TH} (L_{SH} + L_F) \sin \theta_2 \dot{\theta}_2 + r_{COM,HAT} (L_{SH} + L_F) L_{HAT} (\dot{\theta}_2 + \dot{\theta}_3) \sin(\theta_2 + \theta_3) \right\} \dot{\theta}_1 \\
& - M_{HAT} \left\{ r_{COM,HAT} L_{HAT} L_{TH} \sin \theta_3 \dot{\theta}_3 \right\} \dot{\theta}_3 - M_{TH} (r_{COM,TH} L_{TH} (L_{SH} + L_F) \sin \theta_2) \dot{\theta}_1 \dot{\theta}_2 + r_{COM,TH} M_{TH} L_{TH} (L_{SH} + L_F) \sin \theta_2 (\dot{\theta}_1 + \dot{\theta}_2) \dot{\theta}_1 + \\
& M_{HAT} \dot{\theta}_1 \left\{ [L_{TH} (L_{SH} + L_F) \sin \theta_2 + r_{COM,HAT} (L_{SH} + L_F) L_{HAT} \sin(\theta_2 + \theta_3)] (\dot{\theta}_1 + \dot{\theta}_2) + [r_{COM,HAT} L_{HAT} (L_{SH} + L_F) \sin(\theta_2 + \theta_3)] \dot{\theta}_3 \right\} \\
& + (r_{COM,TH} M_{TH} + M_{HAT}) L_{TH} g \cos(\theta_1 + \theta_2) + r_{COM,HAT} M_{HAT} g L_{HAT} \cos(\theta_1 + \theta_2 + \theta_3) = \tau_2
\end{aligned}$$

Equation No.3

$$\begin{aligned}
 & M_{HAT} \left(r_{G,hip} L_{HAT} \right)^2 \ddot{\theta}_3 + M_{HAT} \left\{ r_{COM,HAT} L_{HAT} L_{TH} \cos \theta_3 + \left(r_{G,hip} L_{HAT} \right)^2 \right\} \ddot{\theta}_2 + M_{HAT} \left\{ r_{COM,HAT} L_{HAT} L_{TH} \cos \theta_3 + r_{COM,HAT} L_{HAT} (L_{SH} + L_F) \cos(\theta_2 + \theta_3) + \left(r_{G,hip} L_{HAT} \right)^2 \right\} \ddot{\theta}_1 \\
 & - M_{HAT} \left\{ r_{COM,HAT} L_{HAT} L_{TH} \sin \theta_3 \dot{\theta}_3 \right\} \dot{\theta}_2 - M_{HAT} \left\{ r_{COM,HAT} L_{HAT} L_{TH} \sin \theta_3 \dot{\theta}_3 + r_{COM,HAT} L_{HAT} (L_{SH} + L_F) (\dot{\theta}_2 + \dot{\theta}_3) \sin(\theta_2 + \theta_3) \right\} \dot{\theta}_1 \\
 & + r_{COM,HAT} M_{HAT} L_{HAT} (\dot{\theta}_2 + \dot{\theta}_1 + \dot{\theta}_3) \left[\dot{\theta}_1 (L_{TH} \sin \theta_3 + (L_{SH} + L_F) \sin(\theta_2 + \theta_3)) + L_{TH} \dot{\theta}_2 \sin \theta_3 \right] + r_{COM,HAT} M_{HAT} g L_{HAT} \cos(\theta_1 + \theta_2 + \theta_3) = \tau_3
 \end{aligned}$$

Table A-3 **Characteristics of a three-link model**

Parameter	Description	Value
M_{HAT}	Half the mass of the upper extremity (kg)	18.20
M_{TH}	Mass of the thigh segment (kg)	5.37
M_{SH}	Mass of the shank segment (kg)	3.28
L_{HAT}	Length of the trunk segment (m)	0.461
L_{TH}	Length of the thigh segment (m)	0.392
L_{SH}	Length of the shank segment (m)	0.394
L_F	Length of the foot (m)	0.062
$r_{G,hip}$	Radius of gyration of the upper extremity about the hip joint, as a percent of the trunk length	0.798
$r_{G,knee}$	Radius of gyration of the thigh segment about the knee joint, as a percent of L_{TH}	0.653
$r_{G,ankle}$	Radius of gyration of the shank segment about the ankle joint, as a percent of L_{SH}	0.572
$r_{COM,HAT}$	Proximal center of mass of the upper extremity as a percent of the upper extremity length	0.626
$r_{COM,TH}$	Distal center of mass of the thigh segment as a percent of L_{TH}	0.567
$r_{COM,SH}$	Distal center of mass of the shank segment as a percent of L_{SH}	0.394
θ_1	Ankle angle (rad)	Variable
θ_2	Knee angle (rad)	Variable
θ_3	Hip angle (rad)	Variable
$\dot{\theta}_1$	Ankle angular velocity (rad/s)	Variable
$\dot{\theta}_2$	Knee angular velocity (rad/s)	Variable
$\dot{\theta}_3$	Hip angular velocity (rad/s)	Variable
$\ddot{\theta}_1$	Ankle angular acceleration (rad/s ²)	Variable
$\ddot{\theta}_2$	Knee angular acceleration (rad/s ²)	Variable
$\ddot{\theta}_3$	Hip angular acceleration (rad/s ²)	Variable
τ_1	Ankle torque (Nm)	0
τ_2	Knee torque (Nm)	Variable
τ_3	Hip torque (Nm)	Variable

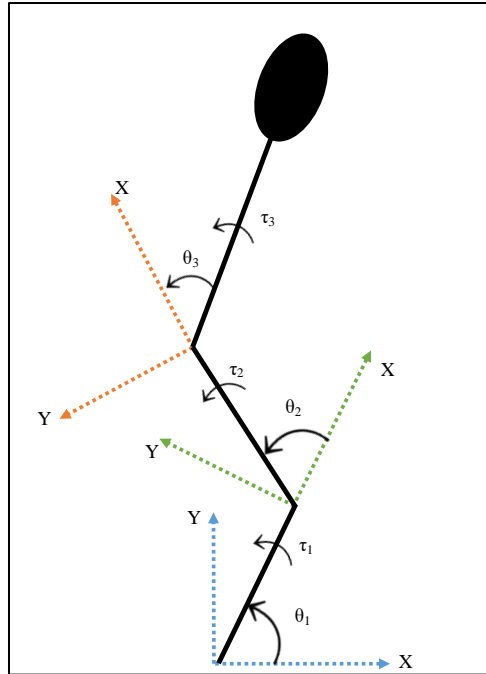


Figure A.3 **Three-link model of a human fall**

Appendix B: Design Variables

Each of the design variables, including the joint angles, angular velocities, and the torques applied to the joints are predefined for a specific fall duration. The fall duration determines the vector length for each design variable. If the vector containing each design variable throughout the fall has the length of l , then x that is the vector containing all the design variables throughout the fall has a length equal to the number of design variables times l . The most general form of vector x , which represents the case of the three-link model, is described in Table B-1.

Table B-1 Characteristics of the vector of design variables

	t_0	$t_0 + dt$	$t_0 + 2dt$...	$t_f - 2dt$	$t_f - dt$	t_f
$X(1:l)$	θ_{1,t_0}	θ_{1,t_0+dt}	θ_{1,t_0+2dt}	...	θ_{1,t_f-2dt}	θ_{1,t_f-dt}	θ_{1,t_f}
$X(l+1:2l)$	θ_{2,t_0}	θ_{2,t_0+dt}	θ_{2,t_0+2dt}	...	θ_{2,t_f-2dt}	θ_{2,t_f-dt}	θ_{2,t_f}
$X(2l+1:3l)$	θ_{3,t_0}	θ_{3,t_0+dt}	θ_{3,t_0+2dt}	...	θ_{3,t_f-2dt}	θ_{3,t_f-dt}	θ_{3,t_f}
$X(3l+1:4l)$	$\dot{\theta}_{1,t_0}$	$\dot{\theta}_{1,t_0+dt}$	$\dot{\theta}_{1,t_0+2dt}$...	$\dot{\theta}_{1,t_f-2dt}$	$\dot{\theta}_{1,t_f-dt}$	$\dot{\theta}_{1,t_f}$
$X(4l+1:5l)$	$\dot{\theta}_{2,t_0}$	$\dot{\theta}_{2,t_0+dt}$	$\dot{\theta}_{2,t_0+2dt}$...	$\dot{\theta}_{2,t_f-2dt}$	$\dot{\theta}_{2,t_f-dt}$	$\dot{\theta}_{2,t_f}$
$X(5l+1:6l)$	$\dot{\theta}_{3,t_0}$	$\dot{\theta}_{3,t_0+dt}$	$\dot{\theta}_{3,t_0+2dt}$...	$\dot{\theta}_{3,t_f-2dt}$	$\dot{\theta}_{3,t_f-dt}$	$\dot{\theta}_{3,t_f}$
$X(6l+1:7l)$	τ_{1,t_0}	τ_{1,t_0+dt}	τ_{1,t_0+2dt}	...	τ_{1,t_f-2dt}	τ_{1,t_f-dt}	τ_{1,t_f}
$X(7l+1:8l)$	τ_{2,t_0}	τ_{2,t_0+dt}	τ_{2,t_0+2dt}	...	τ_{2,t_f-2dt}	τ_{2,t_f-dt}	τ_{2,t_f}
$X(8l+1:9l)$	τ_{3,t_0}	τ_{3,t_0+dt}	τ_{3,t_0+2dt}	...	τ_{3,t_f-2dt}	τ_{3,t_f-dt}	τ_{3,t_f}

In this table t_0, t_f , and dt are the optimization's initial time, final time, and the time step, respectively. The value of each design variable is defined at each time step. As an example, θ_{1,t_0} represents the value of θ_1 at $t=t_0$ and θ_{1,t_f} represents the value of θ_1 at $t=t_f$.

Geometrical constraints are considered in the development of the three-link model of a human fall to assure the validity of the solution. Thus, the value of the hip height is limited to

acquire a positive value at the one-to-the-last step of the fall, and has to acquire a negative value at the last time step.

Appendix C: Constraints Governing the Motion of a Falling Human Model

To recall the description of the constraints, a few parameters from Table 3-2 are reviewed and presented in Table C-1.

Table C-1 Constraints of the optimization

Field Name	Description
A	Matrix for linear inequality constraints
b	Vector for linear inequality constraints
Aeq	Matrix for linear equality constraints
beq	Vector for linear equality constraints
$c(x)$	Function to define nonlinear inequality
$ceq(x)$	Function to define nonlinear equality

In the current optimization problem, there is no linear or nonlinear inequality constraint that needs to be satisfied, thus corresponding parameters to these constraints are defined as described in (C.1).

$$\begin{aligned}
 A.X &\leq b \\
 A &= [] \\
 b &= [] \\
 c &\leq 0 \\
 c &= []
 \end{aligned} \tag{C.1}$$

The linear equalities that have to be satisfied in the optimization problem are the initial joint angles and angular velocities. These values have to remain the same as what is defined initially in the optimization. In (C.2), l is the length of each design variable's vector. $\theta_{1,t_0}, \theta_{2,t_0}, \theta_{3,t_0}$ are the initial ankle, knee, and hip angles, respectively. $\dot{\theta}_{1,t_0}, \dot{\theta}_{2,t_0}, \dot{\theta}_{3,t_0}$ are the initial ankle, knee, and hip angular velocities, respectively.

$$Aeq.X = beq$$

$$Aeq = \begin{bmatrix} 1 & 0 & 0 & 0 & 0 & 0 & \overbrace{0 \dots 0}^{2l} \\ 0 & 1 & 0 & 0 & 0 & 0 & 0 \\ 0 & 0 & 1 & 0 & 0 & 0 & 0 \\ 0 & \dots & 0 & \dots & 0 & \dots & 1 & \dots & 0 & \dots & 0 \\ 0 & 0 & 0 & 0 & 1 & 0 & 0 & 0 \\ 0 & 0 & 0 & 0 & 0 & 1 & 0 & 0 \end{bmatrix} \quad beq = \begin{bmatrix} \theta_{1,t_0} \\ \theta_{2,t_0} \\ \theta_{3,t_0} \\ \dot{\theta}_{1,t_0} \\ \dot{\theta}_{2,t_0} \\ \dot{\theta}_{3,t_0} \end{bmatrix} \quad (C.2)$$

The nonlinear equalities that have to be satisfied in the optimization problem are the initial joint angles and angular velocities. In (C.3), α_{ij} , β_i , and γ_i are the corresponding coefficients used to formulate equations (A.1) to (A.3) in Section (A.3).

$$ceq = 0$$

$$\begin{bmatrix} \alpha_{11} & \alpha_{12} & \alpha_{13} \\ \alpha_{21} & \alpha_{22} & \alpha_{23} \\ \alpha_{31} & \alpha_{32} & \alpha_{33} \end{bmatrix} \begin{bmatrix} \ddot{\theta}_1 \\ \ddot{\theta}_2 \\ \ddot{\theta}_3 \end{bmatrix} = \begin{bmatrix} \beta_1 \\ \beta_2 \\ \beta_3 \end{bmatrix} \Rightarrow \begin{bmatrix} \ddot{\theta}_1 \\ \ddot{\theta}_2 \\ \ddot{\theta}_3 \end{bmatrix} = \begin{bmatrix} \alpha_{11} & \alpha_{12} & \alpha_{13} \\ \alpha_{21} & \alpha_{22} & \alpha_{23} \\ \alpha_{31} & \alpha_{32} & \alpha_{33} \end{bmatrix}^{-1} \begin{bmatrix} \beta_1 \\ \beta_2 \\ \beta_3 \end{bmatrix}$$

$$\begin{bmatrix} \dot{\theta}_1 \\ \dot{\theta}_2 \\ \dot{\theta}_3 \\ \ddot{\theta}_1 \\ \ddot{\theta}_2 \\ \ddot{\theta}_3 \end{bmatrix} = \begin{bmatrix} 0 & 0 & 0 & 1 & 0 & 0 \\ 0 & 0 & 0 & 0 & 1 & 0 \\ 0 & 0 & 0 & 0 & 0 & 1 \\ 0 & 0 & 0 & 0 & 0 & 0 \\ 0 & 0 & 0 & 0 & 0 & 0 \\ 0 & 0 & 0 & 0 & 0 & 0 \end{bmatrix} \begin{bmatrix} \theta_1 \\ \theta_2 \\ \theta_3 \\ \dot{\theta}_1 \\ \dot{\theta}_2 \\ \dot{\theta}_3 \end{bmatrix} + \begin{bmatrix} 0 \\ 0 \\ 0 \\ \gamma_1 \\ \gamma_2 \\ \gamma_3 \end{bmatrix} \quad (C.3)$$

Appendix D: Optimization Problems

The general aim of an optimization problem is to find the best feasible solution that minimizes an objective function while satisfying a set of requirements. The most general form of an optimization problem is defined in (D.1), in which vector x includes the optimization variables, f_0 is the objective function, f_i and b_i include the constraints on the problem, and n is the number of constraints that have to be satisfied in the optimization problem.

$$\begin{aligned} & \text{minimize} && f_0(x) \\ & \text{subject to} && f_i(x) \leq b_i, \quad i = 1, \dots, n \end{aligned} \tag{D.1}$$

Optimization problems are generally categorized based on the form of the objective function and the type of the constraints. A general class of an optimization problem is called convex if the objective function and constraints satisfy the form of an inequality described in (D.2). Convex optimization problems have been the focus of many previous research studies, and effective techniques have been developed to solve these types of problems. However, there is no analytical solution for these types of optimization problems in general [73].

$$f_i(\alpha x + \beta y) \leq \alpha f_i(x) + \beta f_i(y) \tag{D.2}$$

In the particular case where the equality form is satisfied in (D.2) the problem is called a linear optimization program. Nonlinear optimization problems, in which the objective function and the constraints are nonlinear functions of optimization variables, are more difficult to solve. Different methods have been developed to solve nonlinear optimization problems but there is as yet no effective method for solving the general form of nonlinear non-convex programming problems. It was shown that the effectiveness of algorithms developed for nonlinear problems

heavily depends on particular forms of the objective and constraint functions and the number of variables and constraints in the problem [73].

Optimization techniques can also be divided into the two categories of local and global optimization. In a global optimization problem, a global minimum is a point at which the value of the objective function obtains its lowest value. In some optimization problems, it is not feasible to find the global minimum due to the complexity of the form of the optimization problems and the inherent limitations of minimization techniques. In a local minimum optimization problem, the local minimum is a point at which the value of the objective function obtains its lowest value among the nearby points, but there is no guarantee that this point corresponds to the lowest value of the objective function in the global space of the solutions. Compared to global optimization problems, local optimization methods are fast and are widely used when globally optimality of the solution is not required [73].

The most widely used general approach to optimization problems is based on numerical methods. In this approach, an initial estimate of the solution is provided to the optimization and iterative solutions to the optimization problem are examined. Finally, the process is terminated when required convergence criteria are satisfied [74].

As discussed above, the choice of an appropriate optimization technique to solve an optimization problem is governed by the form of the problem, and more specifically the form of the objective function and the constraints. Thus, the technique used to solve the optimization problem proposed in this work was chosen subsequent to the formation of the problem definition. This process will be discussed in more detail in Chapter 3 of this thesis.

Appendix E: Model of a Human-Exoskeleton Fall

Similar to the model of a human fall, a model of a three-link inverted pendulum was used to describe the characteristics of a human-exoskeleton fall (Figure E.1). Characteristics of a hypothetical exoskeleton were added to the already existing three-link model of a human, which was described in Appendix A, Section A.3. The set of governing equations of motion for the model of a human-exoskeleton fall, consisting of three nonlinear, second order differential equation, are defined in (E.1). Corresponding descriptions and value of the exoskeleton's parameters are described in Table E-1. The rest of the parameters in (E.1) have similar descriptions and values as previously defined for the human model (Appendix A, Section A.3). It was assumed that the length of the thigh, shank, and foot segments of the exoskeleton is equal to the corresponding segments of the human body. Also, during the fall, the hip, knee, and the ankle joints of the human model have similar values as corresponding joint angles of the exoskeleton model.

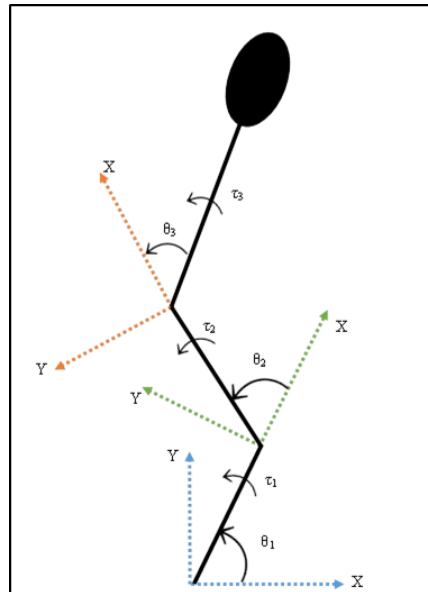


Figure E.1 **Three-link model of a human-exoskeleton fall**

Equation No.1:

$$\begin{aligned}
& \left\{ \left(M_{SH} r_{G,ankle}^2 + \frac{1}{3} M_{eSH} \right) L_{SH}^2 + \left(M_{TH} r_{G,knee}^2 + \frac{1}{3} M_{eTH} \right) L_{TH}^2 + (M_{TH} + M_{eTH})(L_{SH} + L_F)^2 + 2(L_{SH} + L_F)(M_{TH} r_{COM,TH} + M_{eTH} r_{eCOM,TH}) L_{TH} \cos \theta_2 \right. \\
& + \left[M_{HAT} (r_{G,hip} L_{HAT})^2 + \frac{1}{3} M_{eHAT} (L_{eHAT})^2 \right] + (M_{HAT} + M_{eHAT}) L_{TH}^2 + (M_{HAT} + M_{eHAT})(L_{SH} + L_F)^2 + 2(M_{HAT} r_{COM,HAT} L_{HAT} + M_{eHAT} r_{COM,eHAT} L_{eHAT}) L_{TH} \cos \theta_3 \\
& \left. + 2(L_{SH} + L_F)(M_{HAT} r_{COM,HAT} L_{HAT} + M_{eHAT} r_{COM,eHAT} L_{eHAT}) \cos(\theta_2 + \theta_3) + 2L_{TH} (L_{SH} + L_F)(M_{HAT} + M_{eHAT}) \cos \theta_2 \right\} \ddot{\theta}_1 \\
& + \left\{ \left(M_{TH} r_{G,knee}^2 + \frac{1}{3} M_{eTH} \right) L_{TH}^2 + (L_{SH} + L_F)(M_{TH} r_{COM,TH} + M_{eTH} r_{eCOM,TH}) L_{TH} \cos \theta_2 + \left[M_{HAT} (r_{G,hip} L_{HAT})^2 + \frac{1}{3} M_{eHAT} (L_{eHAT})^2 \right] + (M_{HAT} + M_{eHAT}) L_{TH}^2 \right. \\
& + 2(M_{HAT} r_{COM,HAT} L_{HAT} + M_{eHAT} r_{COM,eHAT} L_{eHAT}) L_{TH} \cos \theta_3 + (L_{SH} + L_F)(M_{HAT} r_{COM,HAT} L_{HAT} + M_{eHAT} r_{COM,eHAT} L_{eHAT}) \cos(\theta_2 + \theta_3) \\
& \left. + L_{TH} (L_{SH} + L_F)(M_{HAT} + M_{eHAT}) \cos \theta_2 \right\} \ddot{\theta}_2 \\
& + \left\{ \left[M_{HAT} (r_{G,hip} L_{HAT})^2 + \frac{1}{3} M_{eHAT} (L_{eHAT})^2 \right] + (M_{HAT} r_{COM,HAT} L_{HAT} + M_{eHAT} r_{COM,eHAT} L_{eHAT}) L_{TH} \cos \theta_3 \right. \\
& \left. + (L_{SH} + L_F)(M_{HAT} r_{COM,HAT} L_{HAT} + M_{eHAT} r_{COM,eHAT} L_{eHAT}) \cos(\theta_2 + \theta_3) \right\} \ddot{\theta}_3 \tag{E.1} \\
& - \left\{ 2(M_{HAT} r_{COM,HAT} L_{HAT} + M_{eHAT} r_{COM,eHAT} L_{eHAT}) L_{TH} \sin \theta_3 \dot{\theta}_3 + 2(L_{SH} + L_F)(M_{HAT} r_{COM,HAT} L_{HAT} + M_{eHAT} r_{COM,eHAT} L_{eHAT}) \sin(\theta_2 + \theta_3)(\dot{\theta}_2 + \dot{\theta}_3) \right\} \dot{\theta}_1 \\
& + 2L_{TH} (L_{SH} + L_F)(M_{HAT} + M_{eHAT}) \sin \theta_2 \dot{\theta}_2 \\
& - \left\{ 2(M_{HAT} r_{COM,HAT} L_{HAT} + M_{eHAT} r_{COM,eHAT} L_{eHAT}) L_{TH} \sin \theta_3 \dot{\theta}_3 + (L_{SH} + L_F)(M_{HAT} r_{COM,HAT} L_{HAT} + M_{eHAT} r_{COM,eHAT} L_{eHAT}) \sin(\theta_2 + \theta_3)(\dot{\theta}_2 + \dot{\theta}_3) \right\} \dot{\theta}_2 \\
& + L_{TH} (L_{SH} + L_F)(M_{HAT} + M_{eHAT}) \sin \theta_2 \dot{\theta}_2 \\
& - \left\{ (M_{HAT} r_{COM,HAT} L_{HAT} + M_{eHAT} r_{COM,eHAT} L_{eHAT}) L_{TH} \sin \theta_3 \dot{\theta}_3 + (L_{SH} + L_F)(M_{HAT} r_{COM,HAT} L_{HAT} + M_{eHAT} r_{COM,eHAT} L_{eHAT}) \sin(\theta_2 + \theta_3)(\dot{\theta}_2 + \dot{\theta}_3) \right\} \dot{\theta}_3 \\
& - (L_{SH} + L_F)(M_{TH} r_{COM,TH} + M_{eTH} r_{eCOM,TH}) L_{TH} (2\dot{\theta}_1 + \dot{\theta}_2) \sin \theta_2 \dot{\theta}_2 \\
& + (M_{SH} r_{COM,SH} + M_{eSH} r_{eCOM,eSH}) g L_{SH} \cos \theta_1 \\
& + (M_{TH} r_{COM,TH} + M_{eTH} r_{COM,eTH}) L_{TH} g \cos(\theta_1 + \theta_2) + (M_{TH} + M_{eTH})(L_{SH} + L_F) g \cos \theta_1 \\
& + (M_{HAT} + M_{eHAT})(L_{SH} + L_F) g \cos \theta_1 + (M_{HAT} + M_{eHAT}) L_{TH} g \cos(\theta_1 + \theta_2) + (M_{HAT} r_{COM,HAT} L_{HAT} + M_{eHAT} r_{COM,eHAT} L_{eHAT}) g \cos(\theta_1 + \theta_2 + \theta_3) = \tau_1
\end{aligned}$$

Equation No.2:

$$\begin{aligned}
& \left\{ \left(M_{TH} r_{G,knee}^2 + \frac{1}{3} M_{eTH} \right) L_{TH}^2 + (M_{TH} r_{COM,TH} + M_{eTH} r_{eCOM,TH}) (L_{SH} + L_F) L_{TH} \cos \theta_2 + \left[M_{HAT} (r_{G,hip} L_{HAT})^2 + \frac{1}{3} M_{eHAT} (L_{eHAT})^2 \right] + (M_{HAT} + M_{eHAT}) L_{TH}^2 \right. \\
& \left. + 2(M_{HAT} r_{COM,HAT} L_{HAT} + M_{eHAT} r_{COM,eHAT} L_{eHAT}) L_{TH} \cos \theta_3 + (L_{SH} + L_F) (M_{HAT} r_{COM,HAT} L_{HAT} + M_{eHAT} r_{COM,eHAT} L_{eHAT}) \cos(\theta_2 + \theta_3) \right. \\
& \left. + L_{TH} (M_{HAT} + M_{eHAT}) (L_{SH} + L_F) \cos \theta_2 \right\} \ddot{\theta}_1 \\
& + \left\{ \left(M_{TH} r_{G,knee}^2 + \frac{1}{3} M_{eTH} \right) L_{TH}^2 + \left[M_{HAT} (r_{G,hip} L_{HAT})^2 + \frac{1}{3} M_{eHAT} (L_{eHAT})^2 \right] + (M_{HAT} + M_{eHAT}) L_{TH}^2 + 2(M_{HAT} r_{COM,HAT} L_{HAT} + M_{eHAT} r_{COM,eHAT} L_{eHAT}) L_{TH} \cos \theta_3 \right\} \ddot{\theta}_2 \\
& + \left\{ \left[M_{HAT} (r_{G,hip} L_{HAT})^2 + \frac{1}{3} M_{eHAT} (L_{eHAT})^2 \right] + (M_{HAT} r_{COM,HAT} L_{HAT} + M_{eHAT} r_{COM,eHAT} L_{eHAT}) L_{TH} \cos \theta_3 \right\} \ddot{\theta}_3 \\
& - \left\{ 2(M_{HAT} r_{COM,HAT} L_{HAT} + M_{eHAT} r_{COM,eHAT} L_{eHAT}) L_{TH} \sin \theta_3 \dot{\theta}_3 + (L_{SH} + L_F) (M_{HAT} r_{COM,HAT} L_{HAT} + M_{eHAT} r_{COM,eHAT} L_{eHAT}) \sin(\theta_2 + \theta_3) (\dot{\theta}_2 + \dot{\theta}_3) \right. \\
& \left. + L_{TH} (L_{SH} + L_F) (M_{HAT} + M_{eHAT}) \sin \theta_2 \dot{\theta}_2 \right\} \dot{\theta}_1 \\
& - \left\{ 2(M_{HAT} r_{COM,HAT} L_{HAT} + M_{eHAT} r_{COM,eHAT} L_{eHAT}) L_{TH} \sin \theta_3 \dot{\theta}_3 \right\} \dot{\theta}_2 \\
& - \left\{ (M_{HAT} r_{COM,HAT} L_{HAT} + M_{eHAT} r_{COM,eHAT} L_{eHAT}) L_{TH} \sin \theta_3 \dot{\theta}_3 \right\} \dot{\theta}_3 \\
& + (M_{TH} r_{COM,TH} + M_{eTH} r_{eCOM,TH}) (L_{SH} + L_F) L_{TH} \dot{\theta}_1^2 \sin \theta_2 \\
& + (L_{SH} + L_F) (M_{HAT} r_{COM,HAT} L_{HAT} + M_{eHAT} r_{COM,eHAT} L_{eHAT}) \sin(\theta_2 + \theta_3) \dot{\theta}_1 (\dot{\theta}_1 + \dot{\theta}_2 + \dot{\theta}_3) + L_{TH} (L_{SH} + L_F) (M_{HAT} + M_{eHAT}) \sin \theta_2 (\dot{\theta}_1 + \dot{\theta}_2) \dot{\theta}_1 \\
& + (M_{TH} r_{COM,TH} + M_{eTH} r_{COM,eTH}) L_{TH} g \cos(\theta_1 + \theta_2) + (M_{HAT} + M_{eHAT}) L_{TH} g \cos(\theta_1 + \theta_2) + (M_{HAT} r_{COM,HAT} L_{HAT} + M_{eHAT} r_{COM,eHAT} L_{eHAT}) g \cos(\theta_1 + \theta_2 + \theta_3) = \tau_2
\end{aligned}$$

Equation No.3:

$$\begin{aligned}
& \left\{ \left[M_{HAT} (r_{G,hip} L_{HAT})^2 + \frac{1}{3} M_{eHAT} (L_{eHAT})^2 \right] + (M_{HAT} r_{COM,HAT} L_{HAT} + M_{eHAT} r_{COM,eHAT} L_{eHAT}) L_{TH} \cos \theta_3 \right\} \ddot{\theta}_1 \\
& + (L_{SH} + L_F) (M_{HAT} r_{COM,HAT} L_{HAT} + M_{eHAT} r_{COM,eHAT} L_{eHAT}) \cos(\theta_2 + \theta_3) \\
& + \left\{ \left[M_{HAT} (r_{G,hip} L_{HAT})^2 + \frac{1}{3} M_{eHAT} (L_{eHAT})^2 \right] + (M_{HAT} r_{COM,HAT} L_{HAT} + M_{eHAT} r_{COM,eHAT} L_{eHAT}) L_{TH} \cos \theta_3 \right\} \ddot{\theta}_2 \\
& + \left\{ \left[M_{HAT} (r_{G,hip} L_{HAT})^2 + \frac{1}{3} M_{eHAT} (L_{eHAT})^2 \right] \right\} \ddot{\theta}_3 \\
& - \left\{ (M_{HAT} r_{COM,HAT} L_{HAT} + M_{eHAT} r_{COM,eHAT} L_{eHAT}) L_{TH} \sin \theta_3 \dot{\theta}_3 + (L_{SH} + L_F) (M_{HAT} r_{COM,HAT} L_{HAT} + M_{eHAT} r_{COM,eHAT} L_{eHAT}) \sin(\theta_2 + \theta_3) (\dot{\theta}_2 + \dot{\theta}_3) \right\} \dot{\theta}_1 \\
& - \left\{ (M_{HAT} r_{COM,HAT} L_{HAT} + M_{eHAT} r_{COM,eHAT} L_{eHAT}) L_{TH} \sin \theta_3 \dot{\theta}_3 \right\} \dot{\theta}_2 \\
& + (M_{HAT} r_{COM,HAT} L_{HAT} + M_{eHAT} r_{COM,eHAT} L_{eHAT}) L_{TH} \sin \theta_3 (\dot{\theta}_1 + \dot{\theta}_2 + \dot{\theta}_3) (\dot{\theta}_1 + \dot{\theta}_2) + (L_{SH} + L_F) (M_{HAT} r_{COM,HAT} L_{HAT} + M_{eHAT} r_{COM,eHAT} L_{eHAT}) \sin(\theta_2 + \theta_3) \dot{\theta}_1 (\dot{\theta}_1 + \dot{\theta}_2 + \dot{\theta}_3) \\
& + (M_{HAT} r_{COM,HAT} L_{HAT} + M_{eHAT} r_{COM,eHAT} L_{eHAT}) g \cos(\theta_1 + \theta_2 + \theta_3) = \tau_3
\end{aligned}$$

Table E-1 **Characteristics of the exoskeleton model**

Parameter	Description	Value
M_{eHAT}	Half the mass of the trunk segment (kg)	3.0
M_{eTH}	Mass of the thigh segment (kg)	2.5
M_{eSH}	Mass of the shank segment (kg)	0.5
L_{eHAT}	Length of the trunk segment (m)	0.20
$r_{COM,eHAT}$	Proximal center of mass of the upper extremity as a percent of the trunk length	0.5
$r_{COM,eTH}$	Distal center of mass of the thigh segment as a percent of L_{TH}	0.5
$r_{COM,eSH}$	Distal center of mass of the shank segment as a percent of L_{SH}	0.5

Appendix F: Acceleration/Deceleration Time Calculations

The equations defined in (F.1) were used to calculate the acceleration and deceleration time of the actuator. Parameters used in the following equations are described in Table F-1. Additional information regarding the calculation of the acceleration and deceleration time could be found in [69].

$$t_a = k \times (J_A + J_L) \times \frac{2\pi}{60} \times \frac{N}{T_M - T_L}$$

$$t_d = k \times (J_A + J_L) \times \frac{2\pi}{60} \times \frac{N}{T_M + 2 \times T_F + T_L} \quad (\text{F.1})$$

$$T_F = K_T \times I_R - T_R$$

Table F-1 **Parameters used to calculate the acceleration/deceleration time of the actuator**

Parameter	Description
t_a	Acceleration time (s)
t_d	Deceleration time (s)
k	Acceleration reduction coefficient 1 to 1.5
J_A	Actuator inertia moment (kg.m ²)
J_L	Load inertia moment (kg.m ²)
N	Actuator rotation speed (r/min)
T_M	Maximum actuator torque (Nm)
T_F	Actuator friction torque (Nm)
T_L	Load torque (Nm)
K_T	Torque constant (Nm/A)
T_R	Allowable continuous torque (Nm)
I_R	Allowable continuous current (A)